Design and Implement Towards Enhanced Physical Interactive Performance Robot Bodies

by

Zeyu Ren

Submitted to the Department of Informatics, Bioengineering, Robotics and Systems Engineering
in partial fulfillment of the requirements for the degree of

Doctor of Philosophy

at the

UNIVERSITÀ DEGLI STUDI DI GENOVA
and
ISTITUTO ITALIANO DI TECNOLOGIA

February 2019

Author .....
Zeyu Ren
Università degli Studi di Genova & Istituto Italiano di Tecnologia

Supervisor .....
Dr. Nikos G. Tsagarakis
Senior Researcher Tenured, Principal Investigator
Humanoids and Human Centered Mechatronics Research Line
Istituto Italiano di Tecnologia

Reviewer .....
Prof. Matteo Fumagalli
Department of Mechanical and Manufacturing Engineering
Aalborg University
Prof. Matteo Cianchetti
Leader of Soft Mechatronics, The BioRobotics Institute
Scuola Superiore Sant'Anna

Design and Implement Towards Enhanced Physical Interactive Performance Robot Bodies

by

Zeyu Ren

Submitted to the Department of Informatics, Bioengineering, Robotics and Systems Engineering
on Feb 13, 2019, in partial fulfillment of the
requirements for the degree of
Doctor of Philosophy

Abstract

In this thesis, it will introduce the design principle and implement details towards enhanced physical interactive performance robot bodies, which are more specifically focused on under actuated principle robotic hands and articulated leg robots. Since they both significantly function as the physical interactive robot bodies against external environment, while their current performance can hardly satisfy the requirement of undertaking missions in real application.

Regarding to the enhanced physical interactive performances, my work will emphasis on the three following specific functionalities, high energy efficiency, high strength and physical sturdiness in both robotics actuation and mechanism. For achieving the aforementioned targets, multiple design methods have been applied, firstly the elastic energy storage elements and compliant actuation have been adopted in legged robots as Asymmetrical Compliant Actuation (ACA), implemented for not only single joint but also multiple joints as mono and biarticulation configurations in order to achieve higher energy efficiency motion. Secondly the under actuated principle and modular finger design concept have been utilized on the development of robotic hands for enhancing the grasping strength and physical sturdiness meanwhile maintaining the manipulation dexterity. Lastly, a novel high payload active tuning Parallel Elastic Actuation (PEA) and Series Elastic Actuation (SEA) have been adopted on legged robots for augmenting energy efficiency and physical sturdiness.

My thesis contribution relies on the novel design and implement of robotics bodies for enhancing physical interactive performance and we experimentally verified the design effectiveness in specific designed scenario and practical applications.

Thesis Supervisor: Dr. Nikos G. Tsagarakis
Title: Senior Researcher Tenured, Principal Investigator
Humanoids and Human Centered Mechatronics Research Line
Istituto Italiano di Tecnologia

Acknowledgments

First of all, I would like to express the appreciate to my supervisor Dr. Nikos G. Tsagarakis, who provides me the great opportunity to participate in CENTAURO Project and proceed the research on enhanced physical interactive performance robot bodies design and development. Dr. Nikos G. Tsagarakis not only gave me the specific and helpful guidance in the robotics research field, but also provided me the methodology and attitude towards scientific research and engineer application. Despite of that, Dr. Nikos G. Tsagarakis is a highly self-discipline tutor and delivers much tolerance and freedom to his students, which keeps me in a positive status towards research and life in my three year PhD career.

Afterwards, some highly appreciate and gratitude should be equally given to my colleagues in the research line of Humanoid and Human Centered Mechatronics (HHCM), Department of Advanced Robotics (ADVR), who helped me in specific details in terms of research method, academical writing skills, practical experiments tricks and also the elegant scientific taste. They are Dr. Chengxu Zhou, Dr. Wesley Roozing, Dr. Navvab Kashiri, Dr. Jörn Malzahn, Dr. Yangwei You, PhC Songyan Xin, PhC Rajesh Subburaman, PhC Vishnu Dev Amara etc..

Furthermore, since my PhD research direction are closely related to the mechatronics hardware development, I received generous help and valuable engineering experiences from the technicians in our lab. The significance of these engineering knowledge and experience should not be under estimated or ignored if we are desired to apply the robotics technology into real application, and those knowledge are difficult to be gained from scientific research papers or books. Those technicians are following, Lorenzo Baccelliere, Phil Edward Hudson, Mattia Arena, Paolo Guria, Alessio Margan, Marco Migliorini, Diego Vedelago, Gianluca Pane and Francesco Di Dea etc..

In summary, for all the preliminary results and achievements that i have gained during my PhD career, it's all about a team work, which can hardly be realized individually. Therefore, sincerely be appreciated again for all the people who helped me during my PhD career.

Contents

List of Figures

List of Tables

Chapter 1

Introduction

The design and development of enhanced physical interactive performance robot bodies that can really enter into human society and practical application, for instance where the robots can effectively release human people from hard physical work in extreme environment or care for the elderly people, is currently a worldwide challenge. High energy efficiency, high strength and physical sturdiness are part of the most three important roles in enhanced physical interactive performances and my PhD work is actually based on these to proceed. Naturally this thesis will focus on the introduction of these three aforementioned points, while the other aspects not included in this thesis such as hardware reliability, human friendly and low development cost etc. are also significant and should not be ignored.

Quantities of significant research work has been achieved in the field of utilizing Series Elastic Actuation (SEA) [1, 2, 3, 4, 5, 6, 7, 8, 9, 10], Parallel Elastic Actuation (PEA) [11, 12, 13, 14, 15, 16, 17, 18, 19] and under actuation [20, 21, 22, 23, 24, 25, 26, 27, 28] for chasing the design and development of desired enhanced physical interactive performance robot bodies (robotic hands and anthropomorphic legs) target. As a matter of fact, for chasing the aforementioned targets and based on the practical requirement of European Projects, we designed and developed the anthropomorphic robotics leg named e-Leg, two generation of robotics hands called HERI Hand and HERI II Hand (mounted on Centauro robot). Corresponding design method and experimental validation will be detailed introduced in the following content. This work

not only contributes to the novelty design concept and method, but also provides the details, experiences and tricks in terms of practical engineering and hardware development, which both possess significance for realizing the desired enhanced physical interactive performance robot bodies for real applications.

1.1 Motivations and Objectives

The motivation of designing and developing enhanced physical interactive performance robot bodies is the physical world we living, requires the robot to possess adequate physical interactive ability with external environment, including various of rigid objects as well as soft human bodies. To be more specific, due to the technology limitation of existing power source, the design of robot bodies ought to enable robots to possess much higher energy efficiency in order to achieve higher power endurance, furthermore to release people from physical hard work, robots should be capable of generating high strength motion for undertaking high payload tasks and challenges, finally the physical sturdiness of the robot bodies has to be spotlight since the robot must survive in the external environment from unknown collision. The aforementioned three aspects are significant for the practical applications such as the scenarios in disaster response rescue, physical strength mission under high risk as well as elderly and disabled people caring service.

Among different kinds of robot bodies, we are more focused on the end-effector (robotics hands) and anthropomorphic legs, since they are both the significant parts on robots for interacting with external environment and will directly affect the robotic manipulation and locomotion performance. To be more specific, the design and control of the robotic hands functioned as end-effector directly decides the grasping and manipulation performance, which highly depends on the contact condition between fingers and objects, meanwhile the locomotion ability of the biped robots will be highly relied on the property of corresponding legs design, which will physically contact with the terrain all the time. With respect to the aforementioned reasons, the research object of my thesis will focus on the design of robotics hands and anthro-

pomorphic legs for humanoid robots, to be more specific, the HERI series under-actuated hands (HERI and HERI II) were developed and HERI II Hand is desired to be mounted on Centauro robot to function as a powerful end-effector, the 3-DoF energy efficiency leg named e-Leg was developed for verifying the energy efficiency and high strength motion ability based on series and parallel elastic actuation.

1.2 State of Art

The design and development of enhanced physical interactive performance robotics bodies are a worldwide research topic during the past few decades. The most notable shift is the broad utilization of compliance in robotics actuation in terms of Series Elastic Actuation (SEA) , Parallel Elastic Actuation (PEA) and under actuation.

Series Elastic Actuation (SEA) originates from the work of Pratt in the 90s [1] as shown Fig. 1-1(a). It has been well demonstrated this concept is able to significantly improve energy efficiency [2, 3] as Fig. 1-1(b) shows, torque control performance and stability [4, 5, 6, 7], physical robustness and interaction safety. Especially in field robotics, where environments are uncertain and unexpected collisions are common, the physical robustness and interaction safety of SEAs is highly beneficial [8, 9, 10]. Addition of compliant elements in parallel to the main actuation branches, known as Parallel Elastic Actuation (PEA) has seen less adoption than SEA. However their benefits have been repeatedly demonstrated, in actuator test bench setups [11, 12, 13, 14, 15], hopping robots [19], biped walkers [16, 17] as shown in Fig. 1-1(c)-1-1(d) and humanoids [18].

Basis on the compliant actuation, it is also a significant point relied on the way to implement series and parallel elastic actuation in multi-DoF legged systems. In biological systems, biarticulated muscle structures are common, where a single muscle spans multiple joints. Examples are the rectus femoris and hamstrings, which span the hip and knee joints as an antagonistic pair, the biceps, and the gastrocnemius muscle, which spans the knee and ankle joints. In the field of biomechanics, biarticulated muscles have been identified to transfer mechanical power between joints [29, 30]

(a) Series Elastic Actuator (b) Hopper (c) Stepper (d) Ernie

Figure 1-1: Typical implementation in Series Elastic Actuation (SEA) and Parallel Elastic Actuation (PEA), from left to right: Series Elastic Actuator from MIT, Hopper from University of Pisa and Italian Institute of Technology, Stepper from Sandia National Laboratories, Ernie from Ohio State University.

This principle has been used as a basis for biarticulated robotic actuators. In [31], the transfer of mechanical power between joints was experimentally demonstrated in a leg that models all nine major muscle groups in the human lower limb in the saggital plane. In [32] and [33], biarticulation was used in walking and jumping, respectively. [34] showed how biarticulation can improve the end-effector force ellipsoid. The recently introduced compliant bipedal walker [35] also includes a biarticulated ankle-knee configuration. An alternative mechanical structure that substantially improves efficiency was proposed in [36, 37, 38], which combines a high power SEA branch with a parallel high efficiency energy storage branch. Contrary to most PEA designs, the secondary branch is not passive but employs a secondary motor that allows to adjust the pretension position. In [37] a novel distributed controller was developed that used both branches for energy efficient operation, which experimentally verified the potential of both mechanism and controller on a 1-DoF leg, demonstrating a 65% reduction in electrical power consumption when compared to conventional SEA.

Meanwhile another important design method for chasing the target of developing enhanced physical interactive performance robot bodies is the adoption of under actuation and mechanism compliance, especially in the field of robotic end-effectors (robotic hands) design, which function as one of the most significant robotic bodies interacting physically with external environment. In the past few decades, many multi-finger robotic hands have been developed for both dexterous and robust grasp-

ing. Generally, they can be classified into two categories, fully-actuated and under-actuated hands. Fully-actuated hands, such as UTAH/M.I.T Hand [39], DLR Hand [40], Robonaut 2 Hand [41] and DEXMART Hand [42] etc., are capable of controlling each finger joint independently, thus they are able to mimic most of the sophisticated human hand motions by well-designed control strategies. Meanwhile, their superior capabilities also introduce challenges into the hardware and control designing stage, such as limited space for dozens of actuators, demanding algorithm development due to the redundancy, as well as the concomitant reliability issues and high costs. Therefore, making trade-offs between the actuator quantity and dexterity has been attracting attentions to this end, which flourishes the developments of under-actuated hands, such as RTR II Hand [27], MANUS-HAND [26], Barrett Hand [25], SDM Hand [28], Colombia Hand [24], Ritsumeikan robotic hand [21] and Pisa/IIT Softhand [20] etc. as presented from Fig. 1-2(a) to Fig. 1-2(g).

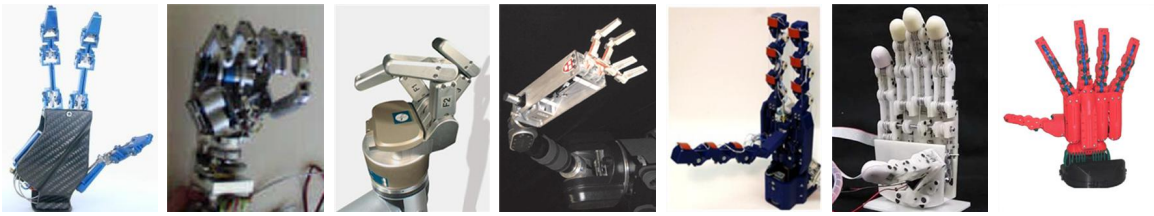

(a) (b) (c) (d) (e) (f) (g)

Figure 1-2: Representative robotics hand based on under actuation, from left to right: RTR2 Hand, MANUS Hand, Barret Hand, SDM Hand, Colombia Hand, Ritsumeikan Hand and PISA/IIT Hand.

The aforementioned different types of under-actuated hands have made greatly progress in terms of anthropomorphic design, dexterous grasping, robust holding, sensor feedback control as well as the low-cost yet robust hardware design. Nevertheless, it is hard for an under-actuated hand to possess all the above-mentioned advantages simultaneously. For instance, Pisa/IIT Softhand [20] is designed with perfect anthropomorphism, superior robustness and excellent self-protection property thanks to its novel compliant structures. However, due to its inherent single-actuator-driven characteristic, dexterous finger manipulation performance would be negatively effected. Ritsumeikan robotic hand [21] is able to achieve pinch, lateral pinch motions and pow-

erful anthropomorphic grasping efficiently with three independent actuators and one solenoid for locking mechanism. However, the deficient in embedded sensors limits its capability in delicate sensitive finger manipulation. As a matter of fact, currently it is quite difficult to come up with a general design method that could perfectly mimic the human hands function, which possesses both high strength powerful grasping and dexterous manipulation ability with delicate sensory feedback in compact integration and low cost. Therefore, the majority design of the robotic hands actually follows a function priority, which desired to enhance some aspects but will naturally sacrifice the others.

1.3 Thesis Contribution

In summary, the contribution of this thesis is mainly relies on the design method and development details of utilizing compliant mechanism and under actuation for achieving enhanced physical interactive performance robotic bodies. Meanwhile on the basis of realized robotic bodies, series of experiments have been proceeded for verifying the design effectiveness in quantitative analysis, which could actually provide specific guidance and reference for other similar robotic bodies design and development considering the long period and high cost of hardware iteration. Last but not least, corresponding engineering experiences and tricks in specific hardware development progress will also be presented, which should not be ignored or under estimated since these are difficult refer from existing papers but are also significant details that directly deciding mechatronics system performance.

To be more specific, in the work regard to the utilization of compliant actuation for energy efficiency and high strength on anthropomorphic robotic leg design, we extended the single one DoF to three DoFs in saggital pitch plane of a robotic leg, where Parallel Elastic Actuation (PEA) units with active pretension tuning mechanism functioned as Energy Storage Branch (ESB) are embedded in different actuation configurations, namely SEA-only, monoarticulation and biarticulation. SEA-only actuation configuration is the traditional joint actuation design and arrangement as

we see in most legged robots, while monoarticulation and biarticulation are come up mainly by considering the allowance or even enhancement of the back-drive ability for joint actuation under high gear ratio, where especially the biarticulation is a novel design inspired by human muscle and tendon structure [43]. On the basis of aforementioned single and multiple actuation configurations, a hardware platform called eLeg [44, 45] was developed, various enhanced energy efficiency and high strength motion were achieved on such a platform through dedicated control strategies, meanwhile specific energy efficiency are quantitatively analysed and evaluated.

Besides, another specific aspect of this thesis contribution relies on the implementation of under actuation principle for high strength grasping and physical sturdiness on robotics hands design and development. My thesis work actually highly emphasised again the significance of under actuation on robotic end-effector design, for its adequate performance in robustness, compliance, reliable and redundancy simplify. And the novelty is focused on the finger module concept implementation, which will at first effectively increase the dexterous manipulation performance in terms of fingers' independence, secondly the utilization of Degree of Actuators (DoAs) in high quantity will highly benefit the high strength grasping property, last but not least daily maintenance convenience will be extremely enhanced since the standard and independent finger module implementation. Following the aforementioned design concept, the hardware platform HERI and HERI II Hand [23, 46] were developed and HERI II Hand was desired to be mounted on Centauro robot [47] for undertaking series of practical test in ***CENTAURO Project*** [1], where its performances in high strength and dexterous grasping, robustness, reliable property are adequately verified.

1.4 Organization of Chapters

Following the Introduction Chapter, the content of this thesis can be divided into three main parts, ranging from Chapter 2 to Chapter 4, which describe each significant

[1] European's H2020 robotics project CENTAURO (644839), CENTAURO – Robust Mobility and Dexterous Manipulation in Disaster Response by Fullbody Telepresence in a Centaur-like Robot

aspect for developing the enhanced physical interactive performance robot bodies, namely energy efficiency, high strength and physical sturdiness respectively.

In Chapter 2, we will present the design method and development details of enhanced physical interactive performance robot bodies in terms of energy efficiency actuation and mechanism. Firstly, we will introduce the important concept of utilizing Asymmetrical Compliant Actuation (ACA) for energy efficiency improvement, where the Powerful Branch (PB) and Energy Storage Branch (ESB) functioning as two parallel branches in asymmetric. Meanwhile these two aforementioned branches could be configured into two different actuation arrangements on multi-DoF anthropomorphic leg, namely monoarticulation and biarticulation, for the further analysis of energy efficiency improvement and comparison. Secondly, we will present the design and distribution details of implementing the aforementioned ACA concept to a 3-DoF (in pitch saggital plane) legged robot, which could be configured into three actuation configurations (SEA-Only, Mono and Bi Articulation Configurations) in rapid time and this will provide the possibility of verifying energy efficiency comparison between three configurations conveniently. Finally, series of experiments are proceeded and corresponding results will be demonstrated in this chapter.

In Chapter 3, another significant aspect for enhanced physical interactive performance robotic bodies design in terms of high strength actuation and mechanism will be presented. On one hand, we will introduce the method of utilizing under actuation and finger module concept for enhancing the robotic hands high strength grasping performance, meanwhile optimised finger distribution and DoA assignment plan will also be demonstrated in order to keep an appropriate balance between high strength and dexterity as well as maintenance convenience. On the other hand, we will specifically present the design method and details of the linear pretension tuning mechanism of compliant energy storage element under high load functioned as Parallel Elastic Actuation (PEA) in legged robots. Here need to be highlighted that the aforementioned high strength linear pretension tuning mechanism can also benefit for further improving energy efficiency as discussed in Chapter 2. Series of experiments for verifying the high strength actuation and mechanism are presented, especially

the robotic hands (HERI and HERI II Hand) weight-grasping ratio evaluation and anthropomorphic legs (eLeg) jumping test with high load.

In Chapter 4, we will discuss the final point for developing enhanced physical interactive performance robotic bodies in terms of physical sturdiness by introducing the corresponding compliant mechanical elements in both robotic hands and anthropomorphic legs, to be more specific, the utilization of under actuation, compliant damping structure and Series Elastic Actuation (SEA). Corresponding evaluation tests including HERI II Hand in real application (CENTAURO project final evaluation camp) and eLeg in 23 kg load jumping are demonstrated for verifying the design effectiveness of physical sturdiness.

In chapter 5, we will firstly conclude the whole thesis work and then present the future work plan in the following three terms, full sensory feedback grasping control algorithm for achieving more precise and powerful grasping on robotic hands, field weakening control strategy for realizing higher eLeg jumping on each Series Elastic Actuator (SEA) and the dedicated pretension tuning control plan for higher eLeg energy efficiency on each Energy Storage Branch (ESB) unit.

Chapter 2

High Motion Energy Efficiency Design

The first topic we will discuss and introduce regard to the design and development of enhanced physical interactive performance robot bodies is the energy efficiency improvement in both actuation and mechanism field. Our work will actually more emphasis on the legged robotics (biped) design, since the traditional joint actuator in high gear ratio will disable the back-drive ability of the joint motion, which will seriously affect the energy efficiency in a negative way. Our idea relies on the design of new actuation and mechanism for enabling or even enhancing the joints back-drive ability while meantime still maintain the high gear ratio actuation plan, since it currently possesses significant improvement in actuator output torque-mass density, which will directly decide the legged robots high strength motion ability.

As a matter of fact, energy efficiency is a significant point that will affect robots performance in real physical world application in short future. Due to the compact geometric size and high integrated system of legged robots, especially biped, it requires the desired power supply to possess a extreme high energy mass density, considering the robots have to carry the power supply for proceeding missions in external environment independently. It is well known that, currently the performance of lithium battery has almost reached its limitation ceiling, in order to improve the robots endurance for undertaking real mission in physical world, the potential of

energy efficiency in actuation and mechanism has to be focused and explored.

2.1 Asymmetrical Compliant Actuation (ACA)

In order to achieve the energy efficiency for legged robots under high gear-ratio actuation, in this section we will firstly introduce the significant concept of utilizing Asymmetrical Compliant Actuation (ACA), which combines the series and parallel elastic actuation together for single joint actuation.

The main components of our series-parallel actuation concept are shown in Fig. 2-1. It consists of two parallel compliant actuation branches, with very different stiffness and power properties. Hence, we refer to this concept as *Asymmetric Compliant Actuation* (ACA) [38, 37].

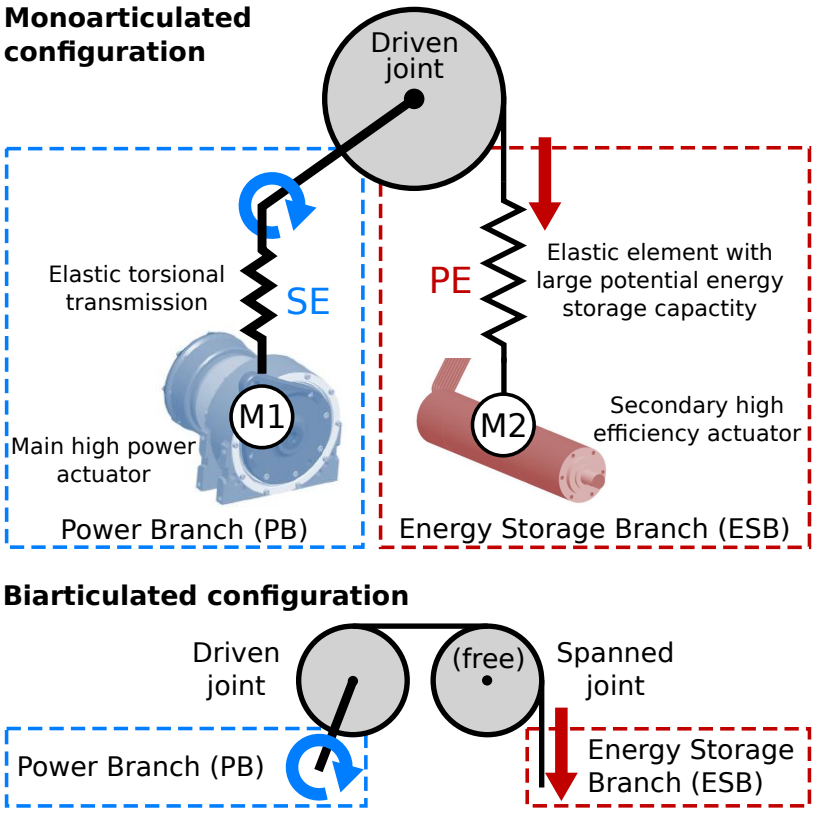

Figure 2-1: The series-parallel actuation concept we refer to as *Asymmetric Compliant Actuation* (ACA), shown in both monoarticulated (top) and biarticulated (bottom) configuration.

The first branch, referred to as the *Power Branch* (PB), is a rotary series-elastic

actuator consisting of a high-power electric motor M1 in series with an elastic element SE. The second branch, referred to as the *Energy Storage Branch* (ESB), comprises a highly-efficient lower power motor M2 with high reduction linear transmission. In the monoarticulated configuration shown on the top of Fig. 2-1, motor M2 is coupled to the driven joint through a linear unidirectional series elastic element PE and pulley. The elastic element PE differs from SE in its significantly lower stiffness and much larger energy storage capacity.

Shown on the bottom of Fig. 2-1 is the ACA concept in biarticulated configuration, where the ESB tendon spans a free pulley on a second (so-called spanned) joint, before driving the first. This configuration results in the elongation of elastic element PE being a function of the configuration of both joints, and the ESB providing torque to both joints. Selection of the pulley radii ratio and stiffness value allows to shape the torque profile as a function of both joint configurations and pretension position of motor M2.

2.1.1 Powerful Branch (PB) Actuation

The actuator we utilized for the Powerful Branch (PB) in Asymmetrical Compliant Actuation (ACA) concept is Series Elastic Actuator (SEA) from *Tree Robotics*[1]. The utilization of Series Elastic Actuation (SEA) technology is mainly for improving the system sturdiness by protecting the reduction gear against external impacts, while at the same time measuring the torque through angle deflection from the integrated torsion bar or compliant element. The actuation units are realised based on two main assemblies: the first assembly is the Kollmorgen flameless brushless DC motor and the second assembly includes a Harmonic Drive (HD) gearbox and a torque sensor unit. The actuators employ a 19-bit Renishaw magnetic encoder measuring the absolute rotor position and serving the Field Oriented control (FOC) implemented on the motor driver, and a 19-bit Renishaw magnetic encoder for measuring the absolute

[1] *Tree Robotics* [47], Technology for Robotics Systems Entering Real Environment, the integrated actuators based on series elastic actuation from Humanoid and Human Centred Mechatronics (HHCM) Research Line, Department of Advanced Robotics (ADVR), Italian Institute of Technology (iit), Link: http://www.treerobotics.eu/

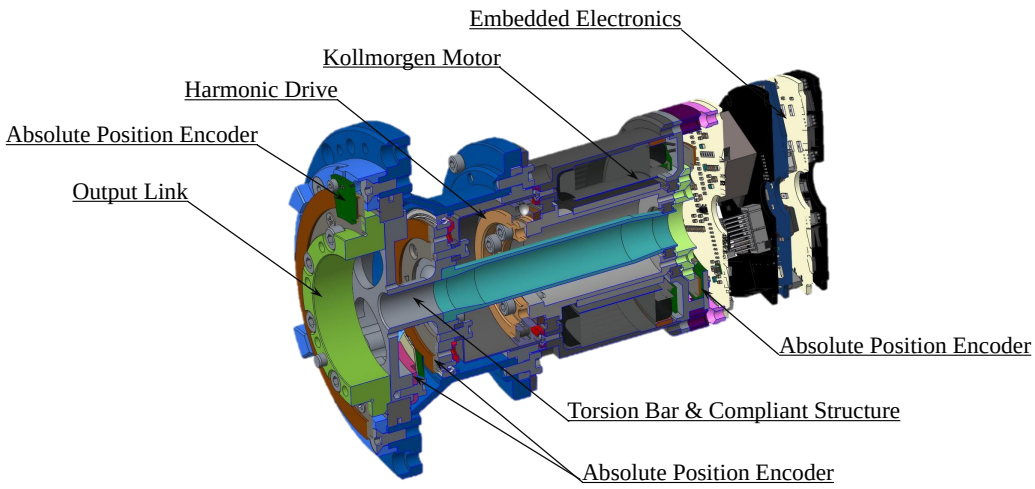

Figure 2-2: Section view of hardware components in Series Elastic Actuator (SEA) from *iit Tree Robotics* for Powerful Branch (PB), Asymmetrical Compliant Actuation (ACA).

link position. All the aforementioned structures related to the series elastic actuation could be refer from Fig. 2-2.

Since we know that the measurement of the torque in legged robots torque-controlled actuators is usually achieved by utilizing strain gauge based principle or angle deflection encoder based method [48], the main difference actually relies on the stiffness selection of the compliant structure equipped with the strain gauge or angle encoder. For the main actuators embedded in Powerful Branch (PB) units on legged robots, it is a trade off to make a decision between high and low stiffness, where the high stiffness will benefit for the torque/position track bandwidth while the low stiffness will increase the transparency and improve system sturdiness. According to the research results about the SEA stiffness selection from [7], the relative low stiffness as well as the angle deflection encoder based for measuring torque are selected by considering physical sturdiness enhancement and system high integration property.

Finally as a result, three identical medium-sized SEAs [32] are used, consisting of Kollmorgen TBMS-6025 motors and 80:1 CPL-20 Harmonic Drive gearboxes, in series with custom planar flexure elements with the stiffness of approx. 5800 Nm/rad. The units can provide peak torque up to 127 Nm and provide torque sensing through deflection measurements of the elastic elements. They feature an integrated design

with power and EtherCAT electronics mounted directly on the actuator.

2.1.2 Energy Storage Branch (ESB) Actuation

In the aforementioned Asymmetrical Compliant Actuation (ACA) concept, Energy Storage Branch (ESB) functions as the significant branch for enhancing the joint back-drive ability by utilizing the compliant element, thus the energy efficiency and explosive motion ability could be improved. As we discussed in previous Thesis Contribution section, the Energy Storage Branch (ESB) ought to possess active elastic element pretension tuning ability by secondary motor embedded. This is also the major novel point of such ESB unit design compared to other passive parallel elastic element functioned as gravity compensators [49].

For the specific design implementation, the main requirements are as following, where we provide approximate target values for the leg knee unit, which is the most demanding joint since the desired high torque and force,

- Large maximum storage capacity, order of 100 J.
- Sufficient torque capacity, up to approximate 100 Nm.
- High torque/weight and energy storage/weight ratio.
- Rapid reconfiguration, ESB units must be mountable and dismountable within 5 minutes.

Several implementations were considered to achieve the desired properties, including metal and pneumatic springs, where the latter was quickly discarded due to higher difficulty for reliable implementation and the need of a secondary (pneumatic) power supply unit.

Three options were considered in more detail: rubber-type elastic cords enclosed in nylon sheaths [36, 37], linear metal extension springs [18, 50], and metal torsion springs [51]. However, due to the requirements of biarticulated configurations and size and weight requirements, as well as integration complexity, torsional springs turned

out to be unsuitable. Linear metal springs appear to be a viable option, however in terms of energy storage capacity to weight ratio they are vastly outperformed by rubber-type elastic materials. Hence, as in the previous prototype [37], the final design is based on rubber-type elastic cords, which we shall refer to as **bungees** for simplicity.

2.2 3-DoF Legged Robot (eLeg) Design

In previous section, we mainly introduced the implementation of Asymmetrical Compliant Actuation (ACA) concept to single joint, while in this section we will present the extension of ACA concept to multi-joint actuation. To be more specific, the implementation of ACA concept on multi-joint anthropomorphic robotic leg will be introduced through detail design of the desired hardware platform (eLeg) in terms of the following two aspects,

- Design of leg body, functioning as the mechanical skeleton together with Series Elastic Actuator (SEA) as Powerful Branch (PB) in Asymmetrical Compliant Actuation (ACA) concept.

- Design of Energy Storage Branch (ESB) units, functioning as another significant parallel branch in Asymmetrical Compliant Actuation (ACA) concept with elastic element (possess pretension active tuning ability) for energy storage, where ESB units can be configured into different actuation configurations (mono and biarticulation) for further optimizing and improving energy efficiency.

By considering the reduction of desired hardware development complexity and cost, while meanwhile maintain the functionality for verifying the design effectiveness of energy efficiency, a hardware platform named eLeg was developed as shown in Fig. 2-3, which is an anthropomorphic robotic leg with 3 DoFs in pitch saggital plane and the concept of Asymmetrical Compliant Actuation (ACA) will be implemented on knee and ankle joint. The corresponding Energy Storage Branch (ESB) units can

be configured into different actuation configurations physically based on this hardware platform.

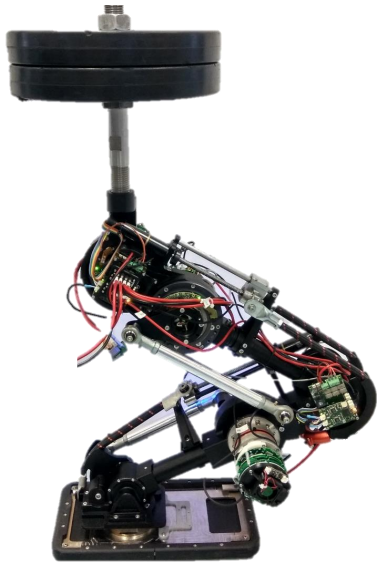

Figure 2-3: Desired hardware platform eLeg, squatting in monoarticulated configuration with 23 kg load.

2.2.1 eLeg Robot Body Design and Development

The design of eLeg prototype is inspired by the human biological counterpart [52] and existing humanoid robot designs. Based on their parameters, target specifications for dimensions and weight were set. The design features three actuated degrees of freedom: ankle, knee and hip. We opted for a leg size slightly under average human size, and aimed for mass not exceeding the human limb and with similar mass distribution; resulting in a anthropomorphic design corresponding to a ≈ 1.50 m humanoid.

The dimensions and major components for the prototype in monoarticulated configuration are shown in Fig. 2-4, and corresponding design parameters and mass distribution are summarized in Table 2.1. The total mass for the SEA-only, monoarticulated and biarticulated actuation configurations are 9.3 kg, 10.9 kg, and 10.9 kg respectively, with the mass of both leg segments (thigh and shank) smaller than that of the human limb in the biarticulated case (Table 2.1). To minimise the leg's inertia with respect to the hip joint, the ankle and knee actuators are placed high on the leg

segments, and drive the joints through parallelogram four-bar linkages. The utilized actuators are three identical medium-sized SEAs [47], for which details are also shown in Table 2.1.

The required range of motion for eLeg joints are highly dependent on the desired motions. To be more precise, two configurations, namely a deep squat posture requiring high ankle and knee flexion [53, 54], and jumping posture in which the ankle is highly extended [54], need to be realized. Hence, the knee joint is designed to achieve a range of motion of $[0°, 130°]$, and the ankle joint is designed to reach a bi-directional working range of $[-69°, 54°]$, which satisfy these requirements. The trunk joint is capable of rotating in a large range of $[-150°, 150°]$ to allow balancing the trunk in any leg posture, and control the center of pressure.

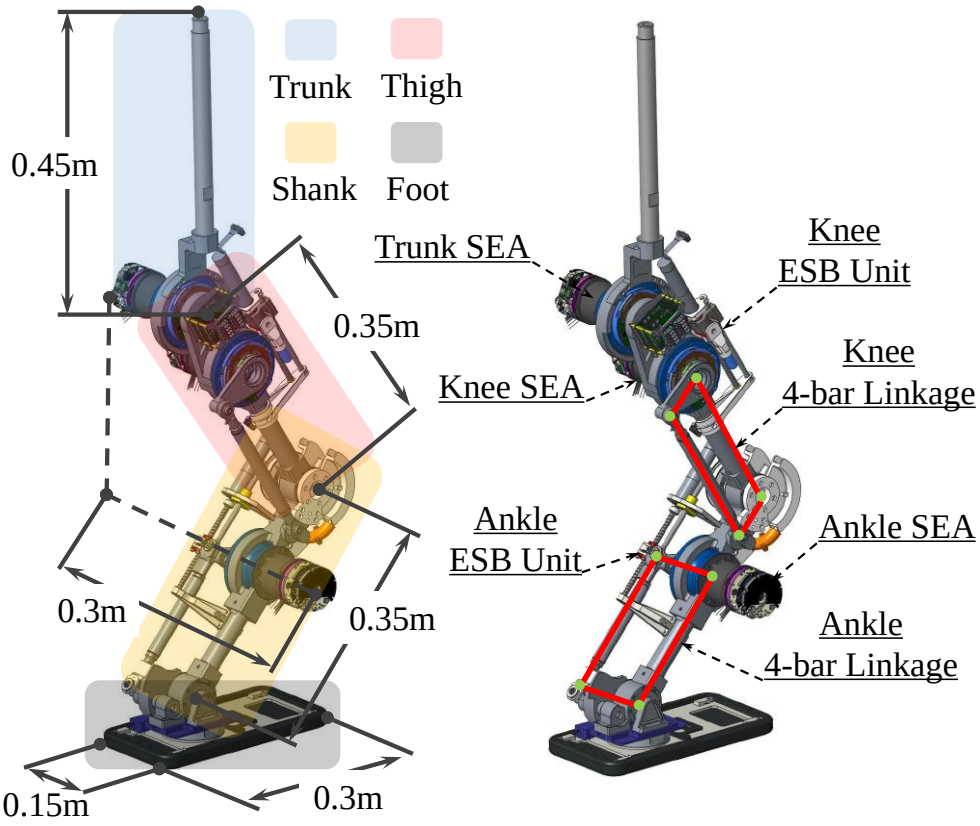

Figure 2-4: The eLeg prototype in monoarticulated configuration, showing overall dimensions and major components.

Table 2.1: The eLeg design and actuation parameters for each actuation configuration.

eLeg Dimensions and Mass Distribution				
	Trunk[(1)]	Thigh	Shank	Foot
Dimensions	0.45 m	0.35 m	0.35 m	$0.28 \times 0.15 \times 0.06$ m
Mass: SEA	1.86 kg, 20.0%	2.79 kg, 30.0%	2.95 kg, 31.7%	1.70 kg, 18.3%
Mass: Monoarticulated	1.86 kg, 17.0%	3.58 kg, 32.8%	3.78 kg, 34.6%	1.70 kg, 15.6%
Mass: Biarticulated	1.86 kg, 17.1%	4.22 kg, 38.9%	3.07 kg, 28.3%	1.70 kg, 15.7%
Mass: Human limb[52]:	n.a.	7.88 kg	3.38 kg	1.13 kg

Joint Actuation SEAs[47, 48] Configuration				
Motor Type	Gearbox Type	Gear Ratio	Stiffness	Peak Torque
Kollmorgen TBMS-6025	Harmonic Drive CPL-20	80 : 1	5800 Nm/rad	127 Nm

Torque Sensing	Position Sensing
Angle deflection based, 69 mNm resolution	Renishaw AksIM 19 bit absolute position encoder

Four-bar Linkage Configuration	
Knee Joint	Ankle Joint
Knee Joint: 0.075 m, 0.075 m, 0.25 m, 0.25 m, Parallelogram Linkage	Ankle Joint: 0.045 m, 0.045 m, 0.215 m, 0.215 m, Parallelogram Linkage

Joint Working Range[(2)]		
Trunk Joint:	Knee Joint:	Ankle Joint:
$[-150°, 150°]$	$[0°, 130°]$	$[-69°, 54°]$

Note: (1) The trunk mass does not include the 23 kg weights load, which will supposed to be mounted on it to simulate the weight of a full humanoid robot; (2) The counter-clockwise rotation direction in Fig. 2-4 is defined as positive joint rotation, while the clockwise rotation direction is defined as negative joint rotation.

2.2.1.1 Interchangeable ESB Units Design

Three actuation configurations were considered, to show both the potential of our proposed actuation concept as well as investigate the effectiveness of biarticulated actuation configurations. Shown in Fig. 2-5, the three concepts are as following:

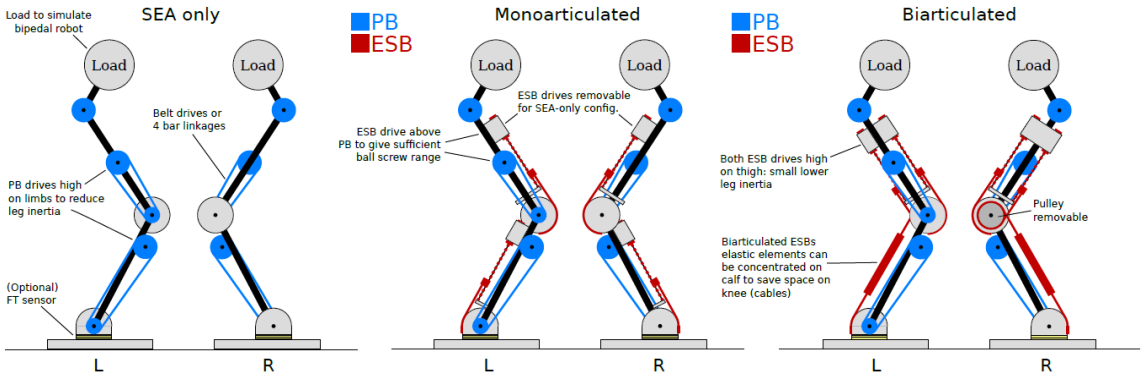

Figure 2-5: Concept drawings of the 3-DoF leg in SEA-only, monoarticulated, and biarticulated actuation configurations. Series-elastic Power Branch (PB) actuation is shown in blue, and the parallel Energy Storage Branches (ESBs) are shown in red.

- **SEA-only**: In the first configuration all joints are driven exclusively by SEAs, to serve as a baseline actuation arrangement which is common in most state-of-the-art articulated robot designs.

- **Monoarticulated**: In the second configuration the ankle and knee joints are augmented with the secondary parallel actuation branch.

- **Biarticulated**: The third configuration again features two joints with parallel actuation branches, however in this case one of the Energy Storage Branches is biarticulated: The ESB for the ankle spans the knee joint and is driven by a motor on the back of the thigh. This tendon spanning both the knee and ankle joints is functionally similar to the gastrocnemius muscle in humans, which allows power transfer from the knee to the ankle joint upon extension.

Since the leg was designed to permit the implementation of three distinct actuation configurations as aforementioned, to show both the potential of our proposed

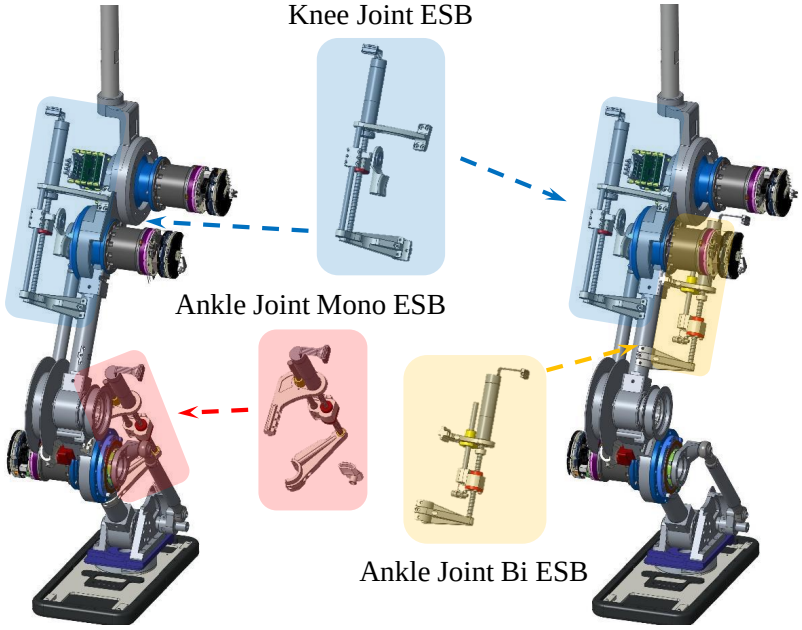

Figure 2-6: Reconfigurable actuation arrangements: monoarticulated (left) and biarticulated (right) configurations.

actuation concept as well as investigate the effectiveness of biarticulated actuation configurations, a significant demand is the switching of monoarticulated or biarticulated from SEA-only configuration ought to be rapid and interchangeable.

As a result, the leg body and ESB units are designed in such way shown as Fig. 2-6, which shows the placement of ESB units for the mono- and biarticulated configurations (SEA-only configuration not shown as it has no ESBs). The elastic elements are not shown. Each ESB unit requires only two connectors and roughly eight screws to mount. In the following section we will elaborate on the detailed design procedure for the ESB units and selection of their parameters.

2.2.2 ESB Unit Design and Implementation

In previous section, the design of eLeg prototype is detailed presented in terms of legged body development and its rapid and interchangeable actuation configuration design, where the Energy Storage Branch (ESB) units can be conveniently assigned and configured into different actuation arrangements for energy efficiency enhancement, and thus its corresponding energy efficiency comparison and analysis could be

easily proceeded with experimental support. As a matter of fact, the design and development of Energy Storage Branch (ESB) units are significant for eLeg robot to achieve energy efficiency and high strength motion ability. In Section 2.1.2, we have already introduced the design requirement of this particular unit as well as its brief design scheme, to be specific, the linear rubber-type elastic bungee functioned as energy storage element with active pretension tuning ability. In this section, we will detail introduce the design and implementation of this specific ESB unit in terms of the following three important aspects:

- Selection of elastic bungee, functioned as energy storage element.
- Design of linear pretension tuning actuation and mechanism.
- Design of ball screw bearing nut with force sensing.

2.2.2.1 Bungee Selection

The design optimisation procedure [38] used to select elastic element (bungee) stiffness, pulley radii and default pretension position of the ESB units assumes a linear stiffness profile of the elastic elements, with zero rest length. However, the rubber-type materials used typically have an S-shaped elongation–force curve, in which force increases rapidly for the first 10-20% (of rest length) of elongation, then flattens out, to increase rapidly again at roughly 80%. Two parameters are dominant in selecting a cord to approximate a desired linear stiffness: the rest length l_r and diameter d. Considering the nonlinearity of the stiffness profile, we determine the linear stiffness k_l of the bungee by linearisation of the aforementioned S-shaped curve from datasheets at 35% elongation, resulting in a good overall fit. The linear stiffness is then given by

$$k_l = \frac{f_p(d)}{0.35\, l_r}, \tag{2.1}$$

where f_p is the extension force at 35% elongation and is dependent on the bungee diameter d.

Table 2.2: ESB units bungee parameter selection, for both monoarticulated (*mono*) and biarticulated (*bi*) actuation configurations. Required elongation and optimal stiffness follow from the design parameter optimisation procedure[(1)] followed by extensive simulation.

Bungee Parameters and Computed Parameters								
Bungee[(2)]	Request Elongation l_e [cm]	Optimised Stiffness k_d [kN/m]	Mininum Length l_m [cm]	Available Length l_a [cm]	Chosen Rest Length l_r [cm]	Chosen Diameter d [mm]	Chosen Stiffness k_l [kN/m]	Stiffness error $(k_l - k_d)/k_d$
Ankle (mono)	7.7	5.4	9.6	12.0	12.0	12	5.8	8.0%
Ankle (bi)	1.9	29.2	2.4	43.3	6.5	18	29.0	-0.6%
Knee (mono)	25.0	8.3	31.3	48.0	45.5	13	7.8	-6.2%
Knee (bi)	29.0	8.3	36.3	48.0	45.5	13	7.8	-6.2%
Bungee Extension Force f_p according to diameters (occurred at 35% elongation)								
Diameter [mm]	10	11	12	13	14	15	18	20
Force [N]	140	180	245	310	420	530	660	790

Note: (1) Specific procedure can be refer from [38]; (2) The bungees are selected from the manufacturer: *Sandow Technic* and in type: *Inserted Tubes Series*.

Besides the desired linear stiffness, there are two length requirements. Firstly, the element should fit within the available space l_a along the leg segment. Secondly, the amount of elongation required should not exceed the allowed elongation of the material, chosen to be 80%. These requirements are summarised as:

$$l_m \leq l_r \leq l_a, \quad \text{where} \quad l_m = \frac{l_e}{0.8}, \tag{2.2}$$

the value of l_e is derived from extensive simulation of the prototype, and l_m denotes the minimum bungee rest length. Table 2.2 lists the previously mentioned ESB elastic element parameters for all three actuation configurations, which result from the design parameter optimisation procedure from [38] followed by extensive simulation. Following selection of rest lengths and diameters, the achieved (linearised) stiffness, their desired values, and error margins are given in Table 2.2, which are within 8%. Finally, the last rows of Table 2.2 list the bungee cord properties as provided by the manufacturer.

2.2.2.2 Actuation and Mechanism Design

The elastic elements must be linearly driven to adjust their pretension. A rotational motor with gearbox combined with a ball screw transmission mechanism are chosen to provide pretension regulation, due to their compact integration, small weight, and large linear motion range. In the following design procedure, we will provide numerical examples for the knee joint ESB, as it is the highest loaded joint in the desired eleg.

Starting with the ball screw, the pitch p is a crucial parameter that is selected as a trade-off between dynamic loading capacity and additional gearbox ratio required to amplify the motor torque prior to the ball screw transmission. The ball screw's permitted dynamic load f_d should be chosen larger than the maximum experienced dynamic force f_d^{max} according to the maximum bungee extension force in Table 2.2, written as:

$$f_d \geq f_d^{max}\, S = \frac{l_e}{2}\, k_l\, S, \tag{2.3}$$

where the values for l_e and k_l are those of the most demanding biarticulated config-

uration, and the safety factor S is set as 1.5. l_e is divided by two due to the fact the bungee is wrapped around at the knee and the other side attaches to the other side of the ball screw nut forming a dual bungee elastic element. The resulting minimum dynamic load is obtained as $f_d \geq 1700\,\mathrm{N}$. Conversely, the generated linear force f_l transmitted through the ball screw and gearbox should not exceed the motor's continuous torque capability, which favours larger total gear ratios. In fact, increasing the transmission ratio reduces the loading on the motor, improving energy efficiency at the cost of reduced adjustment velocity. The maximum continuously generated linear force f_l^{max} and linear velocity v_l are computed as

$$f_l^{max} = I_{max}\, k_\tau\, \eta_m\, \frac{2\pi\, G}{p}, \tag{2.4}$$

$$v_l = V_n\, k_\tau^{-1}\, \frac{p}{2\pi\, G}, \tag{2.5}$$

where k_τ denotes the torque constant of the motor, I_{max} and V_n denote the maximum continuous current and operating voltage of the motor, G denotes the gearbox transmission ratio, and η_m denotes the combined gearbox and ball screw efficiency, set as 0.8 by considering the low operating speeds at high loading.

The resulting maximum generated linear force f_l^{max} and linear velocity v_l are shown in Fig. 2-7 as a function of gearbox ratio G for each of the three ball screw models. From the force requirement derived from the required elongation and stiffness, the maximum generated force f_l^{max} is $\approx 1130\,\mathrm{N}$, shown by the dashed line in Fig. 2-7. While all three ball screws can satisfy this requirement at different gearbox ratios, consider that increased pitch requires a larger gear ratio G which further reduces the overall drivetrain's efficiency. Hence, the final choice of ball screw and gearbox is obtained as small pitch p and small gear ratio G.

Based on this analysis, we finally selected the PRM0805 ball screw with 5 mm pitch and gear ratio $G = 53$ for the knee ESB, indicated by the black dots in Fig. 2-7. With this choice, the maximum linear force is 2595.1 N and linear velocity is 0.05 m/s, which allows to traverse the entire pretension working range in 2.5 seconds, which is

Table 2.3: ESB unit drive train mechanism parameters.

Ball Screw								
Thomson Miniature Ball Screw Series selection[1]								
Type	PRM0401	PRM0504	PRM0601	PRM0606	PRM0801	PRM0805[2]	PRM0808	PRM0812
Diameter d_b, [mm]	4	5	6	6	8	8	8	8
Pitch p [mm]	1	4	1	6	1	5	8	12
Max. dynamic Load f_d [N]	790	720	1200	1450	780	1850	3800	4000

Motor		
Maxon EC 22 Brushless 386675[3]		
Torque Constant	Maximum Continuous Current	Nominal Voltage
k_τ [mNm/A]	I_{max} [A]	V_n [V]
14.2	3.43	48

Gearhead	
Maxon Planetary GP 22 HP	
Knee ESB Units	Ankle ESB Units
53:1 (Mono & bi)	29:1 (Mono & bi)

Note: (1) Considering compact and lightweight design, ball screws up to 8 mm diameter were considered; (2) Finally chosen model; (3) For standardization, the same type of motor is selected for all ESB units.

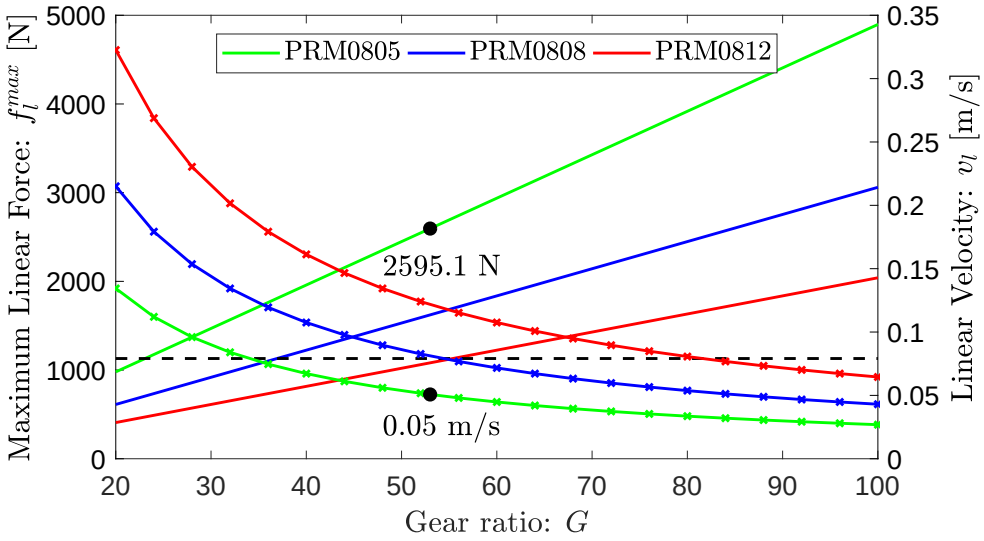

Figure 2-7: Maximum linear generated force f_l^{max} (solid lines) and linear velocity v_l (curves with crosses) for three ball screw types as a function of gearbox transmission ratio G.

sufficient for the parallel branches as fast adjustment is less efficient and not required for accurate joint torque control due to the main series-elastic drives. For the ankle ESB, loading is much smaller than the knee ESB under both mono- and biarticulated configuration. Thus, the same ball screw type and gearbox with lower gear ratio were selected as shown in Table 2.3, allowing for some interchange of components as well if needed.

2.2.2.3 Force-sensing Ball Screw Nut

The installation of the ESB units incorporate two mounting points and a single linear guide to avoid nut rotation as shown in Fig. 2-8(a). Each unit was augmented with an instrumented ball screw nut, with steel cantilever beams and strain gauges to obtain accurate measurements of the linear force applied by the bungees, as well as provide mounting points for the bungee hooks. Such direct bungee force-sensing ability is vital due to the bungee S-shaped nonlinearity property as we mentioned in Section 2.2.2.1, where achieving the linear force from the multiply of bungee stiffness and elongation is not accurate. For the knee joint, the beams were designed to each support 750 N of force. Fig. 2-8(b) shows the finite-element analysis (FEA) results, where the stress

was controlled to be under the yield stress of 17-4PH steel and displacement and strain were controlled to appropriate values to ensure force measuring sensitivity. The strain gauge surfaces were designed to have nearly homogeneous strain. The design achieves excellent force sensing capability, with high linearity, as shown in Fig. 2-8(c).

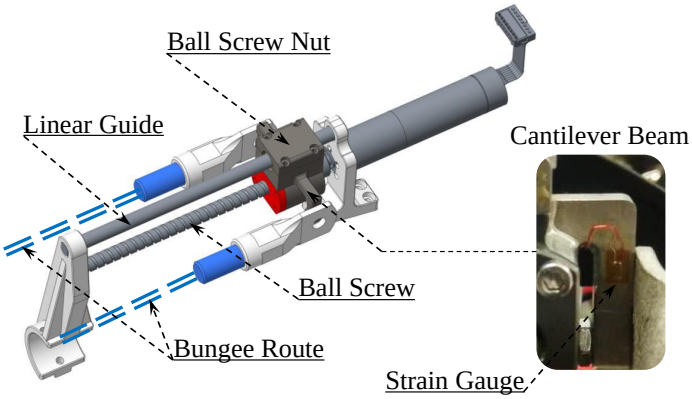

(a) ESB unit components and strain gauge attachment

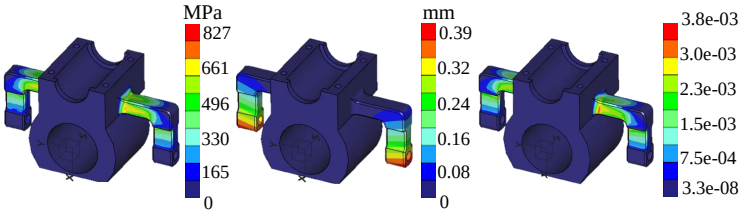

(b) FEA results in stress, displacement and strain

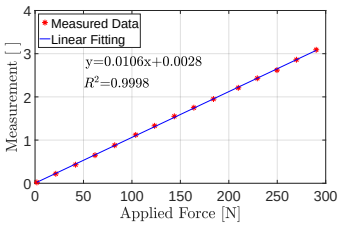

(c) Force-sensing linearity

Figure 2-8: eLeg Knee joint ESB unit development overview and corresponding ball screw nut strain gauge force-sensing presentation.

2.3 Experimental Validation and Results

In this section we will present the corresponding experimental results, which will effectively demonstrate the potential and effectiveness of the eLeg actuation principles and hardware development in terms of energy efficiency. An elliptical squatting motion was performed on all three actuation configurations (SEA-only, mono and biarticulation), consisting of an elliptical Cartesian trajectory of the hip, defined w.r.t. the position of the ankle joint. The joint references were calculated from inverse kinematics, with the trunk link kept vertical. In these preliminary experiments for verifying

the energy efficiency, the main actuators were used in position control mode, with the ESB pretension positions held constant. The hip reference and experimental trajectories are shown in Fig. 2-9, and tracking errors, torque contributions and linear tendons forces are shown from Fig. 2-10, Fig. 2-11 and Fig. 2-12 respectively.

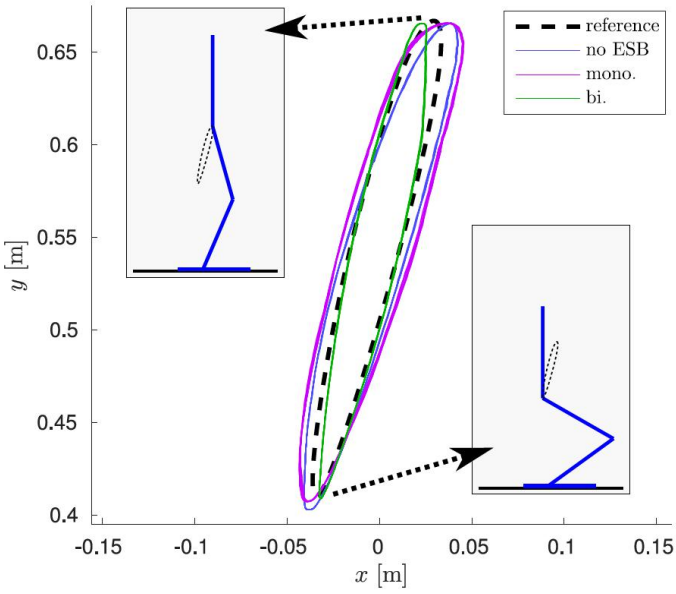

Figure 2-9: Cartesian hip reference (w.r.t. ankle joint) and resulting trajectories for all three configurations, following from the joint tracking performance shown in Fig. 2-10(a) to Fig. 2-10(f)

As can be observed from Fig. 2-10(a) to Fig. 2-10(f), bias in the joint tracking errors due to gravitational loading is significantly reduced in the monoarticulated and biarticulated cases, indicating that the actuators spend less power cancelling gravitational torques, and improving tracking accuracy for this simple position control. The differences in tracking accuracy result in slightly different pose of the leg over time, as indicated by the Cartesian trajectory of the hip, shown in Fig. 2-9. This in turn changes the loading of each joint and the elongation of the elastic elements, as can be observed from Fig. 2-11(a) to Fig. 2-11(i). Furthermore, the current required by the ESB motors to hold the pretension positions of the parallel elements was verified negligible compared to the reduction in power requirements from the SEAs.

The torque measurement results demonstrate a number of key advantages of the parallel actuation design:

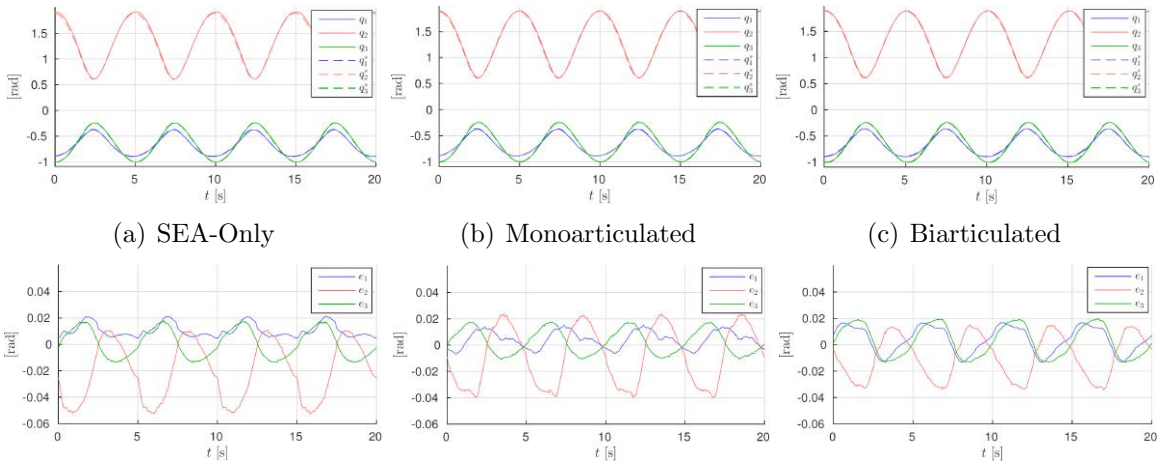

(a) SEA-Only (b) Monoarticulated (c) Biarticulated

(d) SEA-Only (e) Monoarticulated (f) Biarticulated

Figure 2-10: Experimental results for joint position tracking (first row) and its corresponding tracking error (second row) under three articulation actuation configurations. q_1, q_2 and q_3 are the measured angle position trajectory for ankle, knee and hip joint respectively, q^* is the desired angle position trajectory.

- In both cases with Energy Storage Branch units (ESBs), the ESBs significantly reduce the RMS SEA (Powerful Branch) torques for both the ankle and knee joints, shown as dashed lines from Fig. 2-11(a) to Fig. 2-11(i). This results in significantly lower power consumption, which numerical results are presented in Table 2.4, together with the electrical power consumption, calculated using actuator models. We consider only positive (i.e. delivered) electrical power, as negative power is lost as there is no recuperation mechanism. The monoarticulated configuration obtains a **53%** improvement in power consumption, and the biarticulated configuration obtains a **60%** improvement.

- The biarticulated tendon exerts torque on the ankle joint (Fig. 2-11(c)) at more appropriate timing than the monoarticulated ankle tendon (Fig. 2-11(b)), resulting in a decrease in torque required by the SEA, whereas in the monoarticulated configuration it effectively has to 'work against' the ESB elastic element for part of the motion. This is due to the extension of the biarticulated element being a function of both ankle and knee angles, in the same way their configuration changes the ankle loading.

- In this instance, the biarticulated tendon has a counterproductive effect on the required knee SEA torques (Fig. 2-11(f)), as the pretension of the monoarticulated knee tendon was not increased sufficiently to counteract the biarticulated tendon torque, which flexes the leg. This highlights the need for an appropriate control strategy that adjusts the pretension of the parallel tendons.

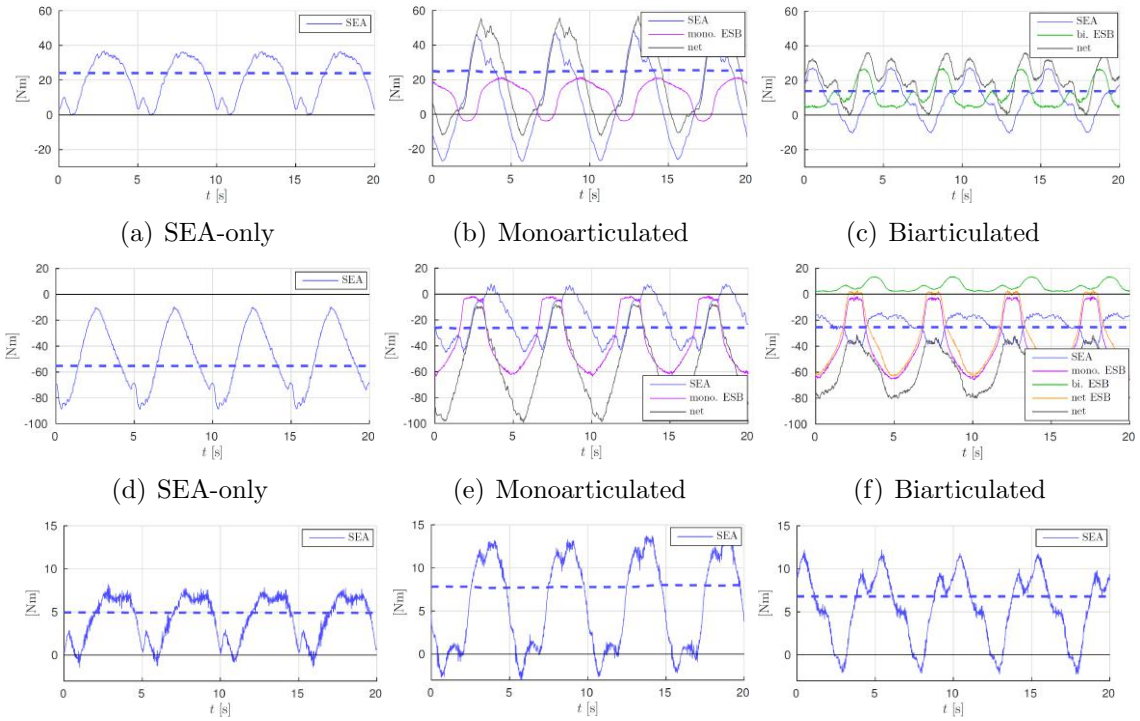

(a) SEA-only (b) Monoarticulated (c) Biarticulated

(d) SEA-only (e) Monoarticulated (f) Biarticulated

(g) SEA-only (h) Monoarticulated (i) Biarticulated

Figure 2-11: Experimental results for the torque generated in corresponding SEA-only, monoarticulated and biarticulated configurations from the ankle joint (first row), knee joint (second row) and trunk joint (third row) respectively. The dashed lines denote RMS SEA torques, over the motion period of 5.0 s (shown numerically in Table 2.4.

These results are in line with expectations based on a simulation study of a 2-DoF leg presented in [38]. From Fig. 2-12 we can be aware of the linear force generated from knee tendon can reach more than 1100 N, it requires the knee ESB unit to possess adequate high strength and physical sturdiness property to realize the active pretension tuning of the bungee during eLeg deep squatting motion, which will definitely further benefit the energy efficiency enhancement. Considering about the paragraph

Table 2.4: RMS and peak Series Elastic Actuator (SEA) torques as well as electrical power consumption over the motion period of 5.0 s. Note we consider only positive (i.e. delivered) electrical power, as there is no recuperation.

	SEA-only	Monoarticulation	Biarticulation
Ankle [Nm RMS]	24.0	24.8	13.7 ↓
Knee [Nm RMS]	55.3	25.8 ↓	25.4 ↓
Hip [Nm RMS]	4.9	7.7	6.8
Ankle [Nm peak]	36	48	27 ↓
Knee [Nm peak]	89	45 ↓	40 ↓
Hip [Nm peak]	8	14	12
Ankle [W]	2.7	1.1	2.6
Knee [W]	30.0	14.2 ↓	9.5 ↓
Hip [W]	0.4	0.1	1.1
Total electrical power [W]	33.1	15.4	13.2
Improvement	-	53%	60%

arrangement of this thesis, we will detail present this further energy efficiency enhancement brought by the high strength ESB unit pretension tuning property in the following Section 3.2.

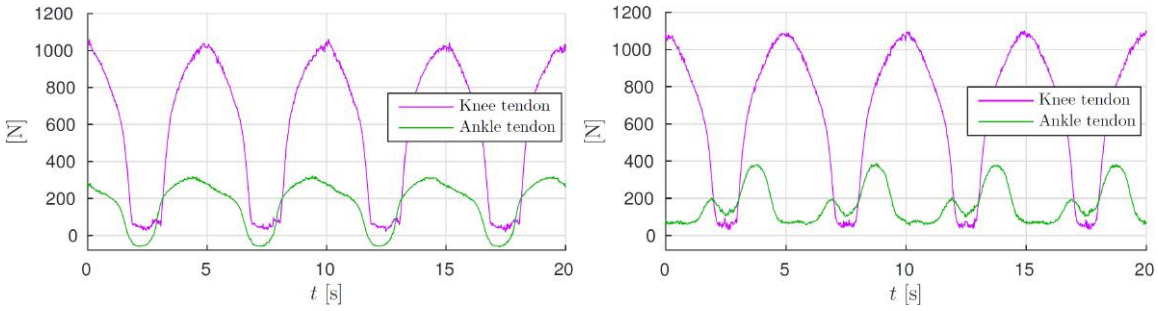

(a) Monoarticulated (b) Biarticulated

Figure 2-12: Experimental results for linear tendon force from knee and ankle joint ESB unit in mono and biarticulated configurations.

2.4 Summary

In this section, we firstly introduced the design concept of utilizing Asymmetrical Compliant Actuation (ACA) on legged robots for enhancing energy efficiency, where the Powerful Branch (PB) and Energy Storage Branch (ESB) consist of it. The Series Elastic Actuators (SEAs) from *iit Tree Robotics* were implemented as Powerful Branch (PB), while Energy Storage Branch (ESB) contains linear elastic bungee and its corresponding pretension tuning actuation and mechanism, functioning as the significant and novelty point for further energy storage and efficiency enhancement.

Secondly, three important actuation configurations in terms of SEA-only, monoarticulation and biarticulation are introduced for extending single joint ACA actuation to multi joints. The eLeg body itself actually functions as SEA-only configuration, which means only the Powerful Branch (PB) consist of SEAs contributes to the eLeg motion ability. Meanwhile the eLeg body ought to possess the actuation reconfigurable potential in terms of switching rapidly between monoarticulation and biarticulation, where the novelty of bio-inspired biarticulation relies on the ESB unit for ankle joint is distributed on the leg thigh part and coupled with the motion of knee joint. This particular biarticulation is inspired from the biological human leg and we are motivated to verify its performance in energy efficiency compared to the traditional monoarticulation.

Thirdly, we presented the mechanical design and development details of eLeg hardware platform, which is a 3-DoF legged robot in pitch saggital plane based on the aforementioned actuation concepts. Since the Energy Storage Branch (ESB) unit directly decides the energy storage and efficiency property, hence we detailed present the mechanical design method and implementation in terms of ESB unit bungee selection, actuation and mechanism design as well as force-sensing ball screw nut design. To be more specific, the stiffness of the bungee applied in ESB units ought to be selected based on the design parameter optimisation procedure [38] followed by extensive simulation, the actuation and mechanism for tuning the pretension is selected from the trade-off between the maximum linear tuning load, velocity as well

as the compact integration demand, the force-sensing ball screw nut design is for achieving the accurate force feedback due to the negative S-shaped nonlinearity of selected bungees.

Finally, in order to preliminary verify the aforementioned design and concept effectiveness, we generated the elliptical trajectory with 23 kg weight distributed at eLeg trunk joint so that the leg robot can realize a cyclic deep squat motion while maintaining the position for pretension tuning. Corresponding results regard to joint position tracking ability, joint torque and linear tendon force from the three actuation configurations (SEA-only, monoarticulation and biarticulation) are plotted, we achieved a significant energy efficiency enhancement by 53% (monoarticulation) and 60% (biarticulation) compared to SEA-only configuration, which directly verifies the design effectiveness in terms of ACA concept utilization and also the bio-inspired biarticulation actuation adoption.

Chapter 3

High Strength Grasping and Motion Design

In previous section, we have discussed and introduced the enhanced physical interactive performance robot bodies design on legged robots energy efficiency actuation and in this section we will present another significant aspect of high strength performance in robotic physical interactive.

High strength performance possesses importance for deciding whether robots have the ability of undertaking high load physical work or achieving high explosive motion, which will directly affect the robot functionalities in real physical application scenario, such as releasing humankind from heavy construction work or dangerous disaster response missions. Nowadays, robots from the lab are still too weak to enter into the real application or physical world, especially the legged robots based on electro magnet principle, the output torque density from the existing actuators sharply limits the robots high strength motion ability. Thus more work have to be focused on designing specific robotic actuation and bodies that can enhance the strength ability.

As a matter of fact, my PhD work will specifically focus on the high strength actuation and mechanism design in robotics hands and legged robots actuators, even though the fact that various of other robotics bodies still matter the whole robots strength performance. To be more specific, the robotic hand grasping strength will highly affect the manipulation performance for practical daily missions like triggering

a drill, knocking a nail or simply robust objects grasping, also the electro magnetic principle actuator strength will determine the legged robots ability for realizing explosive motion, such as jumping, deep squatting or even parkour.

The following content in this section will present the design method and development details for achieving high strength performance target in terms of robotics hands and legged robots actuation. Meanwhile series of experiments and its corresponding results will also be demonstrated to verify the design effectiveness.

3.1 Robotic Hands Strength Grasping Design

It is well known that currently it is difficult to find a general design method for robotic hands to mimic the excellent performance of humankind hands, thus enhancing the robotic hands grasping strength is actually the function priority preference, with no doubt it will sacrifice other performances such as dexterous property to some extent, since powerful and dexterous grasping are in common the performance trade-off among robotic hands design. Following the aforementioned design philosophy, we selected the following three design methods for achieving the target of high strength priority grasping design,

- Under actuation principle.
- Modular finger design concept.
- High strength priority finger distribution and DoA assignment.

Aforementioned methods will all be detail introduced in this section. As a matter of fact, we developed two generations of robotic hands, namely HERI Hand and HERI II Hand as shown in Fig. 3-1, which are both under actuated, HERI Hand is a three-finger hand while the finger quantity and distribution of HERI II Hand can be reconfigurable. Actually HERI II Hand is designed and modified on the basis of HERI Hand, which desired to be mounted on Centauro robot [47] undertaking the manipulation tasks. The design method and development details of these both hands

will be as well introduced in this section. Meanwhile the motivation for the iteration between two hands generation and the physical integration property for HERI II Hand with Centauro will also be stated. Last but not least, series of experiments for verifying the design effectiveness, especially the high strength enhancement performance of robotic hands (HERI and HERI II Hand) and legged robots (eLeg as shown in Fig. 2-3), will be finally presented.

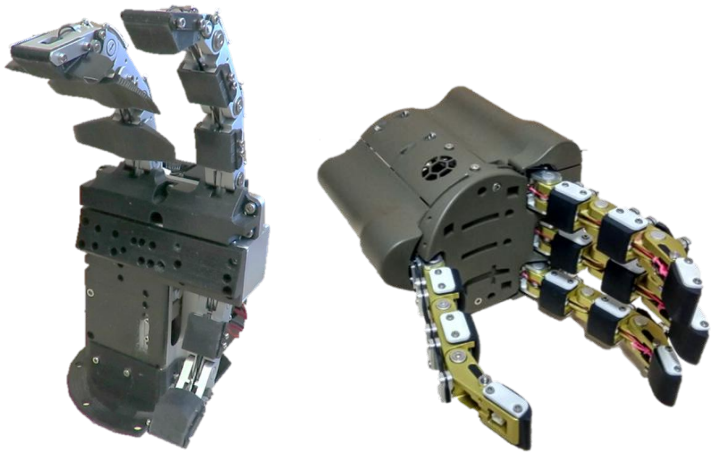

(a) HERI Hand (b) HERI II Hand

Figure 3-1: Hardware development of (a) HERI Hand and (b) HERI II Hand in four-finger configuration.

3.1.1 Under Actuated Finger Design

It is well known that in the field of robotic hands design, under actuation normally possesses higher strength grasping performance than fully actuation under the consideration of low cost, system simplify, compact integration and redundancy reduction. In this section, we will focus on introducing the specific design details of under actuated finger, where HERI and HERI II Hand both utilized such principle and the only modification relies on the fingers of HERI II Hand are reduced in length (compared with HERI Hand) for considering the grasping priority for relative tiny objects. For a more introductory statement, following content regard to the under actuated finger will be based on the fingers of HERI Hand.

3.1.1.1 Finger Phalanx Design

Similarly as human fingers, we consider the design of adopting three phalanxes for normal fingers (index finger, middle finger, ring finger and pinky fingers) whereas for the thumb only two are utilized. With the consideration of reducing fabrication cost and maintenance time, interchangeable and simplification are adopted as two essential principles for the phalanx design. As a result, there are only two types of phalanx modules for all fingers, named Body Phalanx and Tip Phalanx, as shown in Fig. 3-2(a) and Fig. 3-2(b).

(a) Body Phalanx (b) Tip phalanx

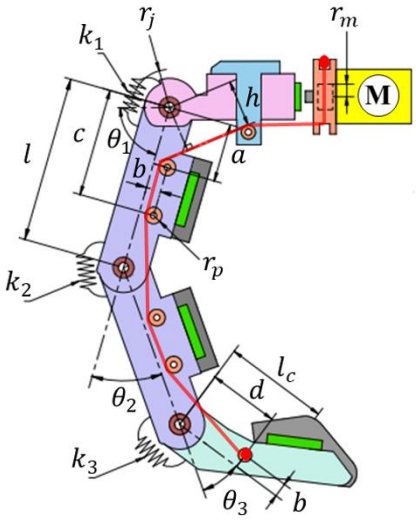

(c) Finger phalanx geometric parameters

Figure 3-2: HERI Hand under actuated finger, consists of Body Phalanx and Tip Phalanx, as well as its corresponding geometric parameters.

Therefore, totally five Body Phalanxes and three Tip Phalanxes are used for constructing the three fingers of HERI hand and their dimensions are decided based on approximately the same size of a normal adult human hand, taking into account

the workspace for grasping common objects, utilizing human tools as well as the size of the robot that the hand will be mounted on.

Since the classic *Da Vinci's Mechanism* [55, p. 55] is adopted as the transmission approach for the under-actuated finger flexion motion, the same pulley layout plan and tendon route are also followed for each phalanx as shown in Fig. 3-2(c). Note that, the torque distribution for each joint is realized by the springs/rubbers with proper stiffness placed at the corresponding joints, despite the fact that the pulley layouts are the same for every body phalanx. Finally, each body and tip phalanx are equipped with the tactile sensor placed in the middle phalanx position. As an example, the detailed geometry dimensions of the third finger are depicted in Fig. 3-2(c) and the values are shown in Table 3.1.

Table 3.1: HERI Hand finger phalanx geometry parameters.

	l	l_c	a	b	c	d	r_p	r_j	r_m
Body phalanx [mm]	40	-	14	3.5	26	-	1.5	9	3.5
Tip phalanx [mm]	-	28	-		-	20	-		

3.1.1.2 Kinematic Analysis and Actuator Selection

The strength of the under-actuated finger in terms of ability to exert a certain grasping force is closely related to the capabilities of its corresponding actuator. It is therefore essential to select the specification of the motor carefully to ensure high strength force tolerance under the severest designed circumstance. In this section, the actuation specification selection process of DoA_1, which is intended for high strength grasping, is detailed as an example. Similar approach is taken for selecting the actuator driving the flexion motion of index and thumb (DoA_2) to satisfy the design requirements and meantime follow the design principles defined in Section 3.1.1.1.

Fig. 3-3 presents the severest grasping scenario in which only DoA_1 is required to keep grasping the object. This scenario is designed with HERI Hand holding a cylindrical object horizontally to the gravity. Therefore only the friction force is utilized for holding the object, which means that there is no extra contact points

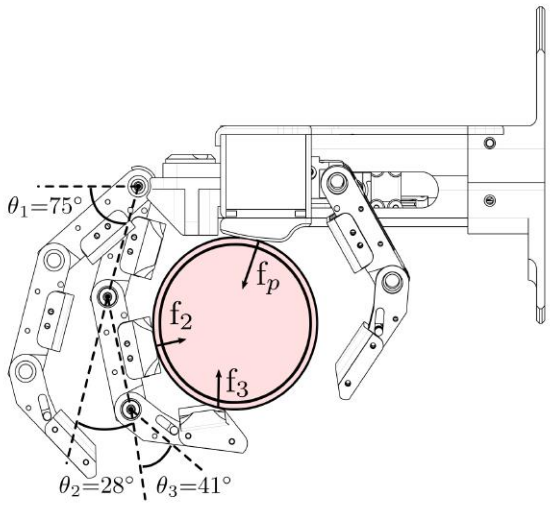

Figure 3-3: Top view for HERI Hand grasping desired object in vertical as severest grasping scenario.

except the vertical surface of phalanxes and the palm. The cylindrical object has a diameter of 60 mm and a mass of 1.5 kg, which is considered as a cylindrical tool that HERI Hand could handle in this situation. As Fig. 3-3 shows, only the middle phalanx, distal phalanx and palm will make contacts with the object in this size and profile, generating the vertical contact forces as f_2, f_3 and f_p respectively. The angles of the finger joints under this grasping scenario can be easily evaluated as $\theta_1 = 75°$, $\theta_2 = 28°$, $\theta_3 = 41°$.

In general cases which are not only limited in Fig. 3-3 scenario, the output motor torque τ_m under a certain posture with contact forces on the phalanxes can be written as

$$\tau_m = (\boldsymbol{J}^T \boldsymbol{F} + \tau_k) \cdot \frac{r_m}{h} \cdot \frac{1}{\eta_m \eta_t} \tag{3.1}$$

where

$$\boldsymbol{J} = \begin{bmatrix} l/2 \\ l/2 + l \cdot \cos\theta_2 \\ l_c + l \cdot \cos(\theta_2 + \theta_3) + l \cdot \cos\theta_3 \end{bmatrix} \tag{3.2}$$

functions as Jacobian Matrix $\boldsymbol{J}$,

$$\boldsymbol{F} = \begin{bmatrix} f_1 & f_2 & f_3 \end{bmatrix}^T \tag{3.3}$$

contains the vertical contact forces exerted at the proximal, middle and distal phalanx, respectively.

$$\tau_k = (k_1\theta_1 + k_2\theta_2 + k_3\theta_3) \cdot r_j^2 \tag{3.4}$$

τ_k is the sum of the torques generated by the spring deflection on each joint. k_1, k_2 and k_3 are the stiffness of the corresponding returning spring connected between two phalanxes at three finger joints, as shown in Fig. 3-2(c). r_j is the distance between the joint rotation centre to the corresponding spring and r_m is the radius of the motor output gear. h is the tendon force arm at the first finger joint and dependency with θ_1, which can be obtained from geometry calculation at a certain finger posture. η_m and η_t are the motor efficiency and tendon transmission efficiency respectively.

Each spring stiffness is defined as following, $k_1 = 230\,\mathrm{N/m}$, $k_2 = 440\,\mathrm{N/m}$ and $k_3 = 740\,\mathrm{N/m}$, which are decided by two constrains. The first is for eliminating the joint deflection caused by the phalanx gravity when the palm facing the ground, which determines the minimum value of k_1 for ensuring the robustness property meanwhile. The second is to avoid the finger *Roll-Back Phenomenon* [55, p. 49], which normally happens during a continuous finger closing motion, that the last phalanx slides against the object resulted in a situation that the finger grasps nothing but itself, which decides the specific ratio between k_1, k_2 and k_3.

As a result, we can utilize (3.1) to calculate the minimum output torque of DoA_1 actuator under the severest single third finger grasping scenario shown in Fig. 3-3. The efficiency coefficients η_m and η_t will be reasonable set for practically estimating the real working conditions. The vertical contact forces f_2, f_3 and f_p in Fig. 3-3 satisfy the relation with the object's gravity in the critical condition where sliding friction would occur, which as following,

$$m \cdot g = \mu \cdot (f_2 + f_3 + f_p) \tag{3.5}$$

where $m = 1.5\,\text{kg}$ is the cylinder's weight, $g = 9.81\,\text{m/s}^2$ is the gravitational constant, $\mu = 0.4$ is the static frictional coefficient between the object and the phalanx rubber.

Fig. 3-4 shows the corresponding motor torque τ_a, which depends on different contact forces f_2 and f_3 distributions. The white curve, whose maximum torque is 0.76 Nm, represents the minimum motor torque which demanded for holding a 1.5 kg cylinder under the critical condition in every different f_2 and f_3 distribution. We finally chosen Maxon EC-Max 22 motor for its compact size and adequate torque output, which is 1.2 Nm and presented as the green transparent plane in Fig. 3-4. The desired motor torque suffices the initial design requirements obviously and meanwhile possesses the maximum capacity to theoretically hold a 2.7 kg cylinder.

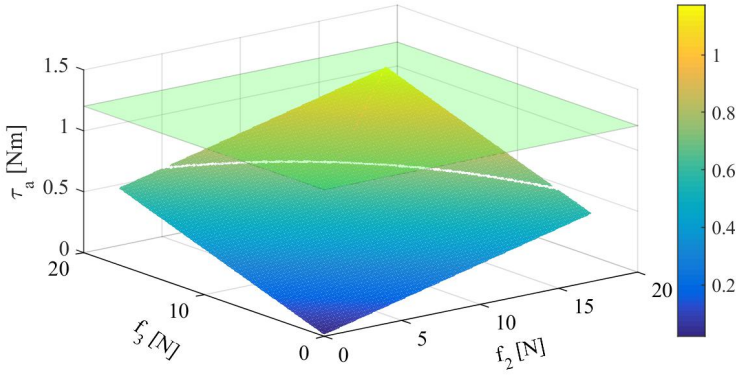

Figure 3-4: HERI Hand, minimum required motor torque τ_a under different contact force combinations.

The above content introduced the details for HERI Hand actuator selection, which is a general and basic method from kinematic analysis of under actuated finger on the basis of *Da Vinci's Mechanism*. Following the same method, the actuator selection for HERI II Hand has also been finished [46] by considering the heavier desired load and lower tendon transmission efficiency in more practical and severe situation. As a result for HERI II Hand actuation selection, the required motor torque is therefore

calculated to be approximately equal to 3 Nm and we eventually selected Maxon DCX22L motor with the gear ratio of 138 that can deliver a continuous torque of 3.3 Nm and a maximum velocity of 7.6 rad/s.

3.1.1.3 Sensor Configuration

Receiving sensory feedback information during finger manipulations is beneficial for interactive and precise finger motion control. The desired under actuated finger is equipped with two types of sensors (same for both HERI and HERI II Hand), namely the absolute angular position sensor for each motor and the tactile sensor for each finger phalanx, which is placed under the elastic rubber layer on each phalanx as shown in Fig. 3-2(c) and Fig 3-5. Meanwhile, the electronic boards embedded in HERI II Hand also provide the ability of reading motor current, which can be further utilized as finger current feedback control.

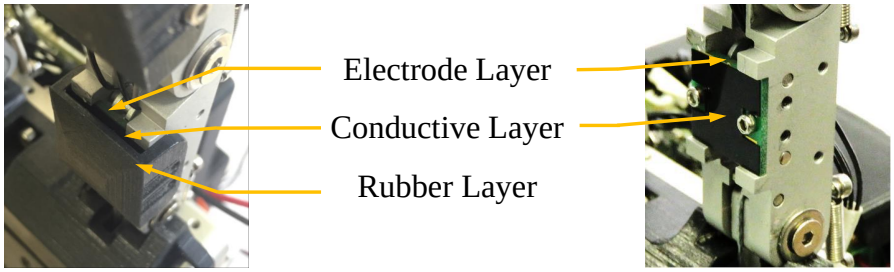

Figure 3-5: Three individual layers for the tactile sensor on each HERI Hand finger phalanx.

The absolute angular position sensor utilized is *AS5048A* from *ams AG*, which is a 14 bit absolute position sensor providing an angle measurement resolution of 0.022 degrees. However for under actuated fingers under tendon transmission, it is actually only the tendon displacement can be estimated by multiplying the angular position sensor feedback angle with the motor tendon pulley radius, while the exact position of each finger phalanx remains unknown due to the properties of under actuation.

The tactile/contact pressure sensors are specially customized designed by using a resistive sensing principle. They are composed by an customized electrode layer, a resistive/conductive layer, and a soft skin top layer as shown in Fig. 3-5. The vertical

component of the external force applied to the phalanxes can be measured by using the resistance change of the sensors after the basic calibration process by vertically placing one 100 g weight above on each of them. The maximum accuracy for the utilized pressure sensor can reach 0.08 N.

3.1.2 Finger Distribution and DoA Assignment

Since we mentioned that nowadays the design of under actuated robotic hands is difficult to fully mimic the structure and function of humankind hands especially in terms of finger distribution and Degree of Actuation (DoA) [1] assignment. To be more specific, the human hands 5 fingers and its corresponding 21 DoAs [56] is actually not the most appropriate design method under current research and technology level considering the acceptable cost, system simplicity, integration compact and redundancy reduction.

In this section, we will mainly introduce the finger distribution and DoA assignment for both HERI Hand and HERI II Hand, where the two hands possess different function priority according to practical requirements. Meanwhile the major motivation of the generation iteration from HERI to HERI II Hand, which is the the grasping strength priority enhancement, will also be detailed introduced.

3.1.2.1 HERI Hand Design Scheme

3.1.2.1.1 Finger Quantity and Distribution At the very initial stage when we design HERI Hand, our consideration is to design an under actuated hand which is competent in both dexterous and high strength manipulation, and meanwhile equipped with sufficient sensors for potential applications utilizing contact force feedback information. Moreover, it should be driven by as few actuators as possible taking into account simplifying mechatronics system and reducing cost at the precondition of not loosing dexterity. For achieving the aforementioned requirements, the main hand

[1] The definition of under actuated mechanism is relied on the quantity of Degree of Actuation (DoA) is fewer than the quantity of Degree of Freedom (DoF). Therefore Degree of Actuation (DoA) concept will be more emphasised in the design field of under actuation.

characteristics in terms of fingers and degree of actuations (DoAs) configurations are determined in this section.

Among the existing under-actuated hands, there are mainly three different designs in terms of finger quantity, which are (i) five-finger hands, (ii) four-finger hands and (iii) three-finger hands. Several examples for each type are as follows,

- Ritsumeikan robotic hand [21] and Pisa/IIT Softhand [20] etc..
- Yale OpenHand Model T [57] etc..
- RTR II [27], SPRING Hand [58] and Barrett Hand [25]etc..

However, by analysing the grip taxonomy [59], which is a thorough investigation for tool usage habit of human hands, we could find that in the majority of high strength grasping performed by the human, the middle finger, ring finger and little finger usually wrap around the object all together in a coordinated manner. Therefore, they can be considered as single Virtual Finger [60] for these grasp tasks and thus inspired us to simplify the hand design by combining the last three fingers main functionalities into only one finger, which naturally leads to three-finger hands type. As a result, the three-finger type was chosen as the finger quantity design of HERI Hand.

In addition, according to the study of human multi-finger force production [61], the coupled motion of last three fingers has the smallest Enslaving Effect among others, which means that combining them together will affect less to other fingers motion. Therefore, imitatively constructing the third finger of HERI Hand by bundling up the last three fingers of human hands is also a reasonable simplification from the biomechanics point of view. The humanoid robot HRP-3 [62] and the five-fingered assistive hand [63] adopted a similar design of a three-finger-combined into one third finger.

To provide larger contact area while at the same time permitting the third combined finger to conform to the object surface along the lateral direction, three wide rubber patches are mounted on phalanxes of the third finger to triple the contact surface, which directly reflects the asymmetrical dimension property of this finger with

respect to the index finger and the thumb. This enables the adoption of the contact area of the combined third finger replicating the flexibility produced by the ring and little fingers.

Therefore, as shown in Fig. 3-1(a), HERI Hand equips with three fingers: the third finger (combining the middle, ring and little fingers), the index finger and the thumb. The thumb is placed oppositely to the index finger to simplify the mechanical design for the realization of pinch motion. Additionally, two rubber-made compliant structures are mounted at the bases of index finger and third finger to avoid the finger structure damage caused by unexpected lateral impacts in the direction of joints rotation axis.

3.1.2.1.2 Degree of Actuation Assignment As the finger quantity and distribution are decided, it comes into the issue for Degree of Actuation (DoA) configurations selection. For the purpose of simplifying the mechanical structure, reducing the cost, and meanwhile maintaining the finger manipulation capabilities to the greatest extent, we finally set the DoA quantity to be three. Fig. 3-6 depicts four possible proposals of the potential three-DoA under-actuation configuration for the desired HERI hand. Fig. 3-6(a) provides independent flexion motion for each finger but lacks the thumb rotation, which will limit the hand dexterous manipulation performance to some extent; Fig. 3-6(b) possesses one kind of unhuman-like grasping motion, namely the combined motion for third finger and thumb but simultaneously allows for independent index flexion motion that can be useful to perform triggering actions e.g. switching on powerful tools; Fig. 3-6(c) merges the motion of index and third finger, which may interfere with each other in some cases where a precision grasp such as palmar pinch is necessary; Fig. 3-6(d) provides the independent flexion motion for third finger, combined flexion motion for index finger and thumb as well as the independent thumb rotation motion.

In summary, options (a) and (c) were excluded as they do not demonstrate any specific advantages with respect to the other two. Under actuation arrangements (b) and (d) provide very similar functionality in terms of robustness and dexterity

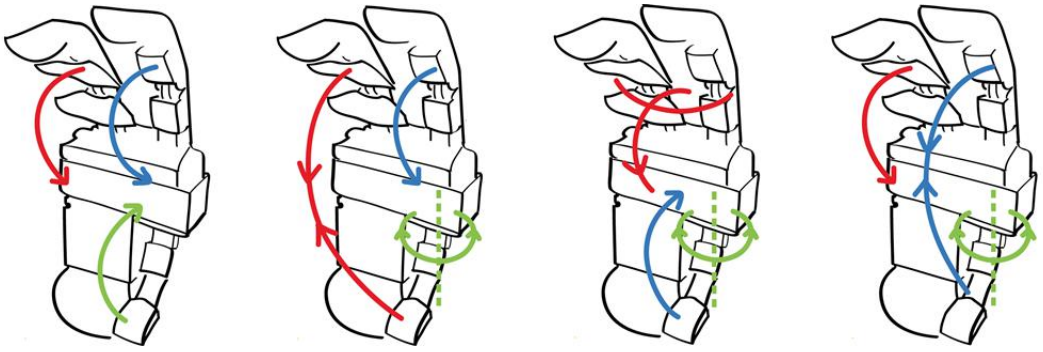

Figure 3-6: Possible potential proposals for assigning Degree of Actuation (DoA) to three-finger under-actuated HERI hand.

as well as have both pros and cons with respect to each other. They could be both selected depending on the choice of the dexterity feature to be highlighted that is the independent index trigger action provided by configuration (b) or the natural index/thumb pitch feature permitted by configuration (d). In this first prototype our choice target was to permit the execution of natural index/thumb pitch action and for this reason configuration (d) was selected in Table 3.2, which presents the significant DoA assignment specifically.

Within the final chosen DoA configuration (d) shown in Table 3.2, we can find that DoA_1 will mainly contribute to the high strength grasping, while DoA_2 and DoA_3 will undertake precise natural pinching and dexterous manipulation, which presents the property for asymmetrical actuation. A special consideration needs to be taken for DoA_2, if either index finger or thumb is stuck by the object during practical grasping, the other finger should be capable of continuously executing the desired motion. Besides, DoA_3 should be independent with DoA_2, that means no coupled motions should exist for the thumb rotation to permit the deterministic placement and control of the thumb opposition.

3.1.2.1.3 Tendon Route Description Since HERI Hand is based on tendon driven, in this section we will specifically introduce the tendon route for achieving the corresponding DoA assignment as shown in Table 3.2.

The main mechanical transmission systems between actuators and end-effectors

Table 3.2: Degree of Actuation (DoA) assignment of HERI Hand.

	DoA_1	DoA_2	DoA_3
Motion Description	Third finger flexion motion	Index finger and thumb combined flexion motion	Thumb rotation

of DoA_1 and DoA_2 are tendon based. The tendon routing design of HERI Hand is significant for achieving adequate grasping performance and mechanical transmission in high efficiency. The *Dacron* rope is used as the specific tendon material for its high strength and wear resistance properties.

As shown in red dashed area in Fig. 3-7, the tendon route depicted in red is designed for DoA_1, namely the strength grasping of the third finger. It is based on the classical *Da Vinci's Mechanism* [55, p. 55] which uses multiple pulleys supported by miniature bearings to significantly decrease the friction between the tendon and the mechanical parts. This sliding friction reduction as well as the short tendon route distance enable DoA_1 to efficiently generate grasping forces.

DoA_2, which is dedicated to the combined flexion motion of index finger and thumb, additional attention was given to ensure its efficient transmission. Its tendon route is combined by two segments as shown in the black dashed area in Fig. 3-7, the green tendon route is the main route connected with DoA_2 motor and then divided into two black branch routes fixed with the tips of thumb and index finger respectively, directly after a *Linear Guide* and a *Movable Pulley* that implement a differential tendon mechanism between the motions of the index and the thumb, which allowing either finger to continue its flexion motion even if the other finger is constrained. However, driving two under-actuated fingers by only one actuator increases the sliding friction between tendon and mechanism due to the complicated tendon route and meanwhile may cause the coupling mechanism's slack issue. For addressing these aforementioned issues, additional pulleys (17 in total) supported by bearings including the essential *Movable Pulley* were used to reduce friction, the slack issue is simultaneously solved by the low tendon friction as well as the pretension

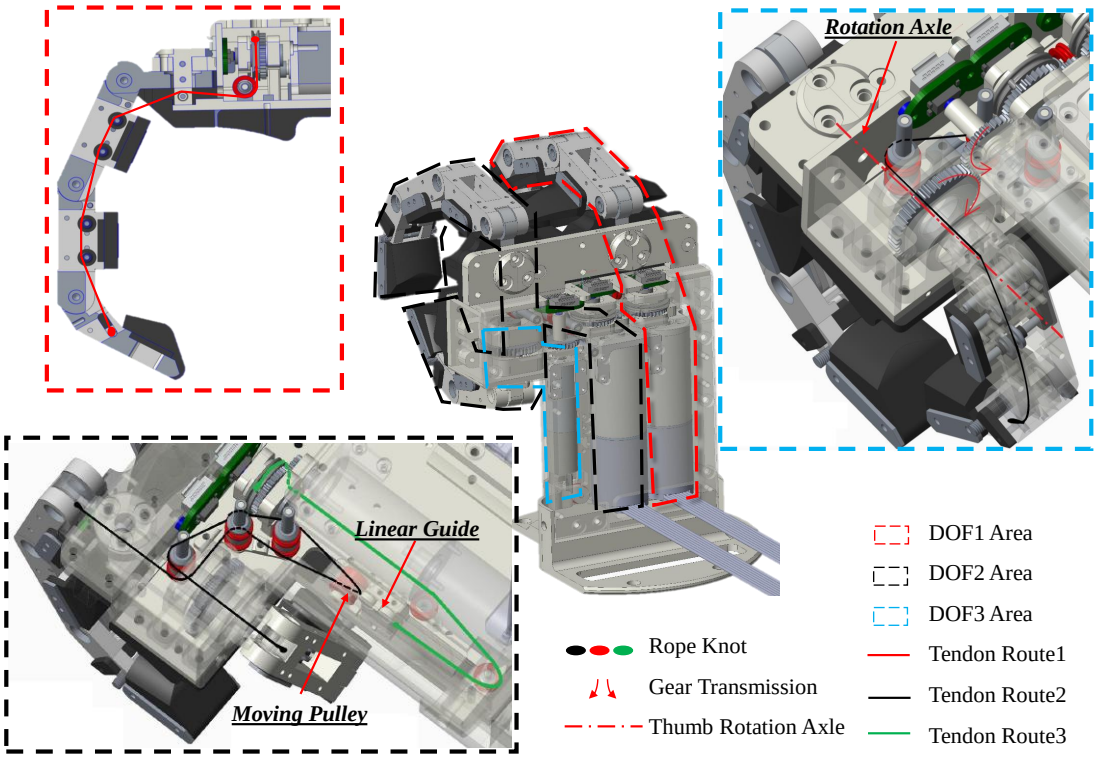

Figure 3-7: Tendon route for driving corresponding DoA of HERI Hand.

force generated by the finger joint springs. DoA_1 transmission is more efficient and can generate higher grasping forces than DoA_2 based on the simple fact that the driving force of DoA_2 is divided for two under-actuated fingers, despite that the two actuators are of the same specification. This asymmetry in the two transmission systems inherently distributes the power grasp functionality to the third finger rather than to the index one.

DoA_3, which is responsible for the thumb rotation, is directly driven by a reliable two-gear transmission as shown in the blue dashed area in Fig. 3-7. It should be independent of DoA_2 and not interfere with the thumb flexion motion, which means that there should not be any displacement for the thumb tendon when it rotates. To achieve this decoupling, the thumb flexion tendon is routed through the centre axis of the thumb rotation joint.

3.1.2.1.4 DoA Configuration Summary Based on the aforementioned sections regard to kinematic analysis, actuator selection, finger distribution, DoA assignment

and the tendon route analysis on HERI Hand, corresponding overall actuation configurations of HERI Hand are summarized in Table 3.3.

Table 3.3: Configuration summary for each DoA actuation components and expected finger grasping force of HERI Hand.

	DoA_1	DoA_2	DoA_3
Motor Type	EC-Max 22, Brushless, Maxon[(1)]		1218A, Brushless, Faulhaber[(2)]
Gearbox Type	Planetary GP 22 C, Maxon		Planetary 12-4, Faulhaber
Gearbox Ratio	104:1		256:1
Continuous Torque	1.2 Nm		0.3 Nm
Peak Torque	1.9 Nm		0.45 Nm
Estimated Transmission Efficiency[(3)]	0.44	0.36	0.5
Tendon Length	145 mm	348 mm & 189 mm[(4)]	-
Number of Tendon Transmission pulleys	6	17	-
Expected Continuous Grasp Force[(5)]	17 N	10 N	-
Expected Peak Grasp Force[(6)]	27 N	15.8 N	-

Note: (1) The selected motor for DoA_1 is powerful enough for DoA_2, for interchangeable principle, the same type was adopted; (2) This motor is selected mainly due to its compact size and appropriate reduction ratio for DoA_3; (3) This is the final efficiency including both the motor efficiency and the tendon transmission efficiency; (4) 348 mm and 189 mm are the length for tendon in black and green respectively, as shown in Fig. 3-7; (5)-(6) This is the force generated from the end-effector phalanx, namely the distal phalanx on corresponding finger.

3.1.2.2 Motivation of Generation Iteration

In this section, we will introduce the motivation for the generation iteration from HERI Hand to HERI II Hand.

3.1.2.2.1 Strength Grasping Priority As the overall design scheme regard to HERI Hand presented in Section 3.1.2.1, our design target is to achieve a performance balance between high strength grasping and dexterous finger manipulation, where specifically DoA_1 is responsible for high strength grasping and DoA_2, DoA_3 are desired to contribute for dexterity. However, from the practical experiments and applications, which will be presented in following Section 3.1.5.1, we found that HERI Hand is actually capable of proceeding relative powerful grasping motion, however it still can not satisfy the high strength grasping requirement in practical application scenario, such as firmly grasping a heavy brick or wood.

The main disadvantages of HERI Hand in terms of high strength grasping priority design are as following,

- Degree of Actuations adoption (only (DoA_1) adopted) for high strength grasping is not enough simply in terms of quantity.
- The differential mechanism embedded in DoA_2 is superb complicated in terms of mechanical structures and tendon routes resulting in low transmission efficiency.
- The dexterous benefits brought by the thumb rotation (DoA_3) is not highlighted enough by considering embedded an extra DoA in such precise and limited mechatronics system by no contribution to the high strength grasping.

As a result, the design of HERI II Hand, which is desired to process much more powerful grasping performance, is mainly following the idea of increasing DoA quantity for high strength grasping. Since we have mentioned that currently it is difficulty to find a general solution for robotic hands to achieve both high strength and dexterous grasping, thus HERI II Hand will lose the dexterity to some extent compared to HERI Hand with no doubt, for instance the thumb rotation namely DoA_3 (corresponding application based on this DoA will be introduced in the following Section 3.1.5.2). Here we have to emphasis, HERI Hand actually achieved a adequate and balanced performance in both strength and dexterity, the motivation for the iteration between these two generations is the functionality priority for higher strength grasping when facing the practical challenge of robotic manipulation scenarios.

3.1.2.2.2 Assembly and Maintenance Simplify Besides of the motivation of enhancing high strength grasping ability, another significant reason we have to consider is the simplify of assembly and maintenance progress. Even though this is more related to the specific engineering and hardware development, we have to still highlight this since the robotic hands functioning as the end-effector will have more chances for suffering from the unknown external collisions, where the physical damage is nearly hard to be totally avoided. The coupling DoAs on HERI Hand (namely DoA_2

and DoA_3) will bring enormous difficulty for daily assembly and maintenance work due to its complex, delicate and coupled structures. Therefore, the design of HERI II Hand will more focus on the simplification of practical assembly and maintenance when under the corresponding design scheme.

3.1.2.3 HERI II Hand Design Scheme

Based on the iteration motivation from HERI to HERI II Hand, one of the important property of HERI II Hand is its configurable finger quantity and arrangement, which means that the specific finger quantity and distribution can be adjusted according to different manipulation requirements. The precondition for the configurable feature is each robotic finger ought to be identical, modular and absolutely driven independently to each other, it can be also concluded that the modular finger concept has to be adopted in HERI II Hand design. This concept actually satisfies our motivation to enhancing strength grasping by utilizing more DoAs and simplify the daily maintenance difficulty as we mentioned in previous section. In the following content of this section, we will introduce the design scheme of HERI II Hand, which is the one taking consideration of manipulation dexterity under the precondition of enhancing strength grasping.

The desired hand base is designed as a cylinder, hence the finger modules can be freely distributed around the cylindrical base as shown in Fig. 3-8(a). Considering placing the fingers opposite to each other is necessary to realise finger pinch manipulation[64]. Two opposing flanges for fixing six finger modules are designed as Fig. 3-8(b) shows, where the two opposing flanges can be divided into three areas for placing finger modules opposite to each other.

For the selection of the arrangement for the finger modules in the two opposing flanges, let consider the three distinct areas of the hand base as shown by the dashed blue lines in Fig. 3-8(c). Each of these three areas can be equipped with one finger at one side (OS), two opposing fingers (TO) or eventually with no fingers (NO). The provided manipulation functionality for each of these cases is reported in Table 3.4 where a consideration related to the cost is also detailed.

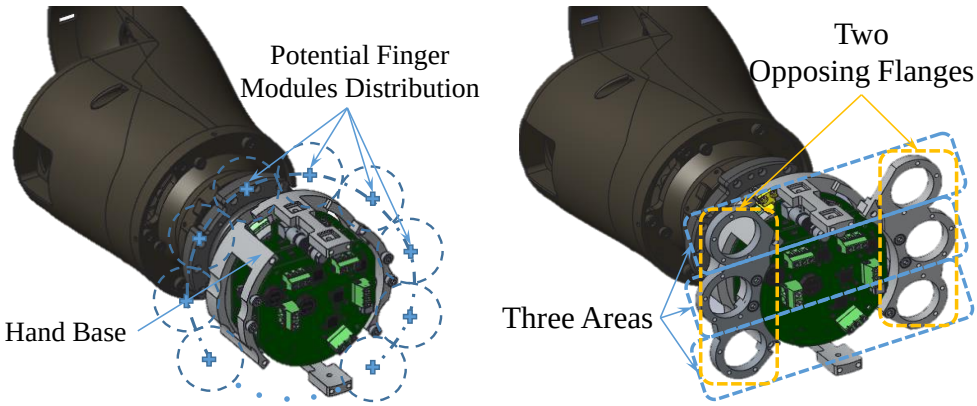

(a) Cylindrical hand base

(b) Two opposing flanges

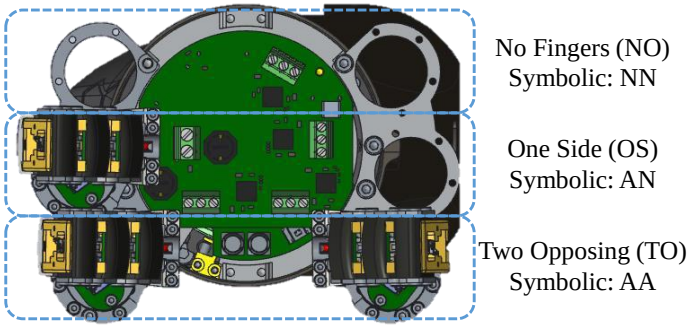

(c) Example for three kinds of finger arrangement

Figure 3-8: Scheme for HERI II Hand finger module arrangement.

Table 3.4: Functionality and cost related figures for the three types of finger arrangement in one dashed blue area.

Finger Arrangement	Symbolic[(1)]	Corresponding Performance Score			
		Robust grasping	Pinch	Trigger	Economic
None (NO)	NN	0	0	0	1
One-Side (OS)	AN or NA	1	0	1	1
Two-Opposite (TO)	AA	1	1	1	0

Note: (1) We use **A** to represent the equipment of finger module at either location in one opposing flange and **N** to represent not equipped.

Several possible finger configurations for composing the whole hand with their corresponding performance scores are presented in Table 3.5, where it can be seen that different finger configurations provide different level of functionality and advantages. HERI II Hand can be configured based on different requirement priority. For instance,

- If the hand is desired for pinch motion, especially for the long cylinder object, the configuration $[AA, AA, AA]^T$ should be adopted as shown in Fig. 3-9(a);

- If the hand is supposed to do the high strength grasping considering also the cost, the configuration $[NA, AN, NA]^T$ could be utilised as presented in Fig. 3-9(b);

- If the hand is designed to achieve a relative balance performance between pinch, high strength grasping, trigger and in low cost, the configurations $[NA, AA, NA]^T$ or $[AA, NN, NA]^T$ could be chosen as Fig. 3-9(c) and 3-9(d) demonstrate.

Table 3.5: Several possible whole hand finger configurations and corresponding performance score.

Finger Configurations(1)	Desired Whole Hand Score			
	Robust grasping	Pinch	Trigger	Economic
[AA, AA, AA]^T	3	3	3	0
[AA, NA, AA]^T	3	2	3	1
[AA, NN, AA]^T	2	2	2	1
[NA, AA, NA]^T	3	1	3	2
[AA, NA, NN]^T	2	1	2	2
[NA, AN, NA]^T	3	0	3	3

Note: (1) We utilise the transpose of a 3×1 Matrix to describe the whole hand configuration based on three types of finger arrangement in Table 3.4.

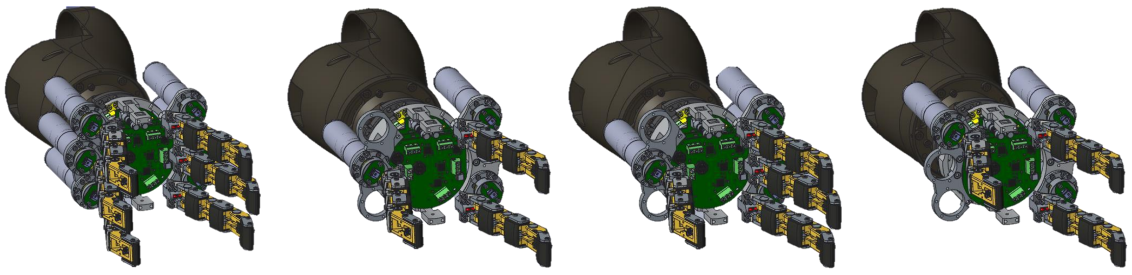

(a) (b) (c) (d)

Figure 3-9: Four types of common finger configuration examples of HERI II Hand.

For the application of HERI II Hand on Centauro Robot[47], the functional priority of high strength grasping while meantime maintaining precise pinch and trigger motion functions are required and considered. As a result, the configuration $[NA, AA, NA]^T$ shown in Fig. 3-1(b) was adopted as the current design scheme of hardware realisation as shown in Fig. 3-1(b).

3.1.3 Finger Module Design and Development

In this section, we will present the design and development details of the specific finger module for HERI II Hand. Fig. 3-10 presents the corresponding components that compose the finger module.

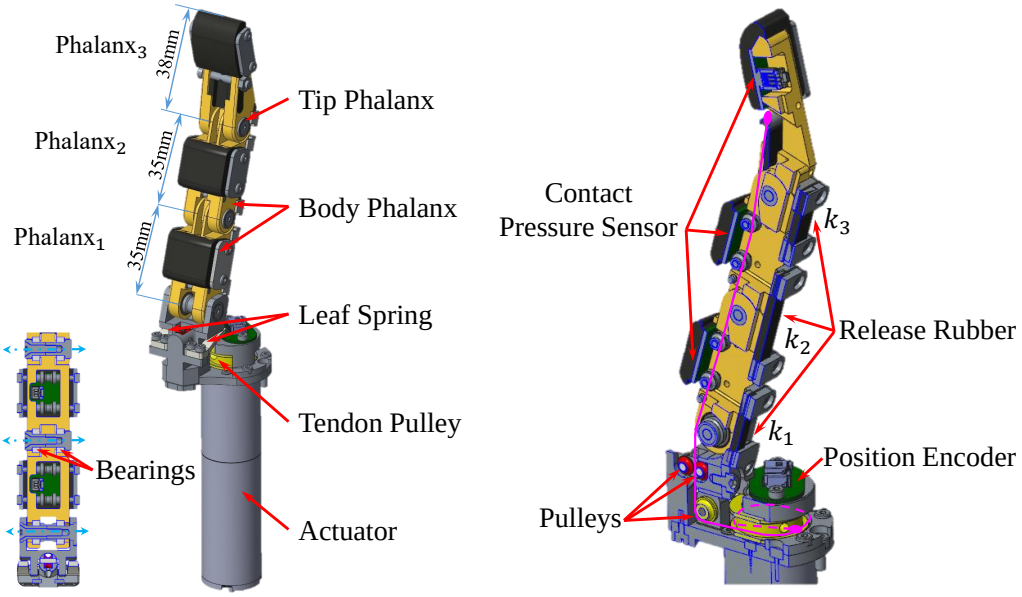

(a) Components anotated (b) Tendon route and sensor configuration

Figure 3-10: HERI II Hand finger module design with components annotated.

The design of an individual finger module, particularly the set of phalanxes, follows the same concept as the first version of the HERI Hand, see Section 3.1.1.1 for the design details. However as mentioned before, the length of body and tip phalanxes, as illustrated in Fig. 3-10(a), is adjusted to reduce the overall length of the hand, and therefore leads to a more compact hand proportional in size to the Centauro forearm presented in [47]. The body and tip phalanxes are 35 mm and 38 mm long respectively, so that the overall finger length is approximately 100 mm in extension condition.

Following the same kinematics analysis procedure as introduced in Section 3.1.1.1, we selected Maxon DCX22L motor with the gear ratio of 138 that can deliver a continuous output torque of 3.3 Nm and a maximum velocity of 7.6 rad/s. Similarly as HERI Hand, We adopted the classic *Da Vinci's Mechanism* [55] approach for the

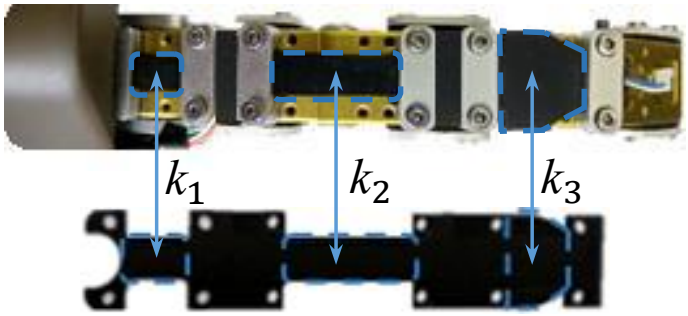

Figure 3-11: Finger release elastic element design on HERI II Hand.

tendon transmission system of the under-actuated finger to render flexion motion as shown in Fig. 3-10(b). The sensor configuration remains the same from HERI Hand to HERI II Hand as presented in Fig. 3-10(b).

Since the tendon transmission according to *Da Vinci's Mechanism* approach can not apply force for finger release, as elaborated in [55], it is essential to design a set of elastic elements for finger phalanx joints to release the finger (extension motion) when finger closing (flexion motion) is not intended/applied. We adopt the elastic rubber of different stiffness level for each phalanx joint, instead of extension springs used in the first version of HERI Hand presented in [23], since it allows fine tuning of the joint stiffness. Furthermore, the rubber superior damping performance decreases the finger tremble in real applications. The rubber element and its mounting on the the finger is shown in Fig. 3-11, where the different stiffness of each joint is achieved by clamping the rubber at two different sections of the rubber. The rubber used in the finger module, when clamped as shown in Fig. 3-11, renders three stiffness values of 880, 950, 1660 N/m from base to tip, that correspond to $k_1 = 0.071$, $k_2 = 0.077$ and $k_3 = 0.134$ Nm/rad, closely matching the values used for the actuator selection analysis.

3.1.4 HERI II Integration Property with Centauro Robot

Since the proposed hand is developed as an end-effector for Centauro Robot[47], we adapt the design with the robot forearm in a way that a compact design embodying essential components is achieved.

Fig. 3-12 reveals HERI II Hand's integration with the Centauro forearm. Starting from the forearm wrist rotation interface, we integrate a 6-axis F/T sensor for connecting the wrist interface to the hand. The hand unit includes a basement part on which all the finger modules, palm and covers are mounted. It contains the main electronics to drive the finger motors and read the sensor information including the F/T sensor and the fingers' sensory data. The specifications of the proposed hand integrated into Centauro robot[47] forearm is reported in Table 3.6.

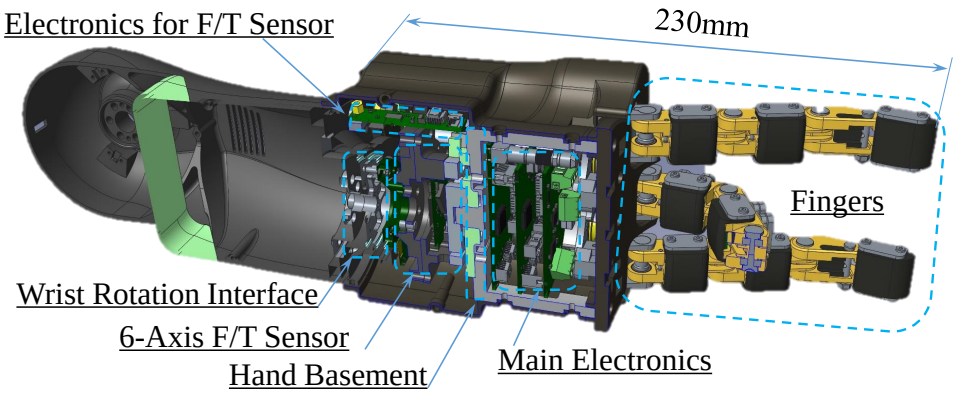

Figure 3-12: HERI II Hand cross section showing the integration of the various electronics and F/T sensor.

Table 3.6: HERI II Hand and finger module specifications.

	HERI II Hand in Fig. 3-1(b) Configuration
Weight	1.6 kg
Overall Dimension	230 mm × 105 mm × 105 mm
	Finger Module
Motor Type	Maxon DCX22L GB KL 48V
Gearbox Type	Maxon Planetary GPX22HP 138:1
Continuous Torque	3.3 Nm
Tendon Guidance Pulleys Number	8
Estimated Transmission Efficiency	$\eta_m = 0.5$, $\eta_t = 0.45$
Tendon Transmission Length	126 mm
Tendon Material	LIROS DSL 0.7 mm
Sensor Configurations	Position & Contact Pressure Sensors, Current Reading
Release Rubber(1) Stiffness	$k_1 = 880$ N/m, $k_2 = 950$ N/m, $k_3 = 1660$ N/m
Weight	298 g

Note: (1) The rubber sheet is from MISUMI RBCM2-20, the different stiffness is achieved by cropping into different sectional area.

3.1.5 Experimental Validation and Results

In previous section, we introduced the design and develop details of HERI Hand and HERI II Hand, especially highlighted the iteration motivation from these two generations, which is for enhancing the high strength grasping. In this section, we will firstly present the corresponding experiments and its results for verifying the modification effectiveness (from HERI to HERI II Hand) in high strength grasping and then secondly meanwhile demonstrate various practical grasping applications for showing both hands dexterity performances.

3.1.5.1 High Strength Grasping Enhancement

For evaluating the high strength grasping performance enhancement from HERI to HERI II Hand, we utilize the specific weight-grasping ratio, where the experiments for achieving this ratio are both proceeded on two hands. Besides, series of HERI II Hand practical high strength grasping applications are also demonstrated.

3.1.5.1.1 Weight-Grasping Ratio Evaluation For verifying the high strength grasping performance of these two desired hands, we specifically designed a testing scenario, where the robotic hand is controlled to vertically grasp heavy objects and the force that handles the grasped object can only come from the static friction generated by finger phalanx contact force. Meanwhile, the corresponding contact force from each finger phalanx will be measured during the complete grasping process since it is one of the directest indicator for the high grasping performance. We will compare the weight-grasping ratio between HERI and HERI II Hand, which is the ratio between the weights of the maximum grasped objects and the utilized robotic hand, since it is a quantitative metrics that can verify and compare the high strength grasping performance among robotic hands.

Through placing metal cubes in different weights one by one into the grasped bottle, we can be aware of the maximum grasping robustness for HERI Hand (utilizing DoA_1 and DoA_2 simultaneously) under this situation, which means in the specific

profile of the grasped cylinder object (75 mm diameter bottle). From Fig. 3-13(a)-(d), totally 1450 g metal cubes were vertically and stably held by HERI Hand, which mass itself is 1190 g. Also from Fig. 3-13(e), we can observe the variation of contact force from three fingers during the process, and the maximum 22 N contact force can be found on Third Finger distal phalanx (TiT_3) when the time is in 13.9 s. This is actually the severest situation for verifying the robotic hand high strength grasping performance since all the vertical supporting force is only generated by the friction force caused by the finger and object contact.

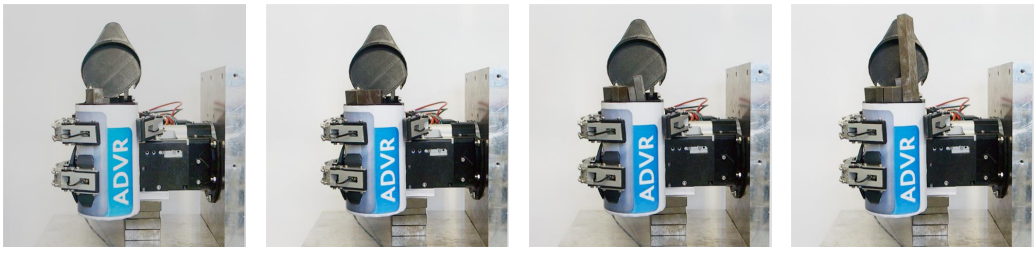

(a) 125 g (b) 650 g (c) 1150 g (d) 1450 g

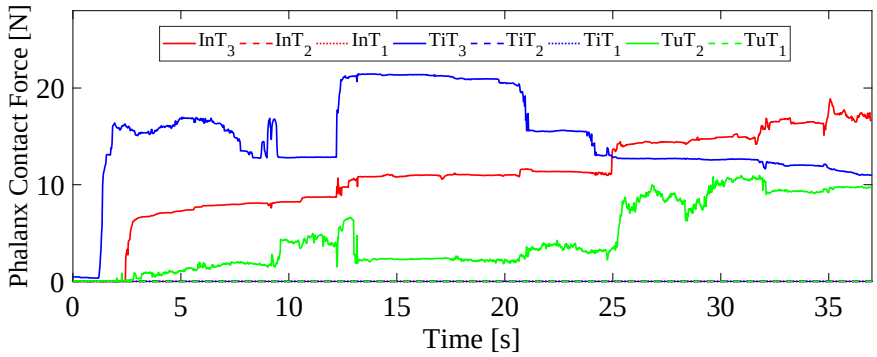

(e) Tactile curves for high strength grasping process

Figure 3-13: HERI Hand high strength grasping for weight-grasping ratio evaluation and the corresponding tactile curves, where InT, TiT and TuT indicate the tactile from Index Finger, Third Finger (The finger utilized in DoA_1) and Thumb respectively, the number order 1, 2 and 3 represent the proximal, middle and distal phalanx correspondingly.

The similar vertical grasping experiment for weight-grasping ratio evaluation has also be proceeded on HERI II Hand, as shown in Fig. 3-14(a). HERI II hand is able to vertically grasp the same cylinder object (75 mm diameter bottle) with 4354 g weight metal cubes inside, which weight itself is 1603 g. Meanwhile all the corresponding tactile information from the phalanxes of four fingers during the experiment are pre-

sented from Fig. 3-14(b) to 3-14(e), where the specific finger naming order could be refer from Fig. 3-14(a). It can be noticed that the maximum contact force from all HERI Hand fingers can reach approximately 40 N, with the comparison of 22 N from HERI Hand.

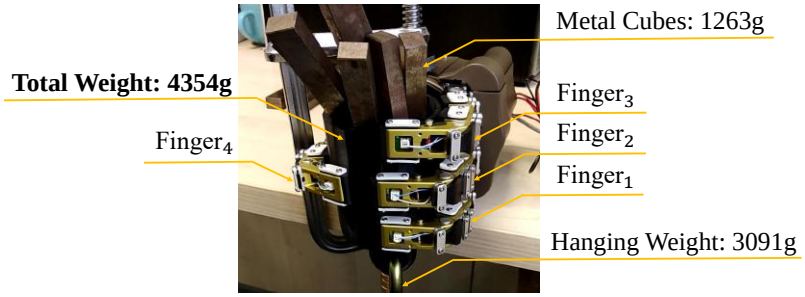

(a) 4354 g vertical grasping experiment and finger naming order

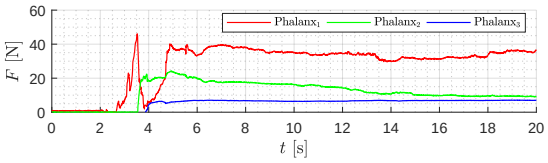

(b) Finger$_1$ contact force curve

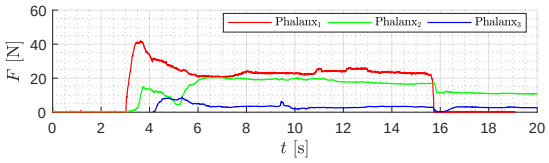

(c) Finger$_2$ contact force curve

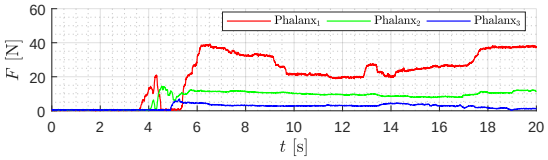

(d) Finger$_3$ contact force curve

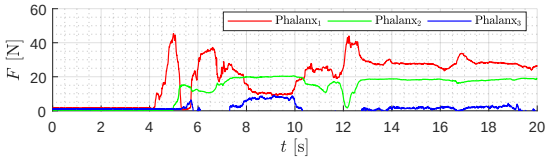

(e) Finger$_4$ contact force curve

Figure 3-14: HERI II Hand high strength grasping for weight-grasping ratio evaluation of vertically holding a cylinder object in 4354 g weight with finger number order annotated, Phalanx$_1$, Phalanx$_2$ and Phalanx$_3$ represent for proximal, middle and distal phalanx respectively.

The measured contact forces from corresponding finger phalanxes possess variation during grasping and meanwhile slightly differ from theoretical calculated forces, which can be observed from Fig. 3-14(b)-3-14(e). The two main potential reasons are as following,

- The contact configuration and pressure are not the same in all fingers and depends on the placement of the object in the hand with respect to HERI II Hand fingers.

- The external disturbance applied on the under-actuated finger during grasping from adding weights will result in the posture variation of the finger[65], which will eventually change the contact force configuration.

If we compare the weight-grasping ratio after this two aforementioned experiments, we can obviously find that, the weight-grasping ratio of HERI II hand is 2.716, which is 2.2 times higher of that of HERI Hand weight-grasping ratio (1.218) in terms of vertical grasping ability. The HERI Hand weights 1190 g mass and can hold a 1450 g weight while the revised HERI II Hand has a mass of 1603 g and is able to hold a 4354 g weight. This actually directly and quantitatively verifies the design and modification effectiveness in terms of high strength grasping between two robotic hands generation iteration.

3.1.5.1.2 HERI II Hand Strength Grasping Application After the quantitative evaluation of the strength grasping performance in terms of weight-grasping ratio, we will here meanwhile present several practical applications that demonstrate its strength grasping ability.

The first application was performed by controlling the hand to grasp a hammer and execute the task of knocking a nail in a wood block as depicted in Fig. 3-15(a). The disturbance during knocking nail applied on four fingers can be detected from contact force curves from Fig. 3-15(b) to 3-15(e). The impact effects can be obviously noticed on Finger_1 as shown in Fig. 3-15(b), demonstrating the high strength grasping of HERI II Hand and its physical resilience to impacts.

The second application was proceed by mounting HERI II Hand on Centauro robot to grasp objects in irregular shape as shown in Fig. 3-16, where a 2.8 kg brick and 3.25 kg long wood were firmly grasped. Since it is well known that, the under actuated hands strength grasping performance is dependent on the profile of the grasped object, besides of the cylinder object in 75 mm in weigh-grasping ratio experiments, we also want to meanwhile demonstrate HERI II Hand strength grasping performance for irregular but more practical objects.

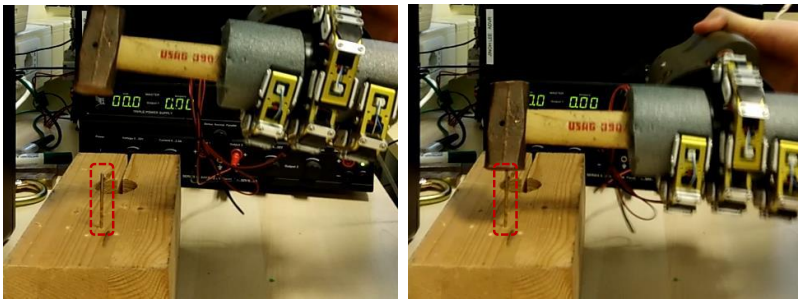

(a) Knocking nail experiment

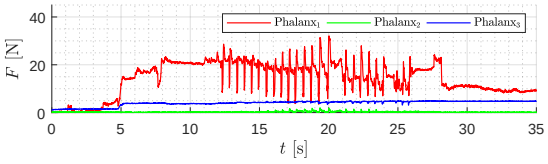

(b) Finger$_1$ contact force curve

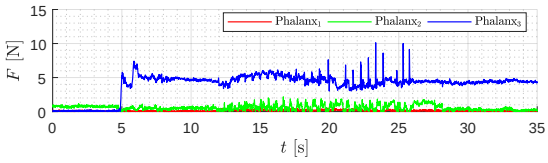

(c) Finger$_2$ contact force curve

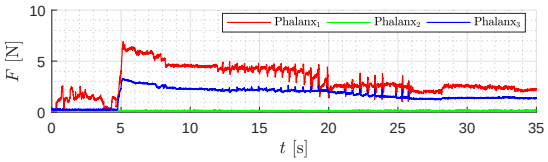

(d) Finger$_3$ contact force curve

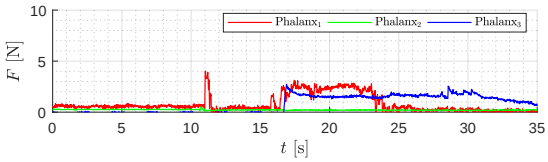

(e) Finger$_4$ contact force curve

Figure 3-15: HERI II Hand high strength grasping for a hammer during the high impact knocking nail task, Phalanx$_1$, Phalanx$_2$ and Phalanx$_3$ represent for proximal, middle and distal phalanx respectively.

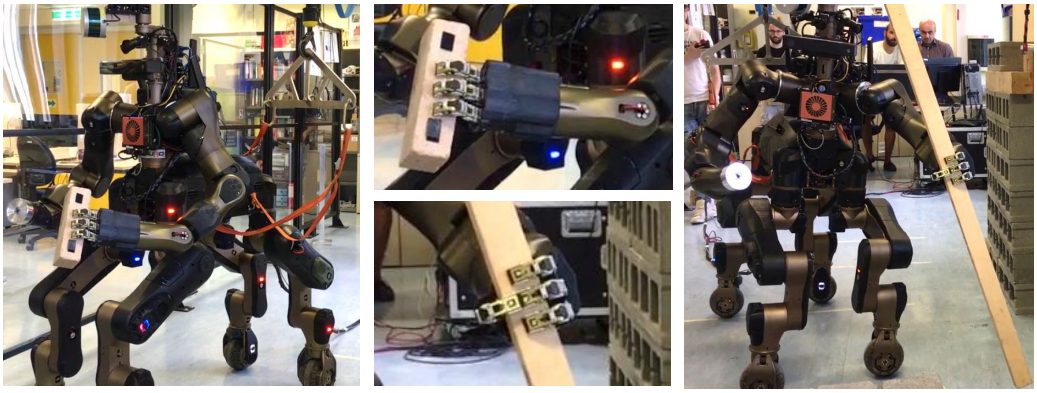

Figure 3-16: HERI II Hand (mounted on Centauro robot) high strength grasping for a 2.8 kg brick (irregular shape) and a 3.25 kg long wood.

3.1.5.2 Dexterous and Delicate Manipulation

Even though we have a functional priority for HERI series of robotics hands to possess strength grasping property, HERI Hand and HERI II Hand are still capable of

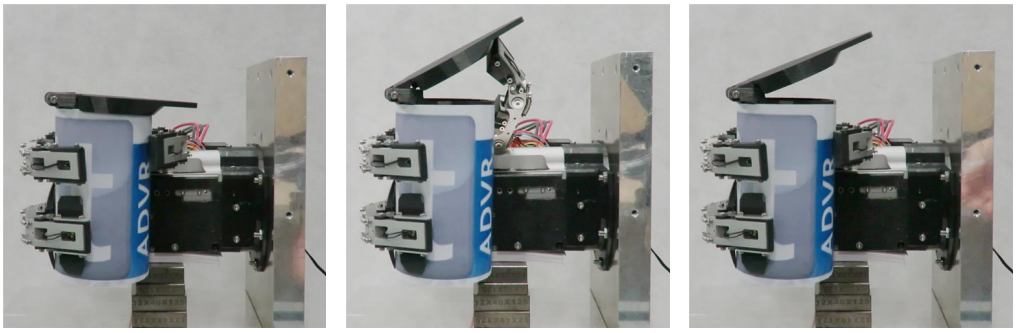

(a) Grasp the cup (b) Open the lid (c) Resume grasp

Figure 3-17: Process for opening a lidded cup utilizing all the three DoAs of HERI Hand simultaneously.

achieving dexterous and delicate manipulation to some extent. In this section, we will present several dexterous and delicate manipulation application from HERI and HERI II Hands.

3.1.5.2.1 HERI Hand Cup lid Open For the purpose of fully taking advantage of all the equipped DoAs on HERI Hand and demonstrating its dexterous performance, a challenging task of involving a certain level of dexterity by executing opening a cup with a hinged lid was carried out. Fig. 3-17 shows this finger manipulation by simultaneously using three DoAs of HERI Hand. The cup was firstly placed by the human operator and then grasped using both DoA_1 and DoA_2 as Fig. 3-17(a) shows. After all the three fingers closed and firmly hold the cup, the thumb was commanded independently to rotate outwards, therefore pushed the lid to open, as shown in Fig. 3-17(b) and finally it rotated back to resume grasping the cup, which is presented in Fig. 3-17(c).

3.1.5.2.2 HERI Hand Delicate Gentle Grasping This experiment was to explore the potential applications of utilizing the embedded sensors, particularly the tactile sensors, to perform high delicate finger manipulations that those without contact force sensing robotic hands have difficulties to realize. A simply admittance controller was developed to demonstrate the effectiveness of integrating the tactile sensor feedback into the controller for grasping an ordinary plastic cup, whose diame-

ter is around 60 mm and thickness is 0.1 mm. This plastic cup was chosen for its easily deformableness which will conspicuously display the compression applied by the fingers. As shown in Fig. 3-18, the admittance controller of each DoA takes the desired joint angular position and the tactile sensor force feedback as inputs, then generates the reference angle sending to the motor. The control principle is that, if the force reading from one of the tactile sensors in a DoA reaches a predefined threshold, the controller will freeze the DoA by keeping sending the last references, and resumes to update the new reference when the threshold condition is not satisfied.

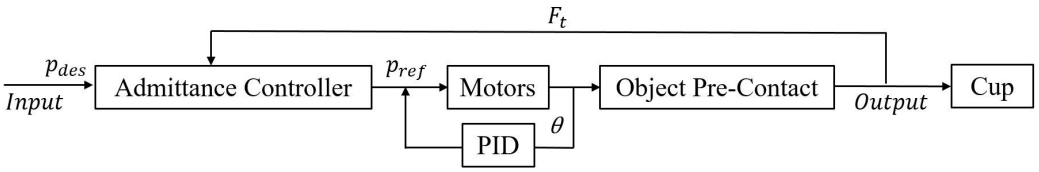

Figure 3-18: Admittance controller for HERI Hand delicate grasping.

Fig. 3-19 shows the practical plastic cup grasping tests without and with the admittance controller using the tactile sensor feedbacks. As shown in Fig. 3-19(a), it is obvious that, using the pure position control of the DoAs without force feedback, directly execution of the desired closing trajectories (shown in Fig. 3-20(b)) deformed the plastic cup. A good comparison can be found in Fig. 3-19(b), the soft elastic cup could hardly be detected the deformation thanks to the utilization of the admittance controller. Meanwhile, we could also observe that the thumb does not make a contact with the plastic cup, since the index finger has already been detected for contacting with it, thus the thumb just stop at its current position as DoA_2 is commanded to stop. Fig. 3-20 present the curve for both phalanx tactile data and absolute angular position data without and with admittance controller. It is obviously that the contact force in Fig. 3-20(c) is much smaller than the contact force in Fig. 3-20(a) due to the utilization of controller for preventing the shape change for soft plastic cup. Fig. 3-20(b) and Fig. 3-20(d) also show the clear comparison for the absolute angular position data between uncontrolled and controlled situation.

It is clear that the soft plastic cup generating the shape change due to the single use of position control. Actually the position command for three DoAs we send is

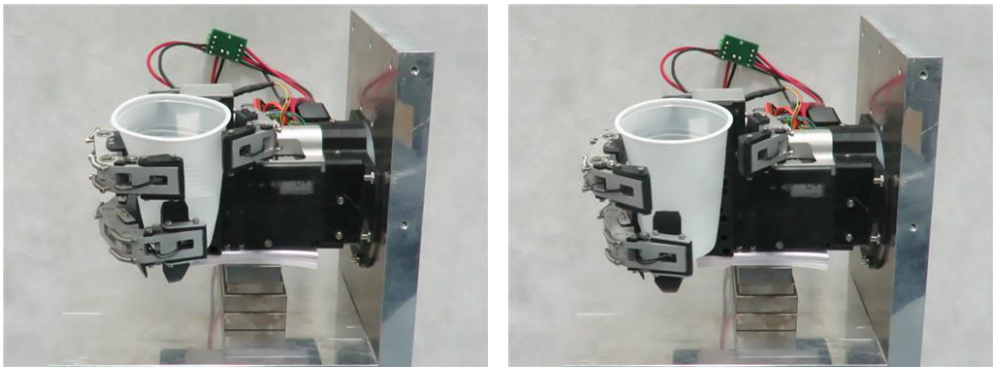

(a) Without admittance controller (b) With admittance controller

Figure 3-19: HERI Hand gentle grasping of a plastic cup (a) without and (b) with admittance controller by utilizing tactile feedback information.

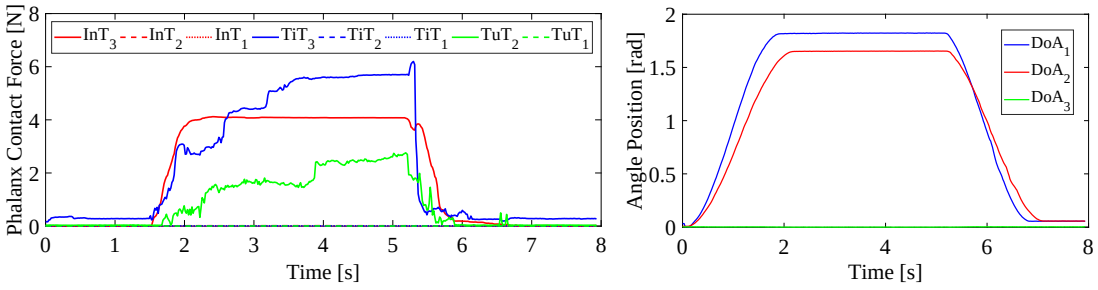

(a) Tactile curve without controller (b) Position curve without controller

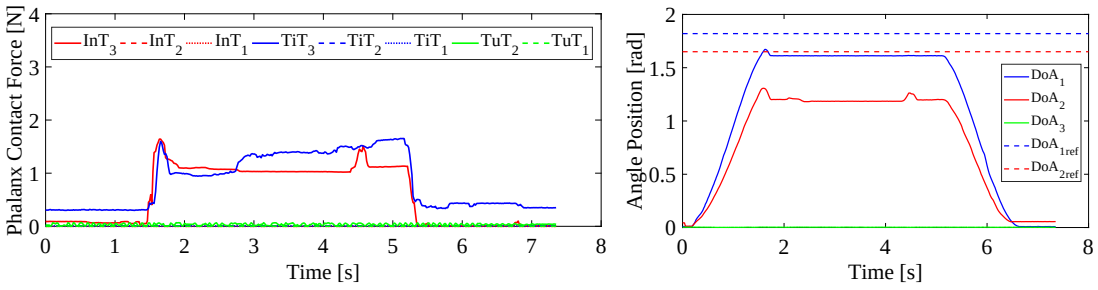

(c) Tactile curve with controller (d) Position curve with controller

Figure 3-20: HERI Hand phalanxes tactile curve and motor position curve without [(a), (b)] and with [(c), (d)] tactile sensor feedback admittance controller, where InT, TiT and TuT indicate the tactile from Index Finger, Third Finger (The finger utilized in DoA_1) and Thumb respectively, the number order 1, 2 and 3 represent the proximal, middle and distal phalanx correspondingly.

not specially analysis for fitting the shape of the cup. Because in majority condition for grasping unknown objects, we can not be aware of the suitable position command that we should deliver to appropriately adapt to the object profile. Therefore, it is significant and necessary for the robotic hands to equip with the tactile sensors

[66] and utilize the corresponding control based on them especially for avoiding soft objects being damaged.

As we mentioned before, the tactile sensor is distributed under elastic rubber on each phalanx as shown in Fig. 3-5, due to the irregular alternation of form on the elastic rubber after collision or contact with grasped objects, the pre-contact force between the tactile sensor and elastic rubber will be unknown modified. This will bring unavoidable negative effect to the calibration of the contact force measured by tactile sensors, this is also the explanation for the value of some contact forces possess positive offset, for instance TiT_3 in Fig. 3-20(c). Nevertheless, preliminary tactile sensors are able to show the variation and brief value of the practical contact force, and that will be capable enough to conduct the finger manipulation based on tactile feedback control such as the application shown in Fig. 3-19.

3.1.5.2.3 HERI Hand Versatility of Objects Grasping It is known that the under actuation of robotics hands can provide the self-adaptive property for objects grasping, which is significant and beneficial for control strategy simplification when grasping objects in different unknown shapes. Here we will demonstrate HERI Hand objects grasping versatility as shown in Fig. 3-21.

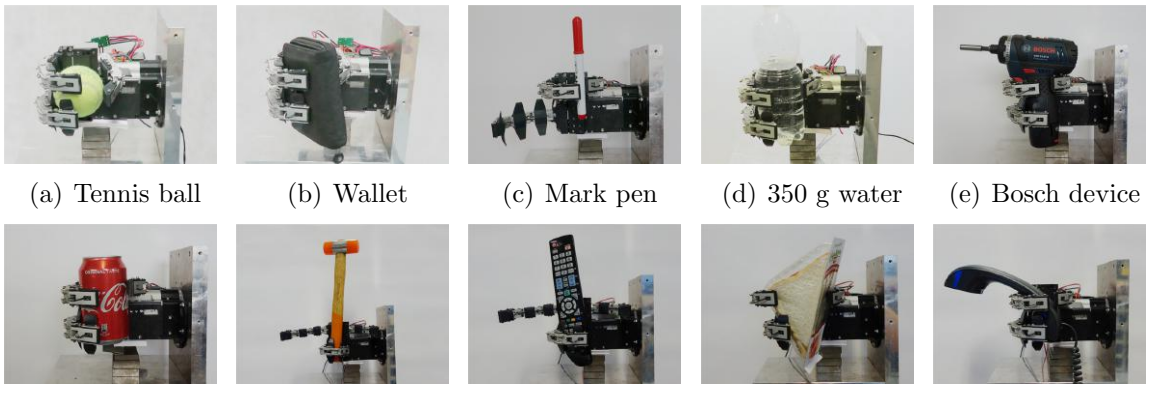

(a) Tennis ball (b) Wallet (c) Mark pen (d) 350 g water (e) Bosch device

(f) Coke can (g) Hammer (h) Remote control (i) Sandwich (j) Telephone

*Note that the metal steels under the hand is for supporting HERI Hand weight, since the connection interface between the hand and the basement are 3D printed in low strength material.

Figure 3-21: HERI Hand versatility of different objects grasping.

3.1.5.2.4 HERI II Hand Finger Independence Dexterity Since the design of HERI II Hand is adopting the modular finger design concept, which will bring the benefits for in-hand manipulation dexterity in terms of finger independence. Its related performance is demonstrated by holding the drill and repeatedly triggering the power on button, which fully utilised the dexterous property in terms of controlling each finger motion independently.

As shown in Fig. 3-22(a), the progress of repeatedly triggering Bosch drill is demonstrated and the corresponding contact force curves of four fingers during the experiment are shown from Fig. 3-22(b)-3-22(e). From Fig. 3-22(d) we can observe two peak contact force curves from Finger_3, which is the finger we controlled to press the trigger button twice. Fig. 3-22(f) demonstrates the curves of reference and measured absolute position of the tendon displacement for driving the under-actuated finger. The position steps are at 9 s and 15 s in Fig. 3-22(f), is evident and correspond to the two triggers motions. The vibration from working drill during the first trigger, caused change in the drill grasping posture. Finger_1, Finger_2 and Finger_4 were used to grasp the drill tighter in order to successfully realise the second trigger. As the drill button location with respect to the finger performing the trigger slightly changed during the second tighter grasping, the reference position of Finger_3 for second trigger was increased for ensuring success as shown in Fig. 3-22(f), which naturally leads to the bigger contact force on finger_3 as presented in Fig. 3-22(d). Finally the currents for driving the motors of four fingers are plotted in Fig. 3-22(g).

3.2 Legged Robots Strength Motion Design

In previous Section 2, we introduced the energy efficiency performance for legged robots design, however only possessing the energy efficiency can not satisfying the requirement of enhanced physical interactive performance, since in most application scenario legged robots ought to generate high strength force or torque to achieve desired explosive motion, such as lifting heavy objects, running or even jumping.

In this section, we will present the design details for achieving legged robots high

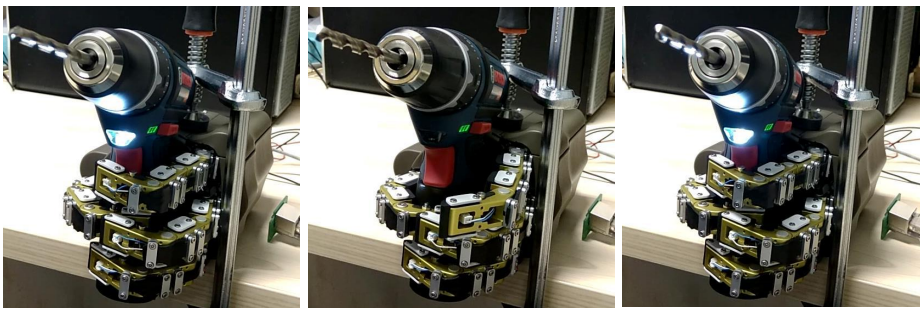

(a) Repeatable trigger experiment

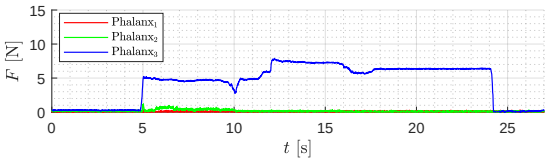

(b) Finger$_1$ tactile curve

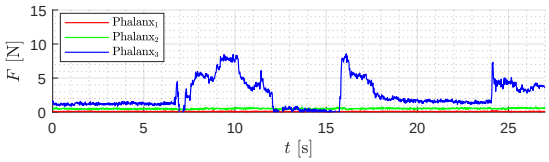

(c) Finger$_2$ tactile curve

(d) Finger$_3$ tactile curve

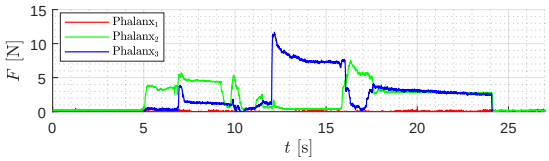

(e) Finger$_4$ tactile curve

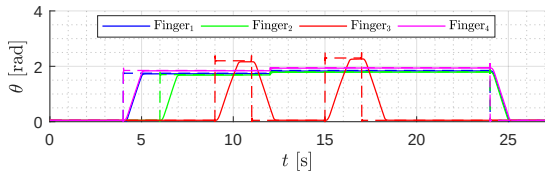

(f) Tendon displacements of four fingers

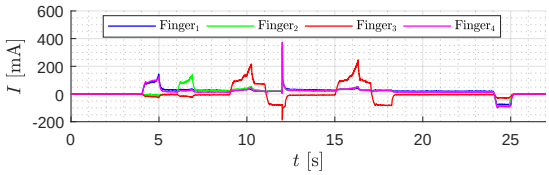

(g) Current curve of four driven motors

Figure 3-22: HERI II Hand dexterous manipulation of trigger drill repeatedly, Phalanx$_1$, Phalanx$_2$ and Phalanx$_3$ represent for proximal, middle and distal phalanx respectively, in (f) dashed line and solid line present reference position curve and measured position curve of four tendon displacements for finger flexion correspondingly.

strength motion in terms of actuators selection for Powerful Branch (PB) and high strength linear pretension tuning mechanism for Energy Storage Branch (ESB) units. Here we have to highlight that, the utilization of Asymmetrical Compliant Actuation (ACA) can not only bring advantages to energy efficiency as introduced in Section 2, but also can highly benefit the high strength motion performance, where the ESB unit can mitigate the torque load applied on Powerful Branch (PB), especially for leg robots knee joint actuation. Series of experiments verifying the design effectiveness

for high strength will be also shown in this section, to be more specific, eLeg jumping with 23 kg full load and ESB unit pretension tuning under high load.

3.2.1 Actuators Selection for High Strength motion

It is well known that from [67], in the field of legged robotics actuation design, there are three common Electro Magnetic (EM) actuator concepts, that manage these trade-offs for robotics are shown in Fig. 3-23.

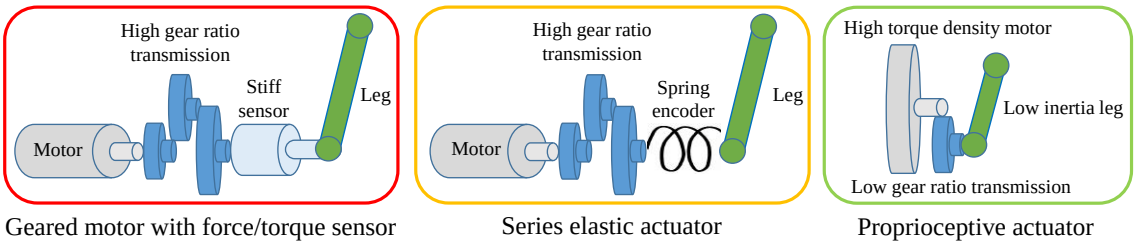

Figure 3-23: Three different Electro Magnetic (EM) actuator concepts, geared motor with force/torque sensor, Series Elastic Actuator (SEA), Proprioceptive force control actuator.

The geared motors with force/torque sensor (in high gear-ratio) are widely utilized in industrial field in terms of robotic arms for manipulation application since its adequate performance in high output torque density, wide bandwidth in position/torque due to the high stiffness as well as its reliable and accurate torque measurement ability through force/torque sensor. However the rigid stiff sensor causes the disadvantage in impact mitigation capability, which will high possibly lead to the damage for the core components of gearbox during unexpected external collision.

Therefore, the implementation of Series Elastic Actuator (SEA) actually solves the main disadvantage of geared motor with force/torque sensor, where the compliant spring with encoder can effectively absorb external impacts. Meanwhile it can also function as the torque measurement sensor by detecting the angle deflection as well as embedded as the energy storage elements for energy efficiency enhancement. But it should also be noticed that, the relatively low stiffness of the compliant structure in SEA will unavoidably shorten the response bandwidth of position/force control, which will eventually negative affect its dynamics motion performance.

Besides of these two aforementioned actuation concepts, nowadays researchers are more focusing on the utilization of proprioceptive actuators, which consist of high torque density motor with low gear ratio transmission instead of traditional high one. Under this configuration, the current feedback is allowed to measure the torque precisely, since the accurate parameter identification of the non-linear and time-varying gear box static friction is achievable in low gear ratio condition (planetary gearbox ix often utilized in this plan). This not only brings the advantage of cost reduction, hardware simplification but also the significant improvement in dynamic motion performance thanks to the high stiffness and low gear ratio. However, the fatal disadvantage for such actuation plan relies on its output torque density. The Elector Magnet (EM) principle based motor has almost reaches its performance limitation in terms of torque density, lacking of the argument from high gear ratio transmission, it is difficulty to implement this actuation concept to biped humanoid robots, which require extreme high output torque density actuation (considering about the hip, knee pitch joint and also the hip roll joint of biped robots).

In order to specifically and quantitatively analysis the performance comparison in terms of output torque density between Series Elastic Actuator (SEA) and proprioceptive actuator, we choose one typical SEA from one biped robot (iit WALK-MAN [68]) and one representative proprioceptive actuator from one quadruped robot (MIT Cheetah [67] [69]). By calculating and comparing their peak output torque density, it is simply to notice that SEA concept roughly possesses 3 times bigger than the proprioceptive actuator concept as shown in Table 3.7. Obviously, the proprioceptive actuator possesses excellent performance in dynamic motion, but our high strength design target for eLeg explosive motion will give more priority to evaluate actuators high output torque density ability.

Based on the aforementioned analysis for the tradeoffs among the three common actuation concepts, we are finally motivated to select the Series Elastic Actuator (SEA). Since one of our significant target of the eLeg design and development is its high strength performance for explosive motion, it is almost impossible for us to select the proprioceptive actuator for achieving such target. Meanwhile considering about

Table 3.7: Performance Comparison between Series Elastic Actuator (SEA) and Proprioceptive Actuator, picking up the typical iit WALKMAN Series Elastic Actuator (SEA) and MIT Cheetah Proprioceptive Actuator.

	SEA, iit WALK-MAN [68] at Trunk Pitch[1]			Proprioceptive Actuator, MIT Cheetah at Trunk Pitch[1]					
				1st Generation (Commercial)			2nd Generation (Costumed Design)		
Motor Type	KollMorgen TBMS-6025X-B			Emoteq HT-5001			MIT[2] [70]		
Motor Performance	Peak Torque [Nm]	Mass [Kg]	Torque Density[3] [Nm/Kg]	Peak Torque [Nm]	Mass [Kg]	Torque Density [Nm/Kg]	Peak Torque [Nm]	Mass [Kg]	Torque Density [Nm/Kg]
	2.56	0.398	6.43	21.3	2.57	8.29	29	1.07	27.1
	Gear Ratio 160:1			Gear Ratio 5.8:1					
Actuator Performance	Peak Torque [Nm]	Mass [Kg]	Torque Density [Nm/Kg]	Peak Torque [Nm]	Mass [Kg]	Torque Density [Nm/Kg]	Peak Torque [Nm]	Mass [Kg]	Torque Density [Nm/Kg]
	314	1.73	181.5	/[4]	/[4]	/[4]	110.25	1.825	60.41

Note: (1) Actuators at trunk pitch for biped and quadruped robots are usually designed to be the most crucial for output torque density demand, hence we select the trunk actuators from both actuation plans for comparison; (2) The motor of the proprioceptive actuator from Cheetah robot is originally from Dr. Niaja Nichole Farve's PhD thesis work [70] in the Department Electrical Engineering and Computer Science, MIT, which is a low-mass but high-torque motor dedicated for quadruped robot; (3) The torque density here actually describes the peak density, where the motor or actuator reaches their maximum torque generating limitation; (4) From the related publish paper, we can not find the corresponding information for the actuator performance based on the Emoteq HT-5001 torque motor.

the impact mitigation performance, the traditional geared motor with force/torque sensor will also be excluded, where the detailed analysis regard to this point will be presented in following Section 4.1.3.

3.2.2 High Strength Linear Pretension Tuning Mechanism

In Section 2.3, it is notable that the linear load on the bungee in knee joint Energy Storage Branch (ESB) unit can reach approximately 1150 N as shown in Fig. 2-12, which is a challenge in the mechanism and actuation design for achieving this high strength linear pretension tuning target. The selection of the ball screw bearing for undertaking the linear transmission task is considered for its high energy efficiency and compact size property. However the traditional design of the ball screw bearing is not suitable for such high payload pretension tuning application and we actually suffered several times from the problem of physically damaging the ball screw bearing nut at initial experiment stage. In this section, we will explain this specific reason and introduce the design method of the ball screw bearing, which is capable of resisting high linear force to adjust the bungee pretension in Energy Storage Branch (ESB) unit.

3.2.2.1 Symmetrical Load Ball Screw Bearing Design

To maximise the structure compactness, all Energy Storage Branch (ESB) units were originally designed to be single-sided, which is a normal design plan utilized in most application, where a single elastic element was used which was pretensioned by the ball screw, as shown in the left-hand side of Fig. 3-24. However, due to very high loading on the knee joint, this led to failure of several ball screws while adjusting pretension under load, due to excessive torsional moments on the nut. Hence, the knee unit was implemented using a single, longer element, both ends of which are attached to the ball screw nut and pass through a track on the knee (right side of Fig. 3-24). As the net line of force is now through the ball screw itself, this reduces the torsional moment on the nut to a minimum.

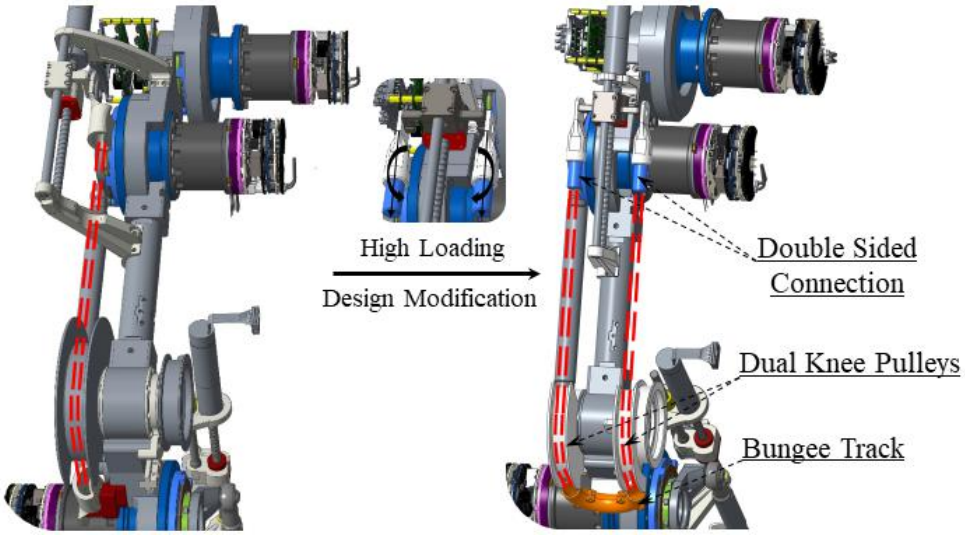

Figure 3-24: Modification of the knee ESB unit to improve high strength pretension tuning against high loading.

A section of eLeg knee joint is shown in Fig. 3-25. It shows both main knee pulleys and the track that connects them, routing the bungee around back to the ESB unit ball screw nut. Inside the right-hand side pulley, the free pulley can be seen that is used for the biarticulated configuration, routing the ankle bungee to its ESB unit on the back of the thigh.

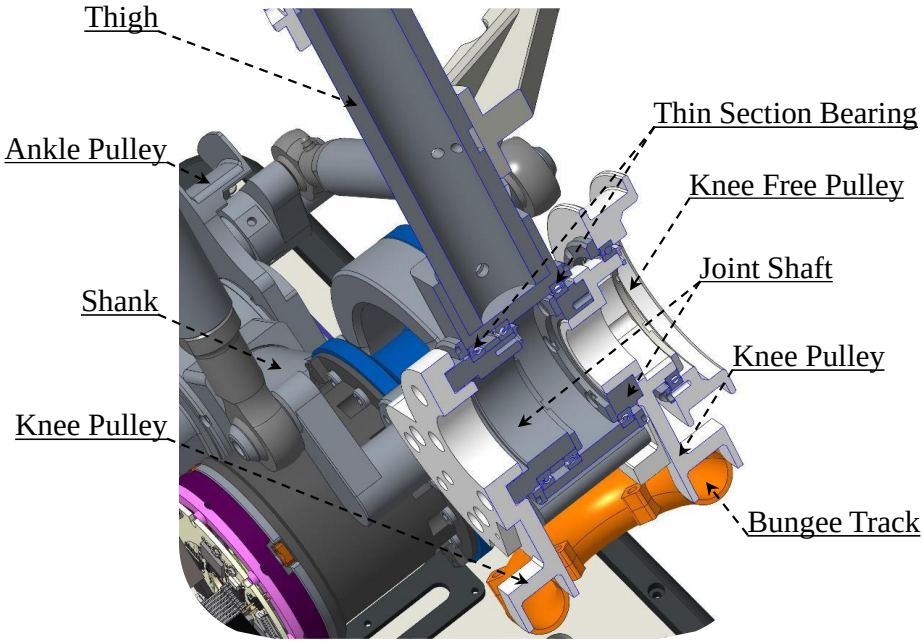

Figure 3-25: Section of eLeg knee joint with components annotated.

3.2.3 Experimental Validation and Results

3.2.3.1 Explosive Jumping Motion with 23 kg Load

For demonstrating the high strength performance of eLeg design in terms of specifically verifying the effectiveness of Series Elastic Actuator (SEA) and Energy Storage Branch (ESB) concept in high strength explosive motion, we designed a experimental scenario, where the eLeg in biarticulation configuration with 23 kg load was controlled to proceed explosive vertical jumping motion.

One highlight regard to such jumping experiment we need to emphasis is the anthropomorphic geometric size and weight of eLeg robot, whose size and weight is originally designed to be similar as a 1.70 m high adult. Specifically explaining about the weight, the self weight of eLeg body is 10.9 kg and the desired load is 23 kg, therefore the total weight of eLeg with load will reach 33.9 kg, considering about the potential of utilizing eLeg to build up a biped humanoid robot, the potential weight can reach 67.8 kg, quite close to a 1.7 m adult weight. Since it is well known that, miniature size robots [71] have already achieved impressive results in extreme jumping locomotion, however quite few researches and efforts have been focused on the anthropomorphic size and weight legged robot jumping. Therefore, even though the eLeg jumping experiment is still under going, we are still highly motivated to present and share some initial experimental results.

Similar to the deep squatting experiment in Section 2.3, we will firstly generate the cartesian trajectory (pure vertical jumping trajectory) of the CoM for the weight distributed at the trunk joint (w.r.t. ankle joint), and then through inverse kinematics the motion trajectory of each Powerful Branch (PB) actuator (ankle, knee and trunk) will be resulted, meanwhile each joint actuator will be controlled under torque control model (joint-level impedance control).

The corresponding jumping experiment is presented in Fig. 3-26, the maximum height (between the back edge of the foot and the ground) can reach 11 cm. Since eLeg main actuators (SEAs) are all distributed for joint pitch direction, we are not capable of controlling the posture of eLeg robot in roll (lateral) or yaw direction,

therefore it can be notable that there existed a slight tilting posture in roll when the leg landed on the ground. Hopefully due to the large size of the foot and well arrangement of the mass distribution, where the CoM of the eLeg is exactly in the middle plane of the robotics body in lateral direction, the eLeg can successfully achieve adequate self-balancing during landing.

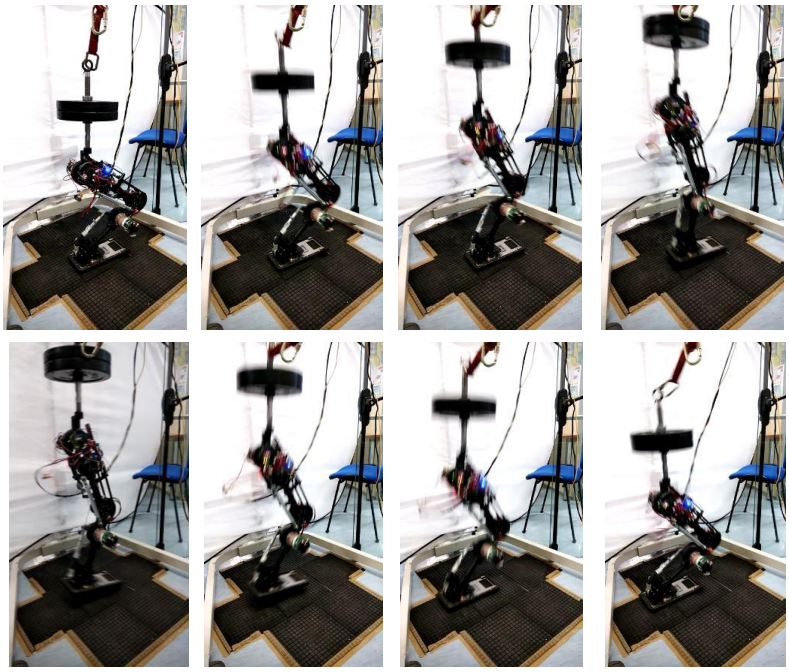

Figure 3-26: eLeg jumping motion with anthropomorphic load (23 kg) in biarticulation, where the maximum height can reach 11 cm.

Fig. 3-27 present the torque information applied on three main joint actuators during jumping motion, we can mainly focus on the knee joint actuator (Fig. 3-27(b)) due to severest load, where the main Series Elastic Actuator (SEA) has the ability to generate 127 Nm peak torque ($\tau_{PB,2}$, occurs at 0.95 s). It is a superb powerful performance in terms of high strength output density, which actually verifies the utilization of Series Elastic Actuator (SEA) for ensuring high strength motion. Meanwhile it is also notable that, the torque generated from knee joint Energy Storage Branch (ESB) units ($\tau_{p,2}$, the sum of $\tau_{p,2}^{mono}$ and $\tau_{p,2}^{bi}$ since biarticulation) can roughly reach 30 Nm during landing progress (within 0.85 s-1.05 s period), which will eventually contribute to the net torque on the knee joint (τ_2) up to 150 Nm (occurs at 0.95 s) for successfully

handling the enormous torque load during landing progress. As a result, apart from the energy efficiency enhancement advantages from Energy Storage Branch (ESB) units, it also verified that such concept utilization can also bring benefits to high strength explosive motion.

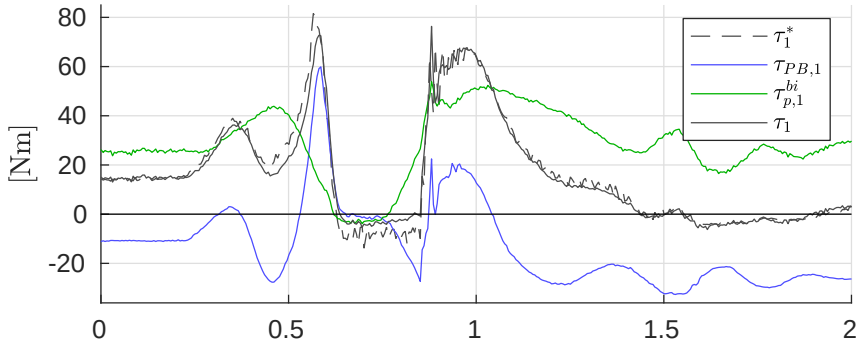

(a) Ankle joint

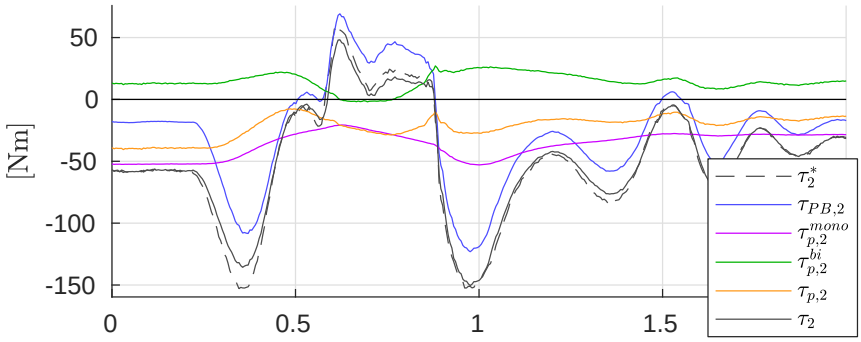

(b) Knee joint

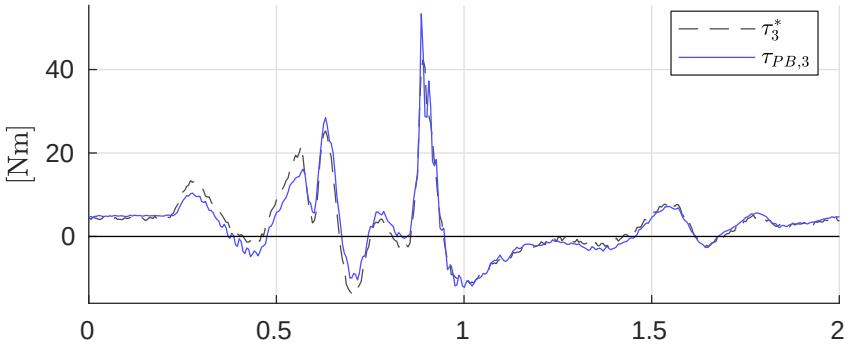

(c) Hip joint

Figure 3-27: Corresponding torque applied on each eLeg joint during 23 kg jumping motion, τ_1 and τ_2 represent the net torque on ankle and knee joint respectively, τ_3 presents the torque from hip joint SEA, τ^* is the desired output torque, τ_{PB} is the torque generated from SEA as Power Branch (PB) (only for ankle and knee joint), τ_p^{mono}, τ_p^{bi} and τ_p are the torque generated from monoarticulation ESB unit, biarticulation ESB unit and net ESB units.

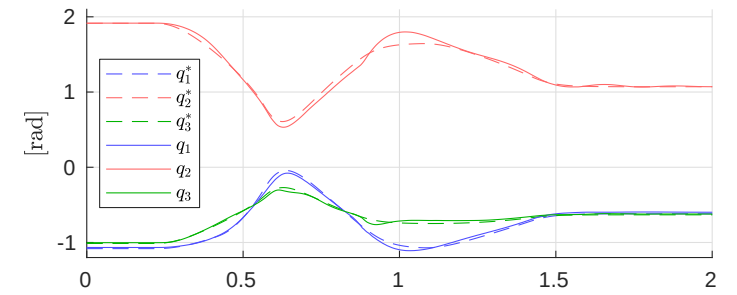

(a) Joints position

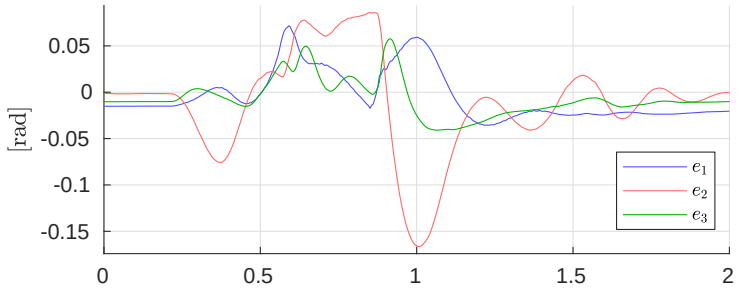

(b) Joints position tracking error

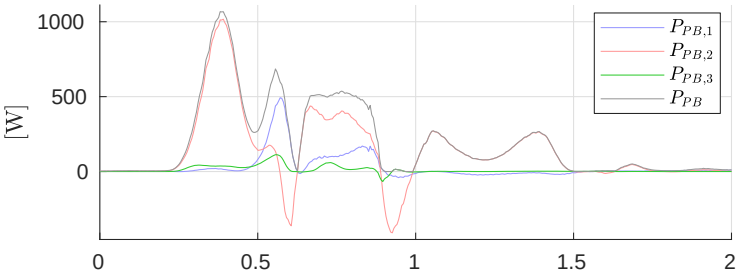

(c) Joints electrical power consumption

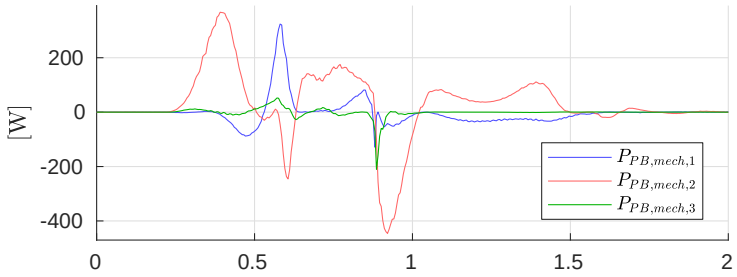

(d) Joints mechanical power consumption

Figure 3-28: SEA as Powerful Branch (PB) position tracking and power consumption in ankle, knee and hip joints, q_1, q_2 and q_3 are the position for ankle, knee and hip joints respectively, (naming order the same for the following) q^* is the desired position trajectory, e is the position tracking error, P_{PB} is the electrical power consumption and $P_{PB,mech}$ represents the mechanical power consumption.

Fig. 3-28(a) and Fig. 3-28(b) present the joint position trajectory and its tracking error for ankle, knee and hip joint during jumping motion, we can notice that the

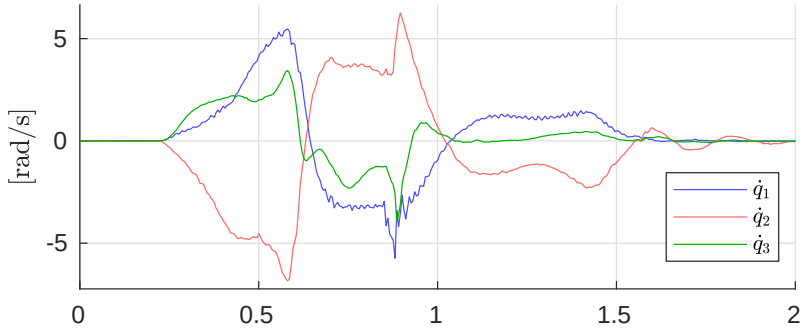

Figure 3-29: Joints velocity during jumping motion, $\dot{q}_1$, $\dot{q}_2$ and $\dot{q}_3$ are for ankle, knee and hip joint respectively.

tracking error of knee joint (e_2) increased when knee joint suffered from high torque load, thus the utilization of Energy Storage Branch (ESB) can also bring benefits for accuracy enhancement of position tracking under high load due to torque/force sharing from SEAs as Powerful Branch (PB). Fig. 3-28(c) and Fig. 3-28(d) present the power consumption in electrical and mechanical respectively, where the peak power for knee joint ($P_{PB,2}$) can reach approximately 1000 W proving the high strength (power density) performance of Series Elastic Actuation (SEA). From Fig. 3-28(d), we can notice the practical power consumption in mechanical is much lower than the electrical one, this relative low energy transfer efficiency is resulted from the enormous heating and friction for explosive motion, which is difficulty to improve due to the existing Elector Magnet (EM) motor principle.

The main issue that limits the maximum jumping height (11 cm) of eLeg is mainly the joint maximum velocity, especially the knee joint as shown in Fig. 3-29, where knee joint SEA has already reached its maximum angular speed (6.6 rad/s). This maximum actuator output speed is actually limited by the maximum speed (5040 rpm, 48 V) of the motor (Kollmorgen-TBMS-6025) embedded. Ideally and theoretically speaking, eLeg robot is not capable of jumping higher than 11 cm with 23 kg load under the current hardware configuration, however eLeg is still supposed to carry more weight load to achieve the same jumping height. To be more specific, from Fig. 3-27(b), we can be aware of that the knee joint (suffered from the highest load) SEA output torque ($\tau_{PB,2}$) has actually not reached its desired maximum value 127 N, meanwhile

the corresponding torque generated by the ESB units ($\tau_{p,2} = \tau_{p,2}^{mono} + \tau_{p,2}^{bi}$) have also much potential to increase, these two aforementioned points will eventually result in enhancing the jumping ability with more load weight while meanwhile remain the maximum knee joint output angular speed (maintaining the same jumping height).

3.2.3.2 ESB Unit Pretension Tuning in High Load Squatting

To demonstrate the effectiveness of the actuation concepts and design procedure for high strength tuning ESB units, we provide experimental data obtained during cyclic deep squatting motions, with the leg in monoarticulated actuation configuration and loaded with 23 kg weight at the trunk. Contrary to our earlier preliminary experiments [44] as shown in Section 2.3, we focus on the knee joint ESB and adjust the pretension during the motion. Furthermore, instead of position control, the entire robot was torque controlled, where the torque generated by the ESB (obtained from the linear force measurements) was subtracted from the impedance torque reference to compute desired SEA torque and achieve accurate joint-level impedance control, i.e.:

$$\tau_{SEA}^{*} = K\left(q^{*} - q\right) + D\left(\dot{q}^{*} - \dot{q}\right) - \tau_{ESB} \tag{3.6}$$

where K, D denote the joint impedance parameters, q^{*} and q denote the joint equilibrium and actual position, respectively, and τ_{ESB} denotes the measured ESB torque.

Fig. 3-30 shows the results. Following two increases in pretension from 5 mm to 85 mm as shown in Fig. 3-30(a) to 3-30(b), the RMS torque provided by the SEA is reduced from 42 Nm to 20 Nm, as the torque provided by the ESB increases as presented in Fig. 3-30(c). Meanwhile, the net knee torque remains constant to achieve the desired motion profile. For demonstration purposes, a low linear adjustment speed of pretension tuning in 3 mm/s was used. After the increase in pretension, the linear force applied on the ball screw mechanism from the bungee can be seen in Fig 3-30(d) to reach 1190 N, which verifies the high strength pretension tuning ability of the ESB

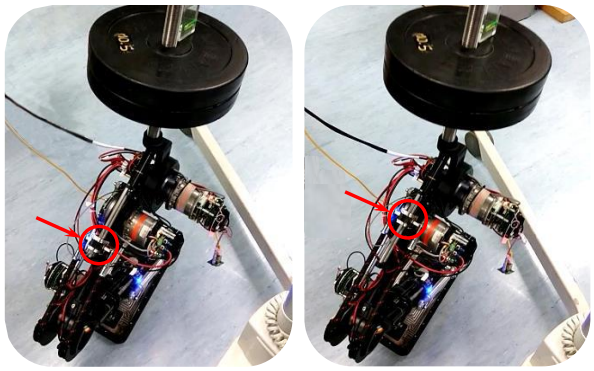

(a) 5 mm pretension (b) 85 mm pretension

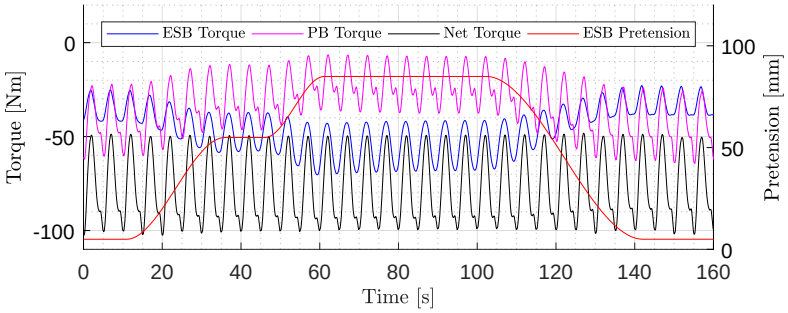

(c) Knee joint PB, ESB, and net torque.

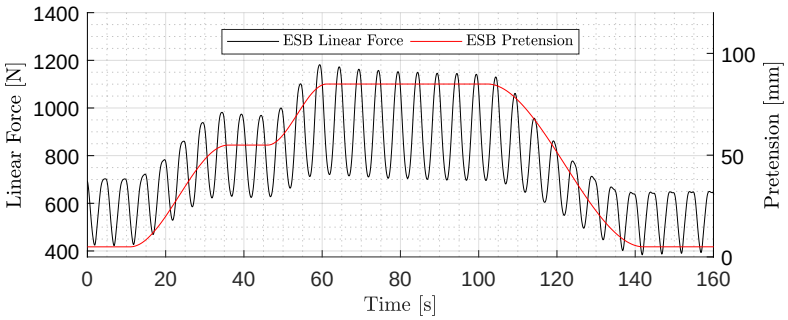

(d) Knee joint linear force as measured by the ESB unit.

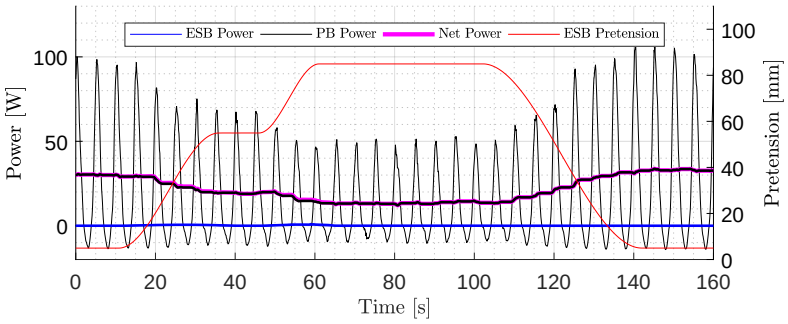

(e) Knee joint PB, ESB and net electrical power.

Figure 3-30: eLeg adjusting knee ESB pretension during cyclic deep squatting motions with 23 kg trunk load.

unit design under high load.

Fig. 3-30(e) shows Powerful Branch (PB), Energy Storage Branch (ESB), and net electrical power consumption on knee joint. Despite the same net torque (and mechanical power) being provided at the joint, the cycle mean net electrical power decreases from 29.7 W to 11.1 W as the ESB is pretensioned, a significant improvement in energy efficiency of **63%** is achieved. Particularly, it can be observed that the power of the ESB unit is negligible. However, it can be observed that at 5 mm pretension the ESB is already providing nearly half of the torque requirements; if the pretensioned case would be compared to the case where the ESB was dismounted (SEA only), the difference in electrical power consumption would be significantly larger.

3.3 Summary

In this section, we mainly discussed the high strength actuation and mechanism design, specifically in term of robotic hands high strength grasping priority design and legged robots explosive motion design.

In the first part regard to robotic hands high strength grasping priority design, we have to highlight again, currently there is nearly no general design method to mimic humankind hands functions perfectly, which means the robotic hands possessing perfect performances in both high strength and dexterity as human being. Therefore, the design method of the desired hands (HERI and HERI II Hand) is following the functionality priority of achieving high strength grasping at first, and meanwhile remaining the dexterity to maximum extent. Hence, firstly we introduced the utilization of under actuation principle by presenting the under actuated finger design in terms of specific finger phalanx, kinematic analysis, actuator selection and sensor configuration. Secondly, we presented the important finger distribution and Degree of Actuation (DoA) assignment scheme for both HERI and HERI II Hand, highlighting the iteration motivation from HERI to HERI II Hand is for further enhancing the high strength grasping ability. Thirdly, a significant concept (Finger Module Design) that we adopted on HERI II Hand to argument the high strength

performance as well as HERI II Hand hardware development details were introduced. Meanwhile, since HERI II Hand is desired to be mounted on Centauro robot [47], so the compact integration property with Centauro forearm was also described. Last but not least, corresponding experiments and results for verifying the design effectiveness were presented, to be more specific, the weight-grasping ratio experiment and its results directly prove the high strength performance enhancement from HERI to HERI II Hand, various of dexterous and delicate manipulation application of HERI and HERI II Hands indicate that we effectively maintain the performance balance for manipulation dexterity under the functionality priority of high strength grasping.

In the second part, firstly we introduced the design method for achieving high strength explosive motion on legged robots. Three common actuators plans for legged robots actuation were introduced and their corresponding actuation characteristics and performances were also analyzed and compared. By considering the high strength explosive motion requirement, SEA actuation was finally selected as the main actuators for Powerful Branch (PB) for its high output torque/mass density. Secondly, for achieving further energy efficiency during deep squatting motion, it requires Energy Storage Branch (ESB) units to possess high strength pretension tuning ability for elastic bungees. We presented the design and development details of corresponding ESB units for linear tuning under high load, especially the symmetrical-load ball screw bearing design was highlighted. Finally, on the basis of all the aforementioned design method, two experiments were processed and its results are presented for verifying the design effectiveness, where the first one is full load (23 kg) jumping test and the second one is the active ESB unit pretension tuning test under high load (23 kg) deep squatting. The experimental results demonstrate that eLeg robot wigh SEA actuation and ESB unit has the ability of jumping up to 11 cm height with 23 kg load, also the ESB unit can successfully tune the pretension of the elastic bungee under high linear load (maximum 1200 N) and result in a **63%** energy efficiency enhancement.

Chapter 4

Robust Physical Sturdiness Design

In previous two sections, we introduced the design method and development details of energy efficiency and high strength for enhancing the physical interactive performance of robot bodies. In this section, we will mainly introduce the design regard to physical sturdiness mechanism specifically in terms of the utilization of compliant structures, which will be embedded on HERI II Hand and eLeg for physical sturdiness enhancement. Series of experiments will be proceeded for verifying its effectiveness.

As a matter of fact, physical sturdiness possesses a significant meaning for physical robotic interactive performance in real external environment and application, where physical interactive in common occurs as unexpected collision that may cause damage to robotic bodies. Although nowadays researchers have developed various of dedicated sensory feedback based control strategy for avoiding physical collision and protecting robot bodies to greatest extent, it is still quite difficult to totally avoid collision especially when urgent situations happens such as the whole robotic system shut down and the dedicated control strategy could not be functional. Based on this situation, it is required the robotic hardware bodies should be equipped with corresponding physical sturdiness mechanisms in order to successfully survive in real practical, complicate and unknown application scenarios, such as disaster response, construction field and elderly people caring.

4.1 Compliant Mechanism Design

Quantities of successful applications for compliant mechanism adoption in robotic design field prove the utilization of soft structures and bodies can effectively improve the physical sturdiness performance in terms of resisting external collisions and impacts, especially our discussed robotic hands and anthropomorphic legs that directly and physically interact with external environments (grasping objects/supporting robot bodies). In this section, we will present the design and development of compliant structures on robotic hands and legged robots, to be specific in terms of under actuated mechanism, damping structure and compliant actuation. Series experiments and corresponding results will be demonstrated for verifying the design effectiveness.

4.1.1 Under Actuated Mechanism in Robotic Hands

In previous Section 3.1.1, we focused on introducing the utilization of under actuation for contributing the high strength grasping of robotic hands. As a matter of fact, another significant advantage for adopting under actuation is its excellent performance in physical sturdiness. For fully actuated hands, miniature motors with low gear ratio as well as rigid mechanical transmission are commonly adopted and embedded in very compact size. Due to relative weak output torque ability, these motors are not able to resist high torque impact from external environment. Applying impedance joint level control in low stiffness on fully actuated hands is also difficult, since one side the aforementioned miniature motors usually can not provide accurate force/torque sensory feedback, the other side is the whole control strategy and system will no doubt become complicated and redundancy simply due to the enormous driven joints quantity. Unlike fully actuated hands [39, 40, 41, 42], finger joints in under actuated hands are in common soft thanks to the under actuation principle and flexible mechanism transmission (tendon) adopted, this will actually provide extremely high potential for resisting external collision to maximum extent. Corresponding experimental verification will be detailed presented in following Section 4.2.1, where during the practical

test a fully actuated hand (Schunk Hand [72]) and a under-actuated hand (HERI II Hand) were mounted on the two arms of Centauro robot [47] for undertaking different functional priority grasping missions.

4.1.2 Damping Mechanism in Robotics Hands

As a matter of fact, facing collisions from external environment, the under actuation on robotic hands will only be functional in finger flexion-close motion direction (defined as pitch positive direction). For further enhancing the physical sturdiness on the adopted *Da Vinci's Mechanism* [55] under actuated finger, we have to still consider the compliance in both finger lateral abduction/adduction motion direction (defined as roll direction) and finger flexion-extension (defined as pitch negative direction), which are similar as the equipped compliance in human hand. In following content, we will introduce the damping mechanism design as passive compliance structures on under actuated fingers (module fingers) of HERI II Hand in both roll and pitch negative direction.

To escalate the physical sturdiness of HERI II Hand finger modules in roll direction, it is essential to overcome the rigidity of the finger in lateral abduction/adduction plane without increasing the actuation and structure complexity. We therefore introduce a spring loaded passive roll joint at the base of the finger unit as shown in Fig. 4-1(a). We limit the deflection range to $\theta_r = \pm 5^\circ$ through mechanical end-stop, and target a desired stiffness of $k_r = 15\,\mathrm{Nm/rad}$ for this compliant joint, thereby standing over 1 kg at the finger tip without reaching full deflection. Fig. 4-1(a) shows the corresponding forces on the finger module. The torque τ_r on the roll joint is given by

$$\begin{aligned} \tau_r &= k_r \cdot \theta_r \\ &= f_t \cdot l_t = f_l \cdot l_l, \end{aligned} \tag{4.1}$$

where l_t and l_l are the finger tip length and leaf spring lever length respectively, and f_t and f_l are the forces associated with these locations. When the maximum deflection

of the joint occurs, the aforesaid stiffness generates $f_l = 130.5\,\mathrm{N}$ on the leaf spring, corresponding to $f_t = 11.9\,\mathrm{N}$, considering that the relevant lengths are $l_l = 10\,\mathrm{mm}$ and $l_t = 110\,\mathrm{mm}$. A leaf spring in accordance with the aforesaid specifications in terms of stiffness and strength, as well al compatible with available space, is therefore designed, on the basis of a clamp-free cantilevered beam concept. The placement of the two leaf springs, for replicating compliance in two directions, is shown in Fig. 4-1(a). The Finite Element Method (FEM) analysis results of the beam, including strain, stress and displacement, are presented in Fig. 4-2, where 17-4PH H900 steel was selected as the leaf spring material. The stiffness of the final design is therefore obtained as 13.2 Nm/rad.

For the modular finger pitch negative direction compliant structure design, we simply embedded a damping rubber at the end of tendon route, where the tendon fixed with a steel rod as shown clearly in Fig. 4-1(b). The material of this specific damping rubber is UPX 8400 in Shore A-45. Each finger phalanx is specifically designed with a mechanical end-stop between each other, when the corresponding phalanxes angle deflection reaches -2°. Such kind of damping and mechanical end-stop design can effectively prevent the tendon from broken due to external collisions, which will finally enhance the physical sturdiness in terms of tendon transmission reliability.

4.1.3 Compliant Actuation Implementation on Legged Robots

In Section 3.2.1, we introduced one of the significant reasons that we selected Series Elastic Actuation (SEA) concept as the Power Branch (PB) actuator on eLeg robot among three common actuation plans, which is its high output torque/mass density that directly enhances the high strength ability for explosive motion.

Actually another important reason for adopting Series Elastic Actuation (SEA) concept relies on its adequate performance for resisting external high impact, which is the performance we seek on actuator hardware level for enhancing physical sturdiness property. It is well known that the utilization of compliant structure, which is in common series embedded between the gearbox and output link in SEA, functioning

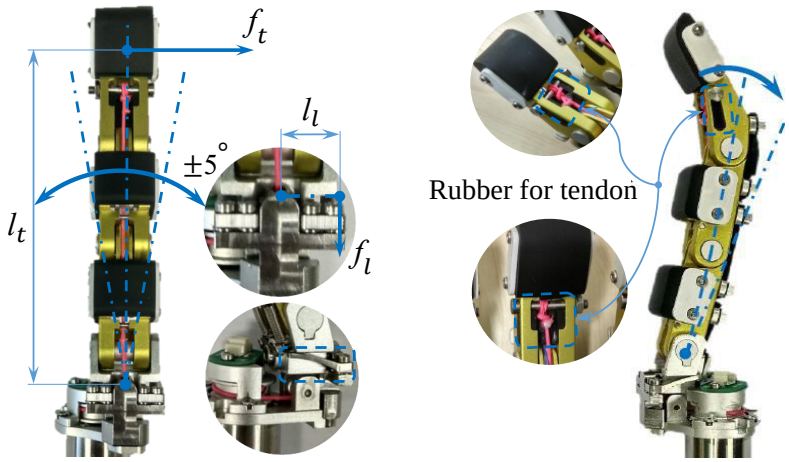

(a) Leaf spring design (b) Damping rubber design

Figure 4-1: Compliant structure in (a) roll and (b) pitch negative direction on the finger module of HERI II Hand.

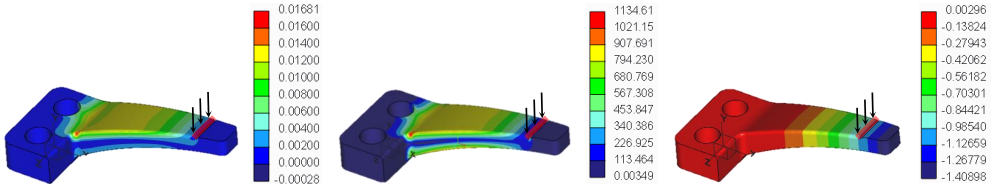

(a) Strain (b) Stress (MPa) (c) Displacement (mm)

Figure 4-2: FEM analysis for leaf spring on the finger module of HERI II Hand.

as a core part to physically absorb external collisions.

In the utilized Series Elastic Actuator (SEA), the compliant structure and its deflection encoder based torque sensor could be shown in Fig. 4-3, the corresponding information about the compliant structure design and deflection encoder based torque sensor could be refer in [48].

Since we know that the selection of the compliant structure stiffness is vital for the whole actuator performance. To be more specific, it is actually a hard trade-off between low-stiffness beneficial transparency and high-stiffness beneficial response bandwidth [73]. Low stiffness selection will no doubt enhance actuator collision resistance performance, but it will unavoidably bring significant negative effects to actuator performances in terms of accurately and agilely tracking desired position and torque trajectory. After tough trade-off and theoretical analysis [73], the optimised

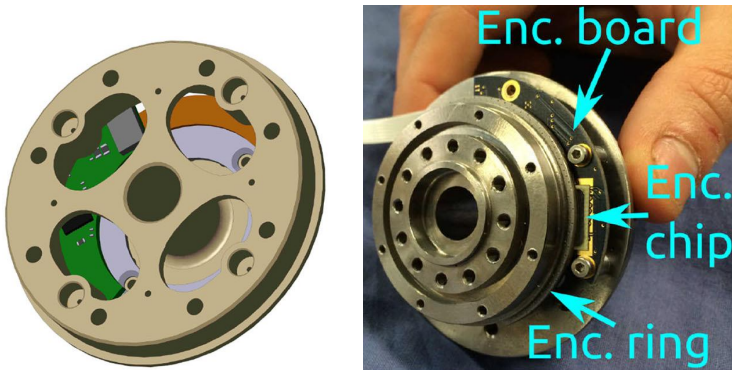

(a) Compliant structure (b) Angle deflection encoder

Figure 4-3: Schematics of the compliant structure with deflection encoder based torque sensor in Series Elastic Actuator for eLeg robot.

stiffness of 5800 Nm/rad was finally selected as Table 2.1 presents.

4.2 Experimental Validation and Results

In this section, we will demonstrate corresponding experimental tests and results for verifying the design effectiveness in terms of physical sturdiness design on robotic hands (HERI II Hand) and legged robots (eLeg).

4.2.1 HERI II Hand in Real Application

During *CENTAURO Project* (as refer in Appendix A) final evaluation camp in *KHG Company* (Karlsurhe, Germany), HERI II Hand (under actuated principle) and Schunk Hand (fully actuated principle) were both mounted on Centauro robot to proceed different requirements of grasping tasks as shown in Fig. 4-4, while under actuated HERI II Hand is desired to process robust and high strength grasping and fully actuated Schunk Hand is responsible for delicate and precise manipulation and grasping.

As a matter of fact, during the 5-day *CENTAURO Project* final evaluation camp, the physical sturdiness performance of fully actuated Schunk Hand can not be comparable regard to HERI II Hand. Even though Schunk Hand is controlled to achieve relative gentle and precise grasping missions, its rigid joints and body structures still suffered from physical damage for several times, even once the damage came from the

Figure 4-4: HERI II Hand and Schunk Hand mounted on Centauro robot in CENTAURO project final evaluation camp.

self-collision between Schunk Hand and Centauro leg during initial posture calibration progress. Schunk Hand possesses a extremely excellent design in terms of anthropomorphic and it can mimic the majority of delicate human hand grasping motion, however from the real application test experience, the fully actuation indeed brought enormous negative effects in terms of physical sturdiness performance. This is actually a quite significant issue that we have to focus on, since without the fundamental reliable physical sturdiness, it is meaningless to discuss about other performances that based on it.

During practical testing, we also noticed that the fully actuated hand often caused a problem when the end-effector approaching the object, where the rigid finger directly pushed the object away or fall down that directly leading to the failure of grasping. This will actually highly require the corresponding manipulation robotic arm to equipped with a high accurate vision feedback, path planning and motion control, while the soft under actuated principle robotic hand could provide relative

error tolerance regard to the aforementioned point.

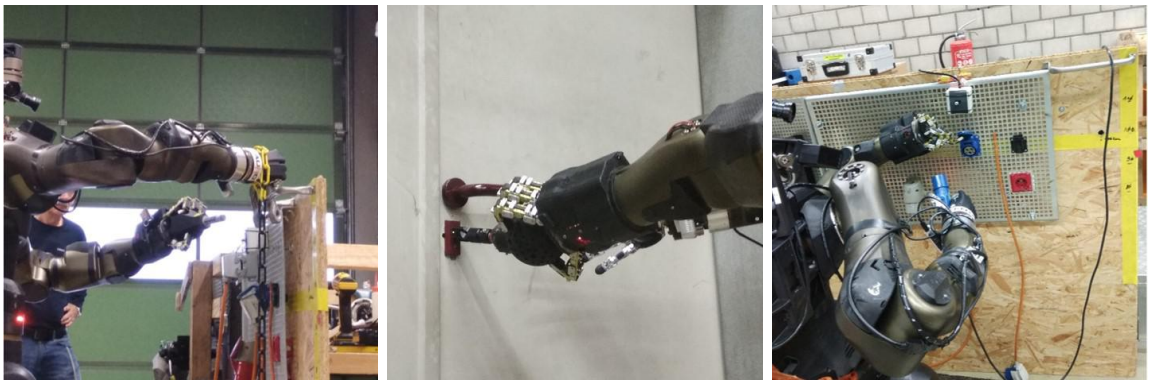

(a) Lock the chain (b) Open door by key (c) Open socket cup

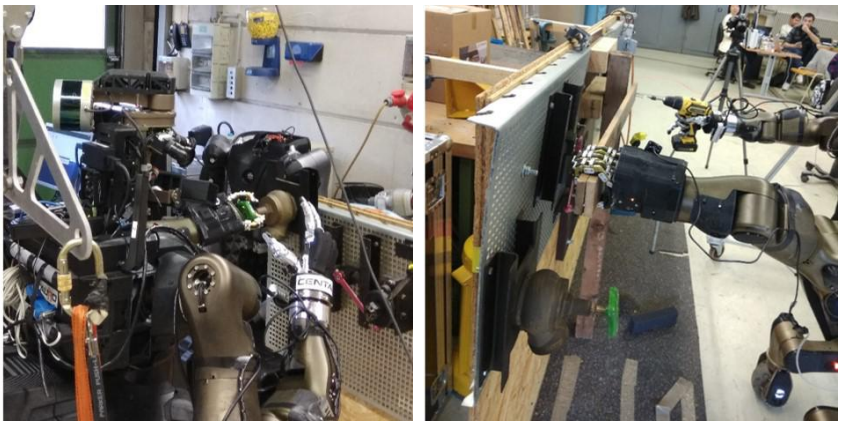

(d) Open valve (e) Fix long wood when drilling

Figure 4-5: HERI II Hand series of grasping applications in real application scenario, *CENTAURO project* final evaluation camp.

Fig. 4-5 demonstrate series of grasping applications of HERI II Hand during practical mission in *CENTAURO project* final evaluation camp. The majority of the external environment is unknown and HERI II Hand can survive and successfully finish the mission as shown in Fig. 4-5(a)-Fig. 4-5(c), such as locking the chain, opening door by key and opening socket cup. Here we have to highlight the application in Fig. 4-5(d) and Fig. 4-5(e), successfully rotating and opening valve as well as fixing long wood when drilling do not only require the HERI II Hand to possess high strength grasping ability as we discussed in the previous section, but also require high physical sturdiness, since the whole hand body will suffer from huge external disturbances and collisions. It is notable that the high level manipulation motion control

and path planning will have some unavoidable inaccuracy in practical application scenario, the compliance mechanism design in HERI II Hand is the key to survive and provides more inaccuracy tolerance for mission accomplishment.

4.2.2 eLeg High Impact Resistance in Jumping

For verifying the effectiveness of the design in terms of resisting collision for eLeg, the same experiment with 23 kg full load jumping was proceeded as shown in previous Section 3.2.3.1. The whole eleg robot weights more than 30 kg with load, we successfully proceeded the jumping testing for more than 100 times without any hardware failure, thanks to the utilization of compliance in both actuation (SEA) and mechanism (sole rubber on foot).

4.3 Summary

Soft is strong.

This is the most significant lesson that we learned from the physical interactive performance robotic body design in terms of physical sturdiness, as you can check quantities of compliant structures were adopted for corresponding robotic hands and legged robots, which possess adequate sturdiness performances in real application.

The most significant design method for enhancing compliance on robotic hands is the under actuation utilization, where each finger joint will become compliant, highly reducing the risk of hardware failure when unexpected external collision occurs. Meanwhile the damping structure adopted for each finger module (HERI II Hand) will allow the compliance in finger lateral direction, further enhancing the physical interactive performance in terms of sturdiness. For legged robots leg body design, which will support the whole robot weight and have high chances suffering from external high load impact, compliance in Series Elastic Actuator (SEA) highly shows its advantage for absorbing collisions.

Series of experiments for verifying the compliant mechanism adopting effectiveness for physical sturdiness have been done. For HERI II Hand, quantities of practical

grasping and manipulation applications have been proceeded in *CENTAURO project* final evaluation camp, various of external collisions have been applied on HERI II Hand without resulting in hardware damage in 5-day testing. Last but not least, the applying of SEA for augmenting physical sturdiness has been verified effectively from the more than 100 times repeatable high load (23 kg) eLeg jumping experiments.

Chapter 5

Conclusion and Future Work

5.1 Conclusion

In this thesis, the work related to the enhanced physical interactive performance robot bodies are detailed introduced in terms of both specific design methods and implement details, with corresponding experimental tests and results that verifying the design effectiveness. Since it is well known that, enhanced physical interactive performance robot bodies design is significant but fundamental for robots entering into real application scenarios in the future and we mainly focus on the exploration of enhanced physical interactive performances in the following three aspects, high energy efficiency, high strength and physical sturdiness particularly on articulated legged robots and robotic hands.

In the first part of the thesis, we mainly introduce the utilization of novel Asymmetrical Compliant Actuation (ACA) concept and prove its capability of enhancing energy efficiency on legged robots. ACA concept actually consists of actuation in Powerful Branch (PB) and Energy Storage Branch (ESB) respectively. A 3-DoF legged robot named eLeg was developed for verifying the design effectiveness by equipping with the interchangeable ESB units. Meanwhile the specific ESB units design method and development details are also presented. Finally, a dedicate designed experiment of using eLeg to process a deep cyclic squat motion with 23 kg load was proceeded, we noticed an energy efficiency enhancement by **53%** and **60%** respectively in mono

and biarticulation, which effectively verified the ACA concept effectiveness.

The second part is focusing on the introduction of design method for enhancing high strength performance, which is applied on robotic hands and legged robots application.

For robotic hands under the design priority of high strength grasping, we firstly introduce the under actuated principle robotic finger design and development details for enhancing high strength grasping. Secondly we present the finger distribution and Degree of Actuation (DoA) arrangement principle on HERI and HERI II Hand as well as the iteration motivation between this two generations, which is considered for further high strength grasping priority. My thesis contribution relies on the novel design and development of robotics bodies for enhanced physical interactive performance and we experimentally verified the design effectiveness in specific designed scenario and practical application. Thirdly a significant design method of using finger module concept on HERI II Hand is described and its development details are demonstrated. Furthermore, since HERI II Hand is designed to be mounted with Centauro robot, the physical integration property between HERI II Hand and Centauro forearm is also presented. Last but not least, various of experiments for verifying the design effectiveness of HERI and HERI II Hands in terms of high grasping strength and dexterous manipulation performances are proceeded. For highlighting, there is a 2.2 times enhancement in terms of weight-grasping ratio from HERI to HERI II Hand by following the aforementioned design method of ensuring high strength grasping priority.

For the design of ensuring legged robots high strength explosive motion, firstly the selection of the actuator to enable the high strength output ability is introduced (namely SEA), then we introduce the specific design of linear pretension tuning mechanism of ESB units under high load by adopting symmetrical load ball screw bearing plan. Finally, eLeg jumping motion with 23 kg load was successfully achieved and prove the correctness of selecting SEA as the main actuation plan for high strength ability. Besides of this, the experiment of ESB unit pretension tuning under high load deep cyclic squatting verified the corresponding high strength design effectiveness and

meanwhile achieved a further **63%** energy efficiency enhancement.

In the third part, we introduce the design method for enhancing physical sturdiness by presenting the compliant mechanism that embedded on desired robotic hand (HERI II Hand) and legged robot (eLeg) in terms of under actuation, damping mechanism and compliant structure in SEAs. Corresponding experiments, such as HERI II Hand real application in *CENTAURO Project* final evaluation camp and eLeg survival in high load (23 kg) jumping impact, proving the compliant mechanism is an effective design method to enhance physical sturdiness, soft is actually strong.

In conclusion, my thesis provides the design method and development details for enhanced physical interactive performance robot bodies, which are specifically in terms of energy efficiency, high strength and physical sturdiness. Not only the theoretical analysis, design principle and corresponding verification experiments and results are introduced, but also the practical engineer development details are presented in this work, which I wish could contribute to this particular robotics hardware development field of enhanced physical interactive performances and even provide beneficial guidance and references to the whole robotic community.

5.2 Future Work

5.2.1 Full Sensory Feedback Grasping Control

Since as we mentioned, HERI series Hands (HERI and HERI II Hand) are equipped with corresponding tactile sensors, absolute angle encoders and current feedback for each finger module as introduced in Session 3.1.1.3. Currently, we successfully utilized the position and tactile sensor feedback to achieve soft and gentle grasping as shown in Fig. 3-19. In our future work, we will develop the dedicated grasping control algorithm of HERI Series Hand by including full sensory feedback, especially the motor current reading.

5.2.2 Field Weakening Control for Higher eLeg Jumping

As we mentioned in Section 3.2.3, the maximum jumping height in biarticulation is limited by the maximum angular speed of knee joint, which is 6.6 rad/s. This is actually restricted by the Kollmorgen TBMS 6025 motor embedded in the actuator, where the normal power supply (48 V) decides the maximum motor speed in 5042 rpm. On the basis of not increasing power supply voltage for safety consideration, we can utilize specific field weakening control method [74] to speed up the maximum motor speed, so that the explosive motion of eLeg can be further enhanced in terms of jumping height.

5.2.3 Dedicated Pretension Tuning Control for Higher eLeg Energy Efficiency

The experiment we proceed in Section 3.2.3.2 for verifying the Energy Storage Branch (ESB) unit pretension adjustment effectiveness for energy efficiency during eLeg deep squatting motion, as we can notice, the tuning pretension is manually set, to be more specific, from 5 mm to 85 mm shown in Fig. 3-30. However, the pretension is not automatically set according to the optimised torque applied on knee joint for higher energy efficiency. Therefore in the short future, we will develop dedicated pretension tuning control strategy for further energy efficiency enhancement.

Appendix A

CENTAURO ROBOT

Disaster scenarios, like the Fukushima nuclear accident, clearly show that the capabilities of today's disaster response robots are not sufficient for providing the needed support to rescue workers.

The CENTAURO project aims at development of a human-robot symbiotic system where a human operator is telepresent with its whole body in a Centaur-like robot, which is capable of robust locomotion and dexterous manipulation in the rough terrain and austere conditions characteristic of disasters.

The CENTAURO robot will consist of a four-legged basis and an anthropomorphic upper body and will be driven by lightweight, compliant actuators. It will be able to navigate in affected man-made environments, including the inside of buildings and stairs, which are cluttered with debris and partially collapsed.

The Centauro system will be capable of using unmodified human tools for solving complex bimanual manipulation tasks, such as connecting a hose or opening a valve, in order to relieve the situation. A human operator will control the robot intuitively using a full-body telepresence suit that provides visual, auditory, and upper body haptic feedback. Rich sensors will provide the necessary situation awareness. Robot percepts and suggested actions will be displayed to the operator with augmented reality techniques. For routine manipulation and navigation tasks, autonomous robot skills will be developed. This will allow for taking the operator partially out of the control loop, which will be necessary to cope with communication latencies and

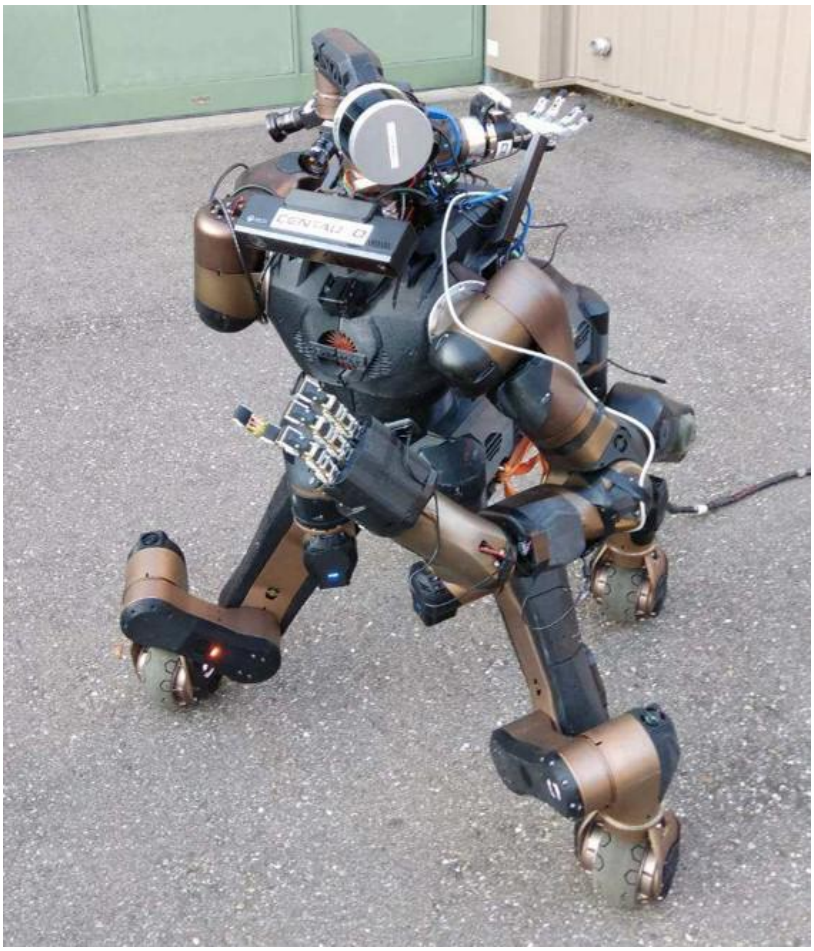

Figure A-1: Centauro robot in final evaluation camp, Karlsruhe, Germany

bandwidth limitations and to reduce the operator workload.

A series of increasingly complex tests with corresponding evaluation criteria will be devised from end-user requirements to systematically benchmark the capabilities of the developed disaster response system.

This project has received funding from the European Union's Horizon 2020 Programme under Grant Agreement 644839 (ICT-23-2014 Robotics).

Appendix B

PUBLICATION

- **Z. Ren**, W. Roozing and N. G. Tsagarakis, "The eLeg: A Novel Efficient Leg Prototype Powered by Adjustable Parallel Compliant Actuation Principles," in *IEEE-RAS International Conference on Humanoid Robots (Humanoids)*, 2018.

- **Z. Ren**, N. Kashiri, C. Zhou and N. G. Tsagarakis, "HERI II: A Robust and Flexible Robotic Hand Based on Modular Finger design and Under Actuation Principles," in *IEEE/RSJ International Conference on Intelligent Robots and Systems (IROS)*, 2018.

- W. Roozing, **Z. Ren**, and N. G. Tsagarakis, "Design of a 3-DoF Leg with Series and Parallel Compliant Actuation for Energy Efficient Articulated Robots," *in IEEE International Conference on Robotics and Automation (ICRA)*, 2018.

- **Z. Ren**, C. Zhou, S. Xin, and N. G. Tsagarakis, "HERI Hand: A Quasi Dexterous and Powerful Hand with Asymmetrical Finger Dimensions and Under Actuation," in *IEEE/RSJ International Conference on Intelligent Robots and Systems (IROS)*, 2017.

- N. Kashiri, L. Baccelliere, L. Muratore, A. Laurenzi, **Z. Ren**, E. Mingo Hoffman, G. Rigano, M. Kamedula, J. Malzahn, S. Cordasco, P. Guria, A. Margan, N. Tsagarakis, "CENTAURO: A Hybrid Locomotion and High Power Resilient Manipulation Platform", in *IEEE Robotics and Automation Letters (RAL)*,

2019, Accepted.

- **Z. Ren**, C. Zhou, and N. G. Tsagarakis, "Development and Application of a Quasi Dexterous and Powerful Hand with Asymmetrical Finger Dimensions and Under Actuation," in *IEEE Transaction on Mechatronics (T-MECH)*. Under Review.

- W. Roozing, **Z. Ren**, and N. G. Tsagarakis, "Development and Control of the eLeg: a 3-DoF Leg with Series and Parallel Compliant Actuation for Energy Efficient Articulated Robots," in *The International Journal of Robotics Research (IJRR)*. Under Review.

Appendix C

Demo

- HERI Hand: $https://www.youtube.com/watch?v=thQotLL9kaQ$
- HERI II Hand: $https://www.youtube.com/watch?v=1P1Z_It2Q5o$
- eLeg design concept: $https://www.youtube.com/watch?v=iu-VFH4TQWY$
- eLeg hardware development: $https://www.youtube.com/watch?v=PDy94M9AAoU$
- eLeg jumping: $https://www.youtube.com/watch?v=v4I6fGqAVz4$

Bibliography

[1] G. A. Pratt and M. M. Williamson, "Series elastic actuators," in *Intelligent Robots and Systems 95.'Human Robot Interaction and Cooperative Robots', Proceedings. 1995 IEEE/RSJ International Conference on*, vol. 1. IEEE, 1995, pp. 399–406.

[2] D. Paluska and H. Herr, "The effect of series elasticity on actuator power and work output: Implications for robotic and prosthetic joint design," *Robotics and Autonomous Systems*, vol. 54, no. 8, pp. 667–673, 2006.

[3] A. Velasco, G. M. Gasparri, M. Garabini, L. Malagia, P. Salaris, and A. Bicchi, "Soft-actuators in cyclic motion: Analytical optimization of stiffness and preload," in *Humanoid Robots (Humanoids), 2013 13th IEEE-RAS International Conference on*. IEEE, 2013, pp. 354–361.

[4] D. W. Robinson, J. E. Pratt, D. J. Paluska, and G. A. Pratt, "Series elastic actuator development for a biomimetic walking robot," in *Advanced Intelligent Mechatronics, 1999. Proceedings. 1999 IEEE/ASME International Conference on*. IEEE, 1999, pp. 561–568.

[5] A. Calanca, R. Muradore, and P. Fiorini, "A review of algorithms for compliant control of stiff and fixed-compliance robots," *IEEE/ASME Transactions on Mechatronics*, vol. 21, no. 2, pp. 613–624, 2016.

[6] H. Vallery, J. Veneman, E. Van Asseldonk, R. Ekkelenkamp, M. Buss, and H. Van Der Kooij, "Compliant actuation of rehabilitation robots," *IEEE Robotics & Automation Magazine*, vol. 15, no. 3, 2008.

[7] W. Roozing, J. Malzahn, N. Kashiri, D. G. Caldwell, and N. G. Tsagarakis, "On the stiffness selection for torque-controlled series-elastic actuators," *IEEE Robotics and Automation Letters*, vol. 2, no. 4, pp. 2255–2262, 2017.

[8] F. Negrello, M. Garabini, M. G. Catalano, J. Malzahn, D. G. Caldwell, A. Bicchi, and N. G. Tsagarakis, "A modular compliant actuator for emerging high performance and fall-resilient humanoids," in *2015 IEEE-RAS 15th International Conference on Humanoid Robots (Humanoids)*. IEEE, 2015, pp. 414–420.

[9] M. Hutter, C. Gehring, D. Jud, A. Lauber, C. D. Bellicoso, V. Tsounis, J. Hwangbo, K. Bodie, P. Fankhauser, M. Bloesch *et al.*, "Anymal-a highly

mobile and dynamic quadrupedal robot," in *2016 IEEE/RSJ International Conference on Intelligent Robots and Systems (IROS)*. IEEE, 2016, pp. 38–44.

[10] N. Paine, J. S. Mehling, J. Holley, N. A. Radford, G. Johnson, C.-L. Fok, and L. Sentis, "Actuator control for the nasa-jsc valkyrie humanoid robot: A decoupled dynamics approach for torque control of series elastic robots," *Journal of Field Robotics*, vol. 32, no. 3, pp. 378–396, 2015.

[11] U. Mettin, P. X. La Hera, L. B. Freidovich, and A. S. Shiriaev, "Parallel elastic actuators as a control tool for preplanned trajectories of underactuated mechanical systems," *The international journal of robotics research*, vol. 29, no. 9, pp. 1186–1198, 2010.

[12] D. F. Häufle, M. Taylor, S. Schmitt, and H. Geyer, "A clutched parallel elastic actuator concept: Towards energy efficient powered legs in prosthetics and robotics," in *2012 4th IEEE RAS & EMBS International Conference on Biomedical Robotics and Biomechatronics (BioRob)*. IEEE, 2012, pp. 1614–1619.

[13] M. Plooij, M. Wisse, and H. Vallery, "Reducing the energy consumption of robots using the bidirectional clutched parallel elastic actuator," *IEEE Transactions on Robotics*, vol. 32, no. 6, pp. 1512–1523, 2016.

[14] G. Mathijssen, R. Furnémont, T. Verstraten, B. Brackx, J. Premec, R. Jiménez, D. Lefeber, and B. Vanderborght, "+ spea introduction: drastic actuator energy requirement reduction by symbiosis of parallel motors, springs and locking mechanisms," in *Robotics and Automation (ICRA), 2016 IEEE International Conference on*. IEEE, 2016, pp. 676–681.

[15] G. Mathijssen, D. Lefeber, and B. Vanderborght, "Variable recruitment of parallel elastic elements: Series–parallel elastic actuators (spea) with dephased mutilated gears," *IEEE/ASME Transactions on Mechatronics*, vol. 20, no. 2, pp. 594–602, 2015.

[16] T. Yang, E. Westervelt, J. P. Schmiedeler, and R. Bockbrader, "Design and control of a planar bipedal robot ernie with parallel knee compliance," *Autonomous robots*, vol. 25, no. 4, p. 317, 2008.

[17] A. Mazumdar, S. J. Spencer, C. Hobart, J. Salton, M. Quigley, T. Wu, S. Bertrand, J. Pratt, and S. P. Buerger, "Parallel elastic elements improve energy efficiency on the steppr bipedal walking robot," *IEEE/ASME Transactions on Mechatronics*, vol. 22, no. 2, pp. 898–908, 2017.

[18] S. Shirata, A. Konno, and M. Uchiyama, "Design and evaluation of a gravity compensation mechanism for a humanoid robot," in *2017 IEEE/RSJ International Conference on Intelligent Robots and Systems (IROS)*. IEEE, 2007, pp. 3635–3640.

[19] X. Liu, A. Rossi, and I. Poulakakis, "Spear: a monopedal robot with switchable parallel elastic actuation," in *Intelligent Robots and Systems (IROS), 2015 IEEE/RSJ International Conference on*. IEEE, 2015, pp. 5142–5147.

[20] M. G. Catalano, G. Grioli, E. Farnioli, A. Serio, C. Piazza, and A. Bicchi, "Adaptive synergies for the design and control of the Pisa/IIT softhand," *The International Journal of Robotics Research*, vol. 33, no. 5, pp. 768–782, 2014.

[21] K. Mitsui, R. Ozawa, and T. Kou, "An under-actuated robotic hand for multiple grasps," in *IEEE/RSJ International Conference on Intelligent Robots and Systems*, 2013, pp. 5475–5480.

[22] R. R. Ma, L. U. Odhner, and A. M. Dollar, "A modular, open-source 3d printed underactuated hand," in *IEEE International Conference on Robotics and Automation*, 2013, pp. 2737–2743.

[23] Z. Ren, C. Zhou, S. Xin, and N. Tsagarakis, "HERI Hand: A Quasi Dexterous and Powerful Hand with Asymmetrical Finger Dimensions and Under Actuation," in *IEEE/RSJ International Conference on Intelligent Robots and Systems*, 2017, pp. 322–328.

[24] L. Wang, J. DelPreto, S. Bhattacharyya, J. Weisz, and P. K. Allen, "A highly-underactuated robotic hand with force and joint angle sensors," in *IEEE/RSJ International Conference on Intelligent Robots and Systems*, 2011, pp. 1380–1385.

[25] A. Edsinger-Gonzales, "Design of a compliant and force sensing hand for a humanoid robot," DTIC Document, Tech. Rep., 2005.

[26] J. Pons, E. Rocon, R. Ceres, D. Reynaerts, B. Saro, S. Levin, and W. Van Moorleghem, "The MANUS-HAND dextrous robotics upper limb prosthesis: mechanical and manipulation aspects," *Autonomous Robots*, vol. 16, no. 2, pp. 143–163, 2004.

[27] B. Massa, S. Roccella, M. C. Carrozza, and P. Dario, "Design and development of an underactuated prosthetic hand," in *IEEE International Conference on Robotics and Automation*, 2002, pp. 3374–3379.

[28] A. M. Dollar and R. D. Howe, "The highly adaptive SDM hand: Design and performance evaluation," *The international journal of robotics research*, vol. 29, no. 5, pp. 585–597, 2010.

[29] G. J. V. I. Schenau, "From rotation to translation: Constraints on multi-joint movements and the unique action of bi-articular muscles," *Human Movement Science*, vol. 8, no. 4, pp. 301–337, 1989.

[30] B. I. Prilutsky and V. M. Zatsiorsky, "Tendon action of two-joint muscles: transfer of mechanical energy between joints during jumping, landing, and running," *Journal of biomechanics*, vol. 27, no. 1, pp. 25–34, 1994.

[31] T. J. Klein and M. A. Lewis, "A robot leg based on mammalian muscle architecture," in *Robotics and Biomimetics (ROBIO), 2009 IEEE International Conference on*. IEEE, 2009, pp. 2521–2526.

[32] F. Iida, J. Rummel, and A. Seyfarth, "Bipedal walking and running with spring-like biarticular muscles," *Journal of biomechanics*, vol. 41, no. 3, pp. 656–667, 2008.

[33] R. Niiyama, A. Nagakubo, and Y. Kuniyoshi, "Mowgli: A bipedal jumping and landing robot with an artificial musculoskeletal system," in *Robotics and Automation, 2007 IEEE International Conference on*. IEEE, 2007, pp. 2546–2551.

[34] V. Salvucci, Y. Kimura, S. Oh, T. Koseki, and Y. Hori, "Comparing approaches for actuator redundancy resolution in biarticularly-actuated robot arms," *IEEE/ASME Transactions on Mechatronics*, vol. 19, no. 2, pp. 765–776, 2014.

[35] F. Loeffl, A. Werner, D. Lakatos, J. Reinecke, S. Wolf, R. Burger, T. Gumpert, F. Schmidt, C. Ott, M. Grebenstein *et al.*, "The dlr c-runner: Concept, design and experiments," in *Humanoid Robots (Humanoids), 2016 IEEE-RAS 16th International Conference on*. IEEE, 2016, pp. 758–765.

[36] N. G. Tsagarakis, H. Dallali, F. Negrello, W. Roozing, G. A. Medrano-Cerda, and D. G. Caldwell, "Compliant antagonistic joint tuning for gravitational load cancellation and improved efficient mobility," in *Humanoid Robots (Humanoids), 2014 14th IEEE-RAS International Conference on*. IEEE, 2014, pp. 924–929.

[37] W. Roozing, Z. Li, G. A. Medrano-Cerda, D. G. Caldwell, and N. G. Tsagarakis, "Development and control of a compliant asymmetric antagonistic actuator for energy efficient mobility," *IEEE/ASME Transactions on Mechatronics*, vol. 21, no. 2, pp. 1080–1091, 2016.

[38] W. Roozing, Z. Li, D. G. Caldwell, and N. G. Tsagarakis, "Design optimisation and control of compliant actuation arrangements in articulated robots for improved energy efficiency," *IEEE Robotics and Automation Letters*, vol. 1, no. 2, pp. 1110–1117, 2016.

[39] S. C. Jacobsen, J. E. Wood, D. Knutti, and K. B. Biggers, "The UTAH/MIT dextrous hand: Work in progress," *The International Journal of Robotics Research*, vol. 3, no. 4, pp. 21–50, 1984.

[40] M. Grebenstein, M. Chalon, G. Hirzinger, and R. Siegwart, "Antagonistically driven finger design for the anthropomorphic DLR hand arm system," in *IEEE-RAS International Conference on Humanoid Robots*, 2010, pp. 609–616.

[41] M. A. Diftler, J. Mehling, M. E. Abdallah, N. A. Radford, L. B. Bridgwater, A. M. Sanders, R. S. Askew, D. M. Linn, J. D. Yamokoski, F. Permenter *et al.*, "Robonaut 2-the first humanoid robot in space," in *IEEE International Conference on Robotics and Automation*, 2011, pp. 2178–2183.

[42] G. Palli, C. Melchiorri, G. Vassura, U. Scarcia, L. Moriello, G. Berselli, A. Cavallo, G. De Maria, C. Natale, S. Pirozzi *et al.*, "The DEXMART hand: Mechatronic design and experimental evaluation of synergy-based control for human-like grasping," *The International Journal of Robotics Research*, vol. 33, no. 5, pp. 799–824, 2014.

[43] J. Sobotta, *Atlas and text-book of human anatomy.* Saunders, 1907, vol. 3.

[44] W. Roozing, R. Zeyu, and N. G. Tsagarakis, "Design of a novel 3-dof leg with series and parallel compliant actuation for energy efficient articulated robots," in *IEEE International Conference on Robotics and Automation*, 2018.

[45] Z. Ren, R. Wesley, and N. G. Tsagarakis, "The eleg: A novel efficient leg prototype powered by adjustable parallel compliant actuation principles," in *IEEE-RAS International Conference on Humanoid Robots (Humanoids)*, 2018.

[46] C. Z. N. G. T. Zeyu Ren, Navvab Kashiri, "Heri ii: A robust and flexible robotic hand based on modular finger design and under actuation principles," in *IEEE/RSJ International Conference on Intelligent Robots and Systems*, 2018.

[47] L. Baccelliere, N. Kashiri, L. Muratore, A. Laurenzi, M. Kamedula, A. Margan, S. Cordasco, J. Malzahn, and N. G. Tsagarakis, "Development of a human size and strength compatible bi-manual platform for realistic heavy manipulation tasks," in *IEEE/RSJ International Conference on Intelligent Robots and Systems*, 2017.

[48] N. Kashiri, J. Malzahn, and N. G. Tsagarakis, "On the sensor design of torque controlled actuators: A comparison study of strain gauge and encoder-based principles." *IEEE Robotics and Automation Letters*, vol. 2, no. 2, pp. 1186–1194, 2017.

[49] Q. Lu, C. Ortega, and O. Ma, "Passive gravity compensation mechanisms: technologies and applications," *Recent Patents on Engineering*, vol. 5, no. 1, pp. 32–44, 2011.

[50] B. Vanderborght, N. G. Tsagarakis, C. Semini, R. Van Ham, and D. G. Caldwell, "Maccepa 2.0: Adjustable compliant actuator with stiffening characteristic for energy efficient hopping," in *Robotics and Automation, 2009. ICRA'09. IEEE International Conference on.* IEEE, 2009, pp. 544–549.

[51] A. Jafari, N. G. Tsagarakis, and D. G. Caldwell, "Awas-ii: A new actuator with adjustable stiffness based on the novel principle of adaptable pivot point and variable lever ratio," in *Robotics and Automation (ICRA), 2011 IEEE International Conference on.* IEEE, 2011, pp. 4638–4643.

[52] A. Tözeren, *Human body dynamics: classical mechanics and human movement.* Springer Science & Business Media, 1999.

[53] N. Dahlkvist, P. Mayo, and B. Seedhom, "Forces during squatting and rising from a deep squat," *Engineering in medicine*, vol. 11, no. 2, pp. 69–76, 1982.

[54] M. F. Bobbert, K. G. Gerritsen, M. C. Litjens, and A. J. Van Soest, "Why is countermovement jump height greater than squat jump height ?" *Medicine and science in sports and exercise*, vol. 28, pp. 1402–1412, 1996.

[55] L. Birglen, T. Laliberté, and C. M. Gosselin, *Underactuated robotic hands*. Springer, 2007, vol. 40.

[56] A. M. Agur and A. F. Dalley, *Grant's atlas of anatomy*. Lippincott Williams & Wilkins, 2009.

[57] R. R. Ma, L. U. Odhner, and A. M. Dollar, "A modular, open-source 3d printed underactuated hand," in *IEEE International Conference on Robotics and Automation*, 2013, pp. 2737–2743.

[58] M. C. Carrozza, C. Suppo, F. Sebastiani, B. Massa, F. Vecchi, R. Lazzarini, M. R. Cutkosky, and P. Dario, "The SPRING hand: development of a self-adaptive prosthesis for restoring natural grasping," *Autonomous Robots*, vol. 16, no. 2, pp. 125–141, 2004.

[59] M. Cutkosky and P. Wright, "Modeling manufacturing grips and correlations with the design of robotic hands," in *IEEE International Conference on Robotics and Automation*, 1986, pp. 1533–1539.

[60] M. A. Arbib, "Coordinated control programs for movements of the hand," *Hand function and the neocortex*, pp. 111–129, 1985.

[61] V. M. Zatsiorsky, Z.-M. Li, and M. L. Latash, "Enslaving effects in multi-finger force production," *Experimental brain research*, vol. 131, no. 2, pp. 187–195, 2000.

[62] K. Kaneko, K. Harada, F. Kanehiro, G. Miyamori, and K. Akachi, "Humanoid robot HRP-3," in *IEEE/RSJ International Conference on Intelligent Robots and Systems*, 2008, pp. 2471–2478.

[63] Y. Hasegawa, Y. Mikami, K. Watanabe, and Y. Sankai, "Five-fingered assistive hand with mechanical compliance of human finger," in *IEEE International Conference on Robotics and Automation*, 2008, pp. 718–724.

[64] T. Feix, J. Romero, H.-B. Schmiedmayer, A. M. Dollar, and D. Kragic, "The grasp taxonomy of human grasp types," *IEEE Transactions on Human-Machine Systems*, vol. 46, no. 1, pp. 66–77, 2016.

[65] R. Balasubramanian, J. T. Belter, and A. M. Dollar, "External disturbances and coupling mechanisms in underactuated hands," in *ASME 2010 International Design Engineering Technical Conferences and Computers and Information in Engineering Conference*. American Society of Mechanical Engineers, 2010, pp. 175–184.

[66] H. Maekawa, K. Tanie, and K. Komoriya, "Tactile sensor based manipulation of an unknown object by a multifingered hand with rolling contact," in *IEEE International Conference on Robotics and Automation*, vol. 1. IEEE, 1995, pp. 743–750.

[67] P. M. Wensing, A. Wang, S. Seok, D. Otten, J. Lang, and S. Kim, "Proprioceptive actuator design in the mit cheetah: Impact mitigation and high-bandwidth physical interaction for dynamic legged robots," *IEEE Transactions on Robotics*, vol. 33, no. 3, pp. 509–522, 2017.

[68] N. G. Tsagarakis, D. G. Caldwell, F. Negrello, W. Choi, L. Baccelliere, V. Loc, J. Noorden, L. Muratore, A. Margan, A. Cardellino *et al.*, "Walk-man: A high-performance humanoid platform for realistic environments," *Journal of Field Robotics*, vol. 34, no. 7, pp. 1225–1259, 2017.

[69] S. Seok, A. Wang, M. Y. Chuah, D. Otten, J. Lang, and S. Kim, "Design principles for highly efficient quadrupeds and implementation on the mit cheetah robot," in *Robotics and Automation (ICRA), 2013 IEEE International Conference on*. IEEE, 2013, pp. 3307–3312.

[70] N. N. Farve, "Design of a low-mass high-torque brushless motor for application in quadruped robotics," Ph.D. dissertation, Massachusetts Institute of Technology, 2012.

[71] D. W. Haldane, J. K. Yim, and R. S. Fearing, "Repetitive extreme-acceleration (14-g) spatial jumping with salto-1p," in *Intelligent Robots and Systems (IROS), 2017 IEEE/RSJ International Conference on*. IEEE, 2017, pp. 3345–3351.

[72] S. W. Ruehl, C. Parlitz, G. Heppner, A. Hermann, A. Roennau, and R. Dillmann, "Experimental evaluation of the schunk 5-finger gripping hand for grasping tasks," in *Robotics and Biomimetics (ROBIO), 2014 IEEE International Conference on*. IEEE, 2014, pp. 2465–2470.

[73] W. Roozing, J. Malzahn, N. Kashiri, D. G. Caldwell, and N. G. Tsagarakis, "On the stiffness selection for torque-controlled series-elastic actuators," *IEEE Robotics and Automation Letters, Vol. 2, No. 4*, 2017.

[74] W. Roozing, N. Kashiri, and N. G. Tsagarakis, "Enhanced explosive motion by field weakening control," in *IEEE/RSJ International Conference on Intelligent Robots and Systems*, 2018.